UNIVERSIDADE DE BRASÍLIA
INSTITUTO DE GEOCIÊNCIAS

O Complexo Máfico-ultramáfico Acamadado de Americano do Brasil e sua mineralização de Ni-Cu-Co

Dissertação de Mestrado Nº 257

Jonas Mota e Silva

Brasília – DF
Agosto de 2009

UNIVERSIDADE DE BRASÍLIA
INSTITUTO DE GEOCIÊNCIAS

O COMPLEXO MÁFICO-ULTRAMÁFICO ACAMADADO DE AMERICANO DO BRASIL E SUA MINERALIZAÇÃO DE Ni-Cu-Co

Jonas Mota e Silva

Orientador: **Prof. Dr. Elton Luiz Dantas**
Co-Orientador: **Prof. Dr. Berhard M. Bühn**

Examinadores: **Prof. Dr. Elson Paiva Oliveira (Unicamp)**
Prof. Dr. Claudinei Gouveia de Oliveira (UnB)

Brasília, agosto de 2009

AGRADECIMENTOS

ÍNDICE

ÍNDICE DE FIGURAS

ÍNDICE DE TABELAS

RESUMO

O Complexo de Americano do Brasil é uma intrusão sin-orogênica máfica-ultramáfica acamadada de 626±8 Ma. Este complexo está associado a um conjunto de outras intrusões correlatas, formadas durante o Ciclo Orogênico Brasiliano/Pan-Africano, no Brasil Central. Essas intrusões são do Arco Magmático de Goiás, que é parte componente da Faixa Brasília. Este estudo visa entender a intrusão das câmaras magmáticas do complexo e suas evoluções. Esta análise permitiu também identificar os processos magmáticos que promoveram a formação dos corpos de minério sulfetado Ni-Cu. Para isso, foram feitos trabalho de campo, descrição de furos de sonda, amostragem, petrografia, química de rocha total (elementos maiores, traço e terras raras) e geoquímica isotópica de S e Sm-Nd.

O Complexo de Americano do Brasil é uma seqüencia acamadada leste/oeste com 12 km de comprimento por 2 km de largura, formado por duas seqüências distintas (Norte e Sul), interpretadas como duas câmaras diferentes tectonicamente colocadas lado-a-lado ao longo de uma zona de falha. As seqüências têm séries de cristalização similares (e.g. ol+chr => ol+cpx+chr => ol+cpx+opx => cpx+opx => opx+plg+cpx), o que é característico de magmas toleíticos.

O complexo possui 3 corpos de minério de Ni-Cu magmático diferentes. Estes estão alojados em três níveis distintos da pilha cumulática: (i) O corpo S2 é de sulfeto semi-maciço a maciço formado durante reinjeção magmática na porção basal dunítica/peridotítica da Seqüencia Norte. (ii) O corpo S1 é de sulfeto disseminado formado por assimilação parcial do gnaisse encaixante, no topo da Seqüencia Sul. (iii) O corpo G2 é de sulfetos em textura em rede (do inglês *net-textured*) de dimensão relativamente pequena hospedado na base pedidotítica/piroxenítica da Seqüencia Sul. Os corpos de minério S2 e G2 possuem porções enriquecidas em Cu-Pt-Pd que foram interpretadas como produto da cristalização fracionada do líquido sulfetado. O δ^{34}S dos corpos de minério e das gotículas (do inglês *droplets*) do complexo estão entre -2,6 e +3,5 ($^0/_{00}$ CDT), indicando uma origem mantélica para os sulfetos.

Por fim, o Complexo de Americano do Brasil e suas intrusões correlatas nos mostram que intrusões máfico-ultramáficas pequenas , falhadas e sinorogenicas na região não devem ser ignoradas quanto ao seu potencial para portar mineralizações sulfetadas econômicas de Ni-Cu(-PGE).

Além deste foco central descrito acima, fez parte desta dissertação de mestrado outros dois estudos secundários: (i) Implantação do método de análise *in-situ* dos isótopos S^{32} e S^{34} utilizando o equipamento LA-MC-ICPMS. Foram alcançadas precisões e acurácias entre 0,3‰ e 0,5‰ (1σ) e estabelecimento de dois padrões internos. (ii) A utilização da técnica de lixiviação por bromo-metanol, que permite abertura dos minerais de sulfeto sem atacar os silicatos ou óxidos. Esta técnica aplicada no Complexo Americano do Brasil teve êxito parcial, pois a pirita da associação sulfetada foi apenas parcialmente dissolvida ao ataque. No entanto, comparando-se os resultados com a análise química de rocha total convencional, foram atingidos dados mais consistentes que permitem analisar a variação da composição do líquido sulfetado ao longo da estratigrafia, bem como, variação na geoquímica do magma silicático ao longo da formação da intrusão acamadada.

ABSTRACT

The "Americano do Brasil" Complex is a 626±8 Ma synorogenic mafic-ultramafic intrusion associated to several other coeval intrusions emplaced during the Brasiliano/Pan-African Orogenic Cycle, in Central Brazil. These intrusions are part of the Goias Magmatic Arc, which is related to the Brasília Belt. This study aim to understand the "Americano do Brasil" Complex's magma chambers emplacement and evolution, identifying the main magmatic processes that have caused its sulfide Ni-Cu orebodies formation. Thus, there we carried out field work, drill hole logging and sampling, petrography, whole-rock major, trace and rare-earth element geochemistry, S and Sm-Nd isotopic geochemistry.

The "Americano do Brasil" Complex consists of a 12 km-long and 2 km-wide EW trending sequence of layered mafic-ultramafic rocks formed by two different sequences (Northern and Southern sequences), interpreted as two different magma chambers, which are now tectonically juxtaposed along a fault zone. The sequences show similar crystallization trends (e.g. ol+chr => ol+cpx+chr => ol+cpx+opx => cpx+opx => opx+plg+cpx), which is a characteristic of tholeiitic magmas.

The complex has three different magmatic Ni-Cu orebodies, formed in three different stratigraphic layers of the cumulus pile: (i) S2 orebody, a semi-massive to massive sulfide reef-type magmatic ore formed during a magma replenishment in the dunite/peridotite basal zone of Northern sequence. (ii) The S1 orebody consists of disseminated sulfide formed by localized gneiss country rock assimilation at the topmost parts of the Southern sequence. (iii) The G2 consists of net-textured relatively small orebody hosted in the Southern sequence's basal websterite and lherzolite zone. The S2 and G2 orebodies have Cu-Pt-Pd-rich portions that were interpreted as a product of the sulfide liquid fractionation. The $\delta^{34}S$ data indicate mantle origin for all complex orebodies and droplets varying between -2.6 and +3.5 ($^{0}/_{00}$ CDT).

The "Americano do Brasil" Complex and several other coeval intrusions of the Goias Magmatic Arc show us that small, faulted and synorogenic mafic-ultramafic intrusions in the region should not be overlooked for their potential for hosting economic Ni-Cu(-PGE) sulfide deposits.

Apart from the described main propose of this master's thesis, there was done two other secondary studies were carried out: (i) Implementation of a method for *in-situ* S^{32} and S^{34} isotopes determination using LA-MC-ICPMS with precisions and accuracy

between 0.3‰ and 0.5‰ (1σ). Two in-house standards were established on the laboratory. (ii) The use of the bromine-methanol leach technique, which permits to determine the mineralogy and chemical composition of the sulfide fraction, even on poor-sulfides (< 1 vol. %) samples. Bromine-methanol leach attacks sulfides leaving the silicates and oxides untouched. The use of this technique on the "Americano do Brasil" Complex was partly successful, because of the partial dissolution of pyrite. Although, compared to traditional whole-rock analyses, the bromine-methanol method provided a more realistic geochemical data to constraint on sulfide liquid compositions along the stratigraphy and on magma geochemical changes during the evolution of layered intrusion.

APRESENTAÇÃO

Introdução

Este trabalho é resultado de pesquisa realizada sobre o complexo que hospeda a única mina de Ni-Cu, em ambiente intrusivo, ativa no país: a de Americano do Brasil, estado de Goiás.

Os depósitos magmáticos sulfetados de Ni-Cu ocorrem em intrusões acamadadas, condutos ou derrames de magma de composição máfica a ultramáfica (Naldrett, 2004). Essas intrusões férteis podem ter magmas parentais de diversas composições, originados em diferentes cenários geotectônicos e em qualquer idade da era geológica. Todavia, na maioria das vezes, essas intrusões estão relacionadas a regimes tectônicos extensionais da crosta, que incluiem riftes continentais ou margens continentais como ocorre nos depósitos classe mundial de Noril'sk na Rússia, Pechenga na Rússia, Voisey's Bay no Canadá e Jinchuan na China (Naldrett, 2004).

Esses depósitos raramente estão associados a regimes tectônicos orogênicos compressivos (Naldrett e Duke, 1980), como no caso do complexo máfico-ultramáfico acamadado de Americano do Brasil (AB). Este complexo é Neoproterozóico (626±8 Ma), sinorogênico toleítico (Nilson, 1981 e Laux *et al.*, 2004), intrudido durante o desenvolvimento da Faixa Brasília e do Arco Magmático de Goiás (Almeida, 1977 e Fuck *et al.,* 1993). Porém, ainda não se sabe se localmente predominava um regime compressivo ou extensivo. O exemplo mundial mais conhecido de depósito de Ni-Cu associado a ambientes orogênicos compressivos é a intrusão Rona, na Noruega. Esta intrusão formou-se em 437±0.5 Ma (Tucker *et al.*, 1990) e está relacionada ao fechamento do Oceano de Iapetus durante o Caledoniano (Ihlen *et al.*, 1997 *apud* Lamberg, 2005). Outros exemplos menos expressivos ocorrem na intrusão Moxie, no Canadá, e nos gabros de Aberdeenshire na Escócia.

O complexo AB faz parte de inúmeras outras intrusões máficas e máficas-ultramáficas (MUM) que ocorrem no Arco Magmático de Goiás e no Complexo Anápolis-Itauçú (Pimentel *et al.*, 2000 e Piuzana *et al.*, 2003), todas provavelmente com idades entre 600 e 630 Ma. Este conjunto de intrusões consolida as adjacências de Americano do Brasil-GO como uma região muito atrativa em termos econômicos no que diz respeito ao potencial para prospecção de depósitos magmáticos (e.g. Ni-Cu, PGE-Ni, Fe-Ti-V e Cu-Au).

Este trabalho se propõe a contribuir com o entendimento da evolução e gênese do complexo AB e de seus corpos de minério de Ni-Cu-Co. Para isso foram empregadas diversas ferramentas como: mapeamento geológico, investigação de galerias subterrâneas, descrição de furos de sondagem, petrografia, geoquímica de rocha total, geoquímica seletiva de sulfetos, análises de PGE, isótopos de Sm-Nd e isótopos de S.

Histórico da Exploração Mineral

O complexo AB foi reconhecido pela primeira vez em 1969 durante as atividades de mapeamento no trabalho de conclusão de curso dos alunos do Instituto de Geociências da Universidade de Brasília (IG / UnB). Durante início e meados da década de 1970 a Metais de Goiás S/A (Metago) assumiu os trabalhos de prospecção e definição dos recursos minerais associados a esta intrusão e outras correlatas. Nesta época foram definidos dois corpos de minério de Ni-Cu sulfetado (S1 e S2) no complexo AB nas margens do Córrego do Salgado. Logo após, foram feitos testes da economicidade da explotação das reservas e foi iniciado o desenvolvimento de uma galeria exploratória. Porém, motivado pelos baixos preços das *commodities* metálicas, a obra foi paralisada em 1980. No início da década de 1990 a área foi reavaliada pelas empresas Western Mining (WMC) e Rio Tinto, que estudaram a área com alguns furos de sondagem e optaram por não fechar negócio de compra com a Metago. Em 2004, diante de uma melhora no cenário econômico mundial, a área foi para licitação pública, que foi vencida pela empresa Prometálica Mineração Ltda, que é uma associação de capital nacional com capital canadense (Grupo Jaguar). Todavia, a exploração econômica dessas reservas só se deu em 2006, quando a Votorantim Metais Ltda (VM) firma uma *joint venture* (JV) com a Prometálica Mineração Centro-Oeste S/A (Prometálica), principalmente motivada pelo alto preço da *commodity* Ni no mercado mundial. Se não houver significativa expansão das suas reservas, a mina em Americano do Brasil será exaurida no final de 2010.

Objetivo

O presente trabalho tem como objetivo principal entender a evolução e gênese do complexo AB e de seus corpos de minério de Ni-Cu-Co, utilizando-se de interpretação geológica, petrográfica e geoquímica por meio de uma abordagem que contemplasse o posicionamento das amostras ao longo da estratigrafia proposta.

Para alcançar tal objetivo foram estabelecidas as seguintes metas centrais:

a. Contextualização do complexo AB na geologia regional, com ênfase no potencial econômico do magmatismo máfico e máfico-ultramáfico – MUM - do Arco Magmático de Goiás;

b. Entendimento do complexo AB quanto ao seu empilhamento estratigráfico e suas implicações petrogenéticas, relações de contato, geometria das camadas e relações temporais;

c. Evolução da câmara, fracionamento magmático e assimilação das rochas encaixantes;

d. Formação dos corpos de minério e seus conteúdos de metais base e nobres;

e. Fracionamento do líquido sulfetado.

Compôs esta pesquisa outro objetivo, de caráter secundário, que foi o da implantação do método de análise de isótopos de S em LA-MC-ICPMS no Laboratório de Geocronologia do Instituto de Geociências da Universidade de Brasília (IG / UnB).

Materiais e métodos

Durante o período 2006 / 2007, foram realizadas atividades de revisão da literatura técnico-científica, mapeamento geológico com descrição de mais de 1000 afloramentos, descrição testemunhos de dezenas de furos sondagem e investigação de galerias subterrâneas. Nesta fase, o autor deste estudo integrou a equipe de exploração mineral da VM do projeto Americano do Brasil, que objetivava obter a expansão das reservas minerais do depósito Ni-Cu-Co através de sondagem *brown field*. Este processo levou a uma compreensão do posicionamento e da geometria das camadas formadoras do complexo, bem como de seus corpos de minério.

Para realização desta etapa do trabalho foram utilizados dados aerogeofísicos (magnetometria e gamaespectometria), geofísica terrestre (magnetometria, IP e TDEM), geoquímica de solo, topografia de detalhe, testemunhos dos furos de sondagem e suas análises químicas. Todos esses dados foram cedidos pelas empresas VM e Prometálica que detinham também os dados da Metago.

As fontes bibliográficas específicas sobre o complexo AB utilizadas, tanto nesta fase inicial como na pesquisa já vinculada ao mestrado, foram os relatórios da Metago que contemplam mapas, seções e cálculo de recursos (Metago, 1978) e a tese de doutorado de Nilson (1981), que contempla mapas, seções dos principais corpos de minério, geoquímica, petrografia e química mineral de silicatos e sulfetos. Além disso,

foram consultados trabalhos mais específicos como a re-interpretação dos dados geofísicos feita no mestrado de Silva (2003) e os recentes dados geocronológicos U-Pb e Sm-Nd apresentados no mestrado de Gioia (1997) e no doutorado de Laux (2004).

Como parte das atividades específicas do programa de mestrado, foi realizada uma amostragem que contemplou a representatividade do complexo como um todo e de suas rochas encaixantes. A amostragem contou também com a colaboração do Prof. Dr. Cesar Ferreira Filho do IG/UnB, totalizou a coleta de 76 amostras, por volta de 1 kg cada uma, sendo que para este estudo foram selecionadas 27.

Parte dessas amostras foi trabalhada no Laboratório de Laminação do IG/UnB para confecção de lâminas delgadas polidas. Foi realizado estudo de micropetrografia, com ênfase na caracterização da fração sulfetada de todas as 27 amostras selecionadas.

A maior fração dessas amostras ficou reservada para geoquímica de rocha total que foi realizada no laboratório ALS Chemex em Toronto no Canadá, com determinação de teores de elementos maiores (fusão com metaborato de lítio e ICP-AES), elementos menores, traço e terras raras (fusão com borato de lítio e ICP-MS), enxofre e carbono (Leco). Amostras de minério com teores elevados de Ni e Cu foram analisados por espectrometria de absorção atômica (AAS) com abertura em tetra-ácido.

Uma porção adicional de amostras foi encaminhada para o Laboratório Labtium Oy na Finlândia para determinação dos teores de Ni, Cu, Co e Fe exclusivamente na fração sulfetada por meio do método de ataque seletivo (brando) com bromo-metanol, conforme descrito por Penttinen *et al.*, 1977 *apud* Lamberg, 2005. Este método com seus resultados e interpretações está apresentado em anexo neste volume.

Visando análise de geoquímica isotópica de Sm-Nd, outra pequena fração foi retirada cominuída, pesada, submetida a sucessivos ataques químicos ácidos com alta temperatura com HNO_3, HF e HCl em cápsulas de Savilex fixadas por bombas, evaporadas em Clean-Box e, por fim, submetida à passagem por colunas catiônicas (Bio-Rad AG50W-X8) em diferentes condições de acidez para separação dos elementos Sm e Nd. A aferição quantitativa desses elementos foi finalmente determinada por aparelho de espectometria de massa por ionização térmica (TIMS). Essa metodologia está detalhada na publicação de Gioia e Pimentel (2000). Todo esse procedimento foi realizado no Laboratório de Geocronologia do IG/UnB.

Uma amostragem adicional mais volumosa, por volta de 2 kg, nos corpos de minério, foi retirada visando caracterizar seus conteúdos de Ni, Co, PGE (Os, Ir, Ru, Rh, Pt e Pd), Au e Cu (metais base e nobres). As determinações dos teores foram feitas

no laboratório Becquerel no Canadá por meio de pré-concentração por fusão com sulfeto de níquel, irradiação e análise por ativação com nêutrons (NAA).

As análises pontuais de isótopos de S foram realizadas por meio do emprego de fusão a laser e leitura em espectrômetro de massa multi-coletor com plasma indutivamente acoplado (LA-MC-ICPMS). Tendo em vista que esse tipo de análise tem caráter inédito no Brasil, o método, que foi desenvolvido no Laboratório de Geocronologia do IG/UnB, está detalhado como anexo neste volume.

Os dados coletados nesses métodos analíticos compuseram a base informacional necessária à realização do objetivo principal desta pesquisa. A geoquímica de rocha total deu suporte aos estudos de evolução, gênese e caracterização química do magmatismo do complexo AB, enquanto que o estudo de geoquímica isotópica de Sm-Nd embasou avaliações sobre contaminação crustal, assimilação de rochas encaixantes e geologia regional e a geoquímica isotópica de S colaborou com inferências sobre assimilação de rochas encaixantes. Por sua vez, as análises de ataque seletivo de sulfetos e análise de PGE dos corpos de minério, compuseram um conjunto mais específico do estudo, que visou caracterizar o conteúdo de metais dos corpos de minério e de segregações menos significativas de sulfeto, bem como colaborar com a interpretação da evolução e fracionamento do líquido sulfetado.

Justificativa

A relevância desta pesquisa destaca-se sobre quatro aspectos principais:

1. O complexo AB hospeda a única mina de Ni-Cu-Co sulfetado, hospedada em ambiente intrusivo, em operação no Brasil, com reservas estimadas para serem exploradas até o final de 2010. O níquel está relacionado à fabricação de aço-inoxidável, superligas, ligas metálicas, baterias recarregáveis, moedas e revestimentos metálicos, que são produtos comuns na indústria de robótica, aviação, marítima, automobilística e química. Toda a cadeia de produção, desde sua extração até a fabricação dos produtos finais, relaciona-se com processos geradores de riquezas e empregos para o país, com impactos de natureza econômica e social. Ao trazer novas informações sobre os processos geológicos que formaram o depósito de Ni-Cu-Co de Americano do Brasil-GO, o presente estudo colabora com as atividades de exploração mineral do complexo AB;

2. Sob o ponto de vista regional, este estudo também contribui para a delimitação e o entendimento do intenso magmatismo máfico e máfico-ultramáfico associados

à porção sul do Arco Magmático de Goiás, denominado de Arco de Arenópolis (Pimentel *et al.*, 2000). Neste âmbito propicia efeitos de natureza econômica e social ao evidenciar o potencial da região para hospedar outras mineralizações magmáticas de Ni-Cu, podendo promover interesses empresariais e governamentais para investimentos na área de prospecção mineral na região;

3. O complexo AB tem suas características ígneas primárias muito bem preservadas, e porta três corpos de minério Ni-Cu-Co, deste modo configura-se como um excelente objeto de estudo para o entendimento de processos geológicos / magmáticos formadores de complexos máfico-ultramáficos acamadados e de seus corpos de minério relacionados. Esta pesquisa discute vários desses processos que incluem a gênese de complexos máficos-ultramáficos, o fracionamento magmático, a contaminação crustal, a assimilação de rochas encaixantes, a saturação e segregação de líquido sulfetado, a acumulação e a formação de depósitos magmáticos, o fracionamento e a química da fração sulfetada. Desta maneira, esta discussão se insere no segmento da ciência geológica que objetiva entender os processos envolvidos na formação desses complexos e de seus depósitos minerais magmáticos associados;

4. Os isótopos de S particionam sob processos biogênicos e, como tal, sulfetos e sulfatos de rochas (meta-) sedimentares costumam apresentar valores de $\delta^{34}S$ negativos e mais variáveis quando comparado aos de origem magmática ou hidrotermal (Faure, 1986). Os sulfetos advindos de rochas ígneas derivadas do manto (e.g. complexos máficos e máficos-ultramáficos) têm composição isotópica homogênea $\delta^{34}S = 0\pm3‰$. Todavia, os grandes depósitos Ni-Cu do mundo, estão hospedados em complexos que apresentam assinatura de contaminação crustal, normalmente associados a seqüências de rochas (meta-) sedimentares, que conferem aos depósitos assinaturas isotópicas negativas. Deste modo, esta ferramenta tem sido amplamente utilizada em depósitos magmáticos Ni-Cu, no sentido de identificar a possível existência de fontes externas de S no magmatismo máfico, associados aos processos de contaminação crustal ou assimilação de encaixantes. Este cenário explicita a relevância deste projeto, com seu objetivo secundário de implantação do método de análise de isótopos de S em LA-MC-ICPMS no Laboratório de Geocronologia do Instituto de Geociências da Universidade de Brasília (IG / UnB).

Localização e Fisiografia

O complexo AB tem aproximadamente 3 x 12 km, sendo que a parte oeste situa-se no município de Mossâmedes e a leste no município de Americano do Brasil, ambos no Estado de Goiás. O centro da intrusão situa-se a 12 km da cidade Americano do Brasil, cujo acesso é feito por estrada de terra de boa qualidade. Essa cidade, por sua vez, fica a 110 km de Goiânia, e pode ser acessada a partir do aeroporto através da perimetral norte em Goiânia, posteriormente rodovias GO-060 e GO-156, todas em bom estado de conservação, durante o período da pesquisa.

Quanto à suas características fisiográficas, a norte da intrusão, gnaisses sustentam um relevo positivo na forma de serra arqueada aproximadamente alongada na direção E-W (Serra das Divisões ou Serra de Santa Marta) dos mais altos da região, atingindo cotas de até 950 m. Esta serra integra um importante divisor de águas entre duas macrobacias hidrográficas, a do Parnaíba, que deságua no Rio Paraná e a do Rio Tocantins. Na escala mais regional, podemos dizer que esta serra está no extremo oeste do compartimento geomorfológico do Planalto Central, que é aplainado aproximadamente na cota 1100 m, sendo recoberto por perfil laterítico relacionado à formação da Superfície Sulamericana de idade Cretácea / Terciária (Costa, 2008). Algumas dezenas de quilômetros mais a oeste, inicia-se a planície aluvionar do Rio Araguaia, principal afluente do Rio Tocantins.

O complexo AB em si, situa-se em relevo negativo comparado às suas encaixantes gnáissicas, tendo um predomínio de relevo de largas colinas e morrotes. Suas porções mais a oeste conformam uma planície recoberta por espessa camada de Latossolo Vermelho e depósitos fluviais recentes, o que dificulta o mapeamento geológico de maior detalhe. A porção central do complexo possui acidentes topográficos mais abruptos, pois está entre a porção leste mais alta (cota ~830 m) e a planície oeste mais baixa (cota ~750 m), o que proporciona boa exposição do topo rochoso.

Escopo do Estudo

Conforme previsto no regulamento do Curso de Pós-graduação em Geologia da Universidade de Brasília e por sugestão do Orientador, esta dissertação de mestrado apresenta-se estruturada na forma de artigo a ser submetido para publicação em periódico científico especializado sobre o tema. Este se encontra apresentado na mesma forma em que será submetido, mantendo o estilo e o formato previstos pelo periódico.

Tal *paper* é intitulado de "*Geology, Petrology and Geochemistry of the "Americano do Brasil" Layered Intrusion and its Ni-Cu Sulfide Deposits, Central Brazil.*", sendo ele elaborado durante os anos de 2008 e 2009. Os autores submeterão o trabalho à revista *Mineralium Deposita*, publicada pela Springer, Alemanha. Este texto tem como objetivo principal apresentar caracterização geológica, estratigráfica, petrográfica, petrológica, geoquímica (elementos maiores, menores, traço, terras raras em rocha total) e geoquímica de isótopos de S e Sm-Nd do complexo AB e de suas encaixantes. Somado a isso, é abordado também discussões sobre a origem e a constituição do complexo AB e sua relação com a geologia regional. Em uma visão de maior detalhe, caracteriza os corpos de minério (S2, S1 e G2) do complexo do ponto de vista geológico, petrográfico, geoquímico e genético.

O artigo mencionado é precedido por um Capítulo de Apresentação, onde estão contidas informações gerais da dissertação que incluem a Introdução, o Histórico da Exploração Mineral, os Objetivos, os Materiais e Métodos, a Justificativa, a Localização e a Fisiografia e, por fim, este próprio Sub-capítulo, nomeado de "Escopo do Estudo". Ao final deste volume encontra-se o Capítulo de Conclusões que apresenta, de forma sintetizada, o conjunto dos resultados da pesquisa, inclusive aqueles já apresentados, mais detalhadamente no artigo. Finalmente, o capítulo de Anexos, que inclui os segmentos que descrevem: i) a técnica e a aplicação do método de ataque (brando) seletivo à fração sulfetada; ii) a metodologia desenvolvida para análise de isótopos de S.

Referências

Almeida F.F.M. (1977). O Cráton do São Francisco. Revista Brasileira de Geociências, 7(4): 349-364.

Costa, M.L. (2008). Evolução da Paisagem, Laterização e Depósitos Minerais Associados. Apostila de Curso, ADIMB. Brasília, Hotel Aracoara, 2008.

Faure, G. (1986). Principles of isotope geology. J Wiley & Sons, NY, 2nd edition, 598 pp.

Fuck, R.A., Jardim de Sá, E.F., Pimentel, M.M., Dardenne, M.A., Soares, A.C.P., 1993. As faixas de dobramentos marginais do Cráton São Francisco: Síntese dos conhecimentos. In: Dominguez, J.M.L., Misi, A. (Eds.), O Cráton do São Francisco, pp. 161–185.

Gioia, S.M.C.L. (1997). Preparação da Metodologia Sm-Nd para Datação de Amostras Geológicas e sua Aplicação em Rochas das Áreas de Firminópolis, Fazenda Nova e Americano do Brasil – GO. Dissertação de Mestrado, Universidade de Brasília, Brasília, Brasil.

Gioia, S.M.C.L. & Pimentel, M.M. (2000). The Sm–Nd isotopic method in the Geochronology Laboratory of the University of Brasília. Ann. Acad. Bras. Cienc. 72, 219–245.

Lamberg, P. (2005). From genetic concepts to practice – Lithogeochemical identification of Ni-Cu mineralized intrusions and localizations of the ore. Bulletin of Geological Society of Finland n. 402, 264 pp.

Laux, J.H. (2004). Evolução do Arco Magmático de Goiás com base em dados geocronológicos U-Pb e Sm-Nd. Tese de Doutorado, Universidade de Brasília, Brasília.

Laux, J.H., Pimentel, M.M., Dantas, E.L., Armstrong, R., Armele, A., Nilson, A.A. (2004). Mafic magmatism associated with the Goiás Magmatic Arc in Anicuns region, Goiás, Central Brazil: Sm-Nd isotopes and new ID-TIMS and SHRIMP U-Pb data. Journal of South America Earth Sciences 16, 599 – 614.

Metago (1978). Complexo máfico ultramáfico de Americano do Brasil, Relatório de Pesquisa, vol I. Relatório de pesquisa DNPM, não publicado.

Naldrett, A.J. and Duke J.M. (1980) – Platinum metals in magmatic sulfide ores. Science, 208, 1417-1424.

Nilson, A.A. (1981). The nature of Americano do Brasil mafic-ultramafic complex and associated sulfide mineralization, Goiás, Brazil. PhD Thesis, University of Western Ontario, 460 pp.

Pentinnen, U., Palosaari, V., Siura, T. (1977) – Selective dissolution and determination of sulfides in nickel ores by the bromine-methanol method. Bulletin of Geological Society of Finland 49(2), 79 – 84.

Pimentel, M.M., Fuck, R.A., Gioia, D.M.C.L. (2000). The Neoproterozoic Goiás Magmatic Arc, Central Brazil: a review and new Sm–Nd isotopic data. Revista Brasileira de Geociências 30 (1), 35–39.

Piuzana, D., Pimentel, M.M., Fuck, R.A., Armstrong, R.A., (2003). Neoproterozoic granulite facies metamorphism and contemporaneous granite magmatism in the

Brasília Belt, Central Brazil: regional implications of new SHRIMP U–Pb and Sm–Nd data. Precambrian Research, 125: 245–273.

Silva, C.A. (2003). Geofísica de superfície no Complexo de Americano do Brasil, GO – interpretação e integração. Dissertação de Mestrado, Universidade de Brasília, Brasília – DF.

Tucker, R.D., Boyd, R. and Barnes, S-J. (1990). A U-Pb zircon age for Rona intrusion, N. Norway: New evidence of basic magmatism in the Scandinavian Caledonides in Early Silurian time. Norsk Geologisk Tidsskrift, 70: 229-239.

Geology, Petrology and Geochemistry of the Americano do Brasil Layered Intrusion and its Ni-Cu Sulfide Deposits, Central Brazil.

Jonas Mota e Silva, Cesar Fonseca Ferreira Filho*, Bernhard Manfred Bühn, Elton Luiz Dantas

Instituto de Geociências, Universidade de Brasília, Brasília, DF. 70910-900. Brazil.

* Corresponding author. Fax +55 61 3347 4062.

E-mail address: jonas.silva@vmetais.com.br (J. Mota e Silva).

E-mail address: cesarf@unb.br (C. Ferreira Filho).

Abstract The "Americano do Brasil" Complex (ABC) is a 626±8 Ma synorogenic mafic-ultramafic intrusion associated to several other coeval intrusions emplaced during the Brasiliano/Pan-African Orogenic Cycle, in Central Brazil. These intrusions are part of the Goias Magmatic Arc, which is related to the Brasília Belt. This paper aim to understand the ABC magma chambers emplacement and evolution, identifying the main magmatic processes that have caused its Ni-Cu orebodies formation. Thus, there were done field work, drill hole logging and sampling, petrography, whole-rock major, trace and rare-earth elements geochemistry, S and Sm-Nd isotopic geochemistry.

The ABC Complex consists of a 12 km-long and 2 km-wide EW trending sequence of layered mafic-ultramafic rocks formed by two different sequences (Northern and Southern sequences), interpreted as two different magma chambers, which are now tectonically juxtaposed along a fault zone. The sequences show similar crystallization trends (e.g. ol+chr => ol+cpx+chr => ol+cpx+opx => cpx+opx => opx+plg+cpx), which is a characteristic of tholeiitic magmas.

The complex has three different magmatic Ni-Cu orebodies, formed in three different stratigraphic layers of the cumulus pile: (i) S2 orebody, a semi-massive to massive reef-type magmatic ore formed during a magma replenishment in the dunite/peridotite basal zone of Northern sequence. (ii) The S1 orebody consists of disseminated sulfide formed by localized gneiss country rock assimilation on topper parts of Southern sequence. (iii) The G2 consists of net-textured relatively small orebody hosted in the Southern sequence's basal websterite and lherzolite zone. The S2 and G2 orebodies have Cu-Pt-Pd-rich portions that were interpreted as a product of the

sulfide liquid fractionation. The δ^{34}S indicates mantle origin for all complex orebodies and droplets varying between -2.6 and +3.5 ($^0/_{00}$ CDT).

Finally, the ABC and coeval intrusions of the Goias Magmatic Arc show that small, faulted and synorogenic mafic-ultramafic intrusions in the region should not be overlooked for their potential to host economic Ni-Cu(-PGE) sulfide deposits.

Keywords: Ni-Cu sulfide deposit - Synorogenic mafic-ultramafic intrusion – Massive reef-type magmatic ore - Sulfide liquid fractionation

Introduction

Magmatic Ni-Cu sulfide deposits are hosted in layered intrusions, magma conduits or lava flows of mafic to ultramafic compositions (Naldrett, 2004). They are formed during the emplacement of mantle-derived magmas of different compositions in widely distinct tectonic settings. The processes related to these magmatic ores formation are: (i) partial melting of the mantle, (ii) transfer of magma to crust, (iii) saturation in S and formation of the sulfide phase that collects the metals and (iv) concentration of that phase (Naldrett, 1989, 2004, Barnes and Maier, 1999 and Lamberg, 2005). The only exception is the Sudbury Igneous Complex, which has been interpreted to result from a meteorite impact (Giblin, 1984; Krough *et al.,* 1984).

Intrusion-related Ni-Cu sulfide deposits are typically associated with extensional tectonics in the crust, including rifted continental crust or continental margin, as represented by the occurrences from Noril'sk, in Russia, Duluth, in the United States, Pechenga, in Russia, Voisey's Bay, in Canada and Jinchuan, in China (Naldrett, 2004). However this type of deposit is rarely associated with orogenic compressive tectonic settings.

The world's important deposits of Ni-Cu sulfides occur almost exclusively at the base of their associated igneous bodies, which implies that the magmas involved were saturated in sulfide, and carrying excess sulfide at the time of their final emplacement (Naldrett, 1999). Sulfide saturation of magmas is not enough itself to produce an ore deposit. The appropriate physical environment is required to mix the sulfide liquid with enough magma to produce a sulfide fraction enriched in chalcophile metals. Moreover,

the sulfide mass must be concentrated in a restricted locality to result in an ore grade (Naldrett, 1999).

Contamination is a key aspect to drive the magmas to sulfide saturation and for Ni-Cu giant deposits formation. World wide examples reveal particular processes of contamination related to Ni-Cu deposits formation: (i) externally-derived sulfur was stressed as a key ingredient by Keays *et al.* (1997) and was identified using sulfur isotopes in Noril'sk (Godlevsky and Grienko, 1963; Gorbachev and Grinenko, 1973, Grinenko, 1985; Li *et al.,* 2003), Stillwater (Zientek and Ripley, 1990), Bushveld (Buchanan *et al.*, 1981) and its satellite intrusion Uitikomst (Li *et al.*, 2002); (ii) crustal contamination with strong light rare earth element (LREE) and incompatible trace elements enrichment as in Jinchuan deposit (Song *et al*., 2006; Tang *et al.*, 2007); and (iii) siliceous assimilation (Irvine, 1975) from country rocks, as a means of lowering sulfide solubility, was suggested for the Sudbury deposit where S may have been of magmatic origin (Naldrett *et al*., 1986). The orebodies hosted in the feeder structure of Voisey's Bay have the geochemical signature of all the three contamination processes (Li and Naldrett, 1999, Ripley *et al*., 1999).

The "Americano do Brasil" Complex (ABC), Central Brazil, is associated with several Neoproterozoic synorogenic mafic and mafic-ultramafic intrusions (Laux *et al.,* 2004). These intrusions are located at the eastern border of the Neoproterozoic Goiás Magmatic Arc, an extensive juvenile terrain of the Brasiliano orogeny (Pimentel *et al.,* 2000). This complex is the only intrusion with an operating Ni-Cu sulfide mine in Brazil. The mining activities started in 2006 and renewed the academic interest for magmatic processes forming Ni-Cu sulfide mineralizations in the Goiás Magmatic Arc. Previous studies of the ABC provided mainly geological and petrographic descriptions of the intrusion and its Ni-Cu sulfide deposits (Nilson, 1981; Nilson *et al*., 1986).

In this paper we intend to understand the mineralization process within the petrologic evolution of the layered intrusion, providing constraints for the stratigraphic and petrologic evolution of the ABC. In a more detailed approach we interpret the orebodies genesis in the light of assimilation of siliceous and S-rich country rocks, magma replenishment and REE and trace elements contamination. The results of a field and petrologic-geochemical study of the ABC and its Ni-Cu sulfide deposits provide new insights for the formation of Ni-Cu sulfide deposits within layered intrusions, expanding the exploration opportunities for orogenic environments in general.

Exploration Review

The ABC was discovered in 1969 during regional mapping projects developed by the University of Brasília. The Ni-Cu sulfide mineralization was identified during regional exploration by the Brazilian company METAGO in the early 70'. Systematic drilling by METAGO in 1975-1978 indicated a small Ni-Cu deposit (*ca.* 5 Mt @ 0.62 %Ni, 0.65 %Cu). The development of this deposit by METAGO (including experimental underground mining and hydrometallurgical plant) started in 1980, but were discontinued shortly after. Except for intermittent re-evaluations performed by different mining companies, including Western Mining Co. in 1993 and RTZ Corp. in 1995, the deposit was dormant until acquisition by Prometalica Ltd. in 2004. A re-evaluation of the reserves, underground mining and conventional sulfide flotation process (concentrator) were developed through a joint venture between the Prometalica Ltd. and Votorantim Metais Ltd. Production of Ni at *ca.* 6,000 t per year of Ni in concentrate started in 2006 with proven reserves to sustain production until 2010. This mining operation triggered an exploration rush in the nearby layered complexes, as well as an extensive brown field exploration by Votorantim Metais Ltd. in the ABC. Exploration activities were mainly discontinued after the abrupt decrease of metal prices in the third and fourth quarter of 2008.

Regional Geology

The Tocantins Province (Almeida, 1977), in Central Brazil, which hosts the ABC, consists of three orogenic belts formed during the Neoproterozoic Brasiliano/Pan-African cycle: the Paraguai, the Araguaia and the Brasília belts. They were formed during the collision of three major cratonic blocks in Brazil, the Amazon to the west, São Francisco to the east, and the sediment-covered Paraná craton to the south (Pimentel *et al.*, 2000 – Figure 1). The ABC is located within the Brasilia Belt (Dardenne *et al.*, 2000; Pimentel *et al.*, 2000), which is made of:

    i)   an extensive fold-and-thrust belt that consists of a metamorphosed siliciclastic and carbonate sequence from a passive margin deposition of the western part of the São Francisco Craton, known from the west to east as Araxá, Ibiá and Canastra Group followed by Paracatú,

Vazante and Serra do Garrote Formation (Almeida *et al*., 1981; Fuck *et al*., 1993, 1994, 2001; Dardenne, 2000; Pimentel *et al*., 2000);

ii) exposure of older terrains made of Archean greenstone belts and tonalite–trondhjemite–granodiorite (TTG) associations, known as the Goiás Massif, which also includes the three large layered intrusions Barro Alto, Niquelandia and Cana Brava. These latter intrusions are interpreted as a disrupted single continuous magmatic structure formed by two juxtaposed sequences (Ferreira Filho, 1998; Ferreira Filho *et al*., 1998) of 1.25 Ga and 800 Ma, uplifted by a N-S thrust fault (Pimentel *et al.,* 2004, 2006; Ferreira Filho *et al.*, 2009);

iii) the Anápolis-Itauçú Complex, which is a large NW-oriented metamorphic complex made of Neoproterozoic para- and orthogranulites and highly deformed granites (Piuzana *et al.,* 2003; Laux *et al.*, 2005); and

iv) the Neoproterozoic juvenile Goiás Magmatic Arc underlying extensive areas in the western part of the Brasilia Belt (Pimentel *et al.*, 2000; Junges *et al.,* 2002; Laux *et al.*, 2004).

The Brasilia Belt contains several base metals and gold deposits and mines (Figure 1). The nickel exploration in the Tocantins province is mainly related to lateritic ores, formed by two active mines at Niquelandia Complex, an unexploited deposit in Barro Alto Complex and alkaline-ultramafic plugs to the west of the Arenóplois Magmatic Arc (e.g. Montes Claros and Santa Fé – Figure 1).

Goiás Magmatic Arc

The Goiás Magmatic Arc is located on the western part of the Brasília Belt and, since last decade, is interpreted as a large area of Neoproterozoic juvenile continental crust formed during plate convergence roughly between 900 and 630 Ma (Pimentel and Fuck, 1992; Pimentel *et al*., 1991, 1997; Junges *et al*., 2002). It is divided by the Goiás Massif into two parts, which are the northern arc (Mara Rosa) and the southern one (Arenópolis). All rocks were metamorphosed under upper greenschist to amphibolite facies conditions, but have kept their major geochemical and isotopic features indicating the juvenile nature of the igneous protoliths (Junges *et al*., 2002). Recent data suggest that igneous activity in the Goiás Magmatic Arc took place in two episodes: between

890 - 800 Ma, in an intraoceanic setting made of magnetite series tonalitic rocks; and between 660 - 600 Ma, likely in an active continental margin at the end of the Brasiliano Orogenic Cycle (Laux *et al*., 2005). The U-Pb TIMS (Thermal Ionization Mass Spectrometer) age of the ABC of 626±8 Ma (Laux *et al*., 2004) and its geological association suggest that the complex was formed during the second magmatic episode.

In the central-east part of the Arenópolis Magmatic Arc, in the contact with the Anápolis-Itauçú Complex, the Anicuns-Itaberaí volcano-sedimentary sequence is exposed. It is formed by metavolcanic and metaplutonic amphibolites, metapelitic rocks with minor iron formations, cherts, marbles and ultramafic rocks. Recent U-Pb data suggest that this sequence probably makes part of the Arenóplis magmatic arc (Laux *et al*., 2004) formed during the first magmatism episode (890 – 800 Ma).

Anápolis-Itauçú Complex

The Anápolis–Itauçú Complex underlies a large area in the central-southern part of the Brasília Belt and consists of a NW–SE elongated (240 km × 60 km) exposure of high-grade metamorphic rocks and granites. The complex is separated from the low-grade metamorphic metasedimentary rocks of the Araxá Group by poorly exposed low- and high-angle shear zones (Piuzana, 2003). Recent studies suggest that the Anápolis-Itauçú Complex, composed of para- and ortho-granulites, represents a metamorphic complex made of Araxa group and Arenópolis Magmatic Arc protoliths (Piuzana *et al*., 2003; Hollanda *et al*., 2003; Laux *et al*., 2005). The rocks were metamorphosed at ultra-high-temperature conditions 1050ºC and 10 kbar represented by sapphirine- and quartz-bearing garnet-orthopyroxene-sillimanite granulites (Moraes *et al*., 2001). U–Pb data for zircons of these granulites range from 649 to 634 Ma (Baldwin and Brown, 2008).

Mafic and Mafic-Ultramafic intrusions

The magmatism in the Arenópolis Magmatic Arc and the Anápolis-Itauçú Complex comprises the two main magmatic episodes mentioned. The second one at *ca.* 630 – 600 Ma contains several mafic and mafic-ultramafic (MUM) intrusions. This magmatism is probably the consequence of a localized extensional event in the orogenic system related to pressure release with partial mantle fusion on the final arc uplift (Pimentel *et al*., 2004). Recent U-Pb and Sm-Nd data presented by Laux *et al.* (2004)

support the idea that many of the MUM intrusions in the Arenópolis Magmatic Arc are coeval with the ABC. The distribution of the intrusions is shown in Figure 2, the isotopic data are presented in Table 1 and its geochronological timeline on Figure 3.

The 630-600 Ma orogenic MUM intrusions in the Arenópolis Magmatic Arc have similar petrological characteristics (e.g. cumulus phases succession) suggesting that they formed from similar parental magmas. Only two of the intrusions (Córrego Seco and Santa Barbara) have a gabbro-dioritic nature and may represent intrusions crystallized from more evolved parental magmas.

Most intrusions are covered by thick lateritic soil. An aeromagnetic survey conducted by the Goias State, however, has recently identified several magnetic anomalies which may be related to unexposed and yet unknown intrusions (Figure 4).

Table 1. Geochronological and isotopic data of the MUM intrusions probably coeval to ABC.

intrusion	rock association	U-Pb age (Ma)	K-Ar age (Ma)	Sm-Nd isochron age (Ma)	eNd (T)	reference
Americano do Brasil	dunite, wehrlite, lherzolite, websterite, gabbronorite and diorite	631±6 and 626±8 (intrusion); 856±15 (country)	610±50		between +2.1and +2.7 (intrusion); between +2.8 and +4.8 (country)	Laux *et al.*, 2004; Pimentel *et al.*, 2004a; Gioia, 1997
Corrego Seco	gabbro and anorthosite	623±13; 622±6				Laux *et al.*, 2004; Pimentel *et al.* 2004[a]
Mangabal	dunite, wehrlite, websterite, gabbronorite and diorite		612±8			Gioia, 1997
Santa Barbara	gabbro and anorthosite	612±6; 598±8			+2.2; +2.6	Laux *et al.*, 2004
Goianira-Trindade	lherzolite, websterite and gabbronorite	626 ± 2		*ca.* 621		Hollanda *et al.*, 2003
Taquaral	lherzolite, websterite and gabbronorite	621 ± 36				Pimentel *et al.*, 2004a
Agua Claras	lherzolite, websterite and gabbronorite			*ca.* 642		Pimentel *et al.*, 2003
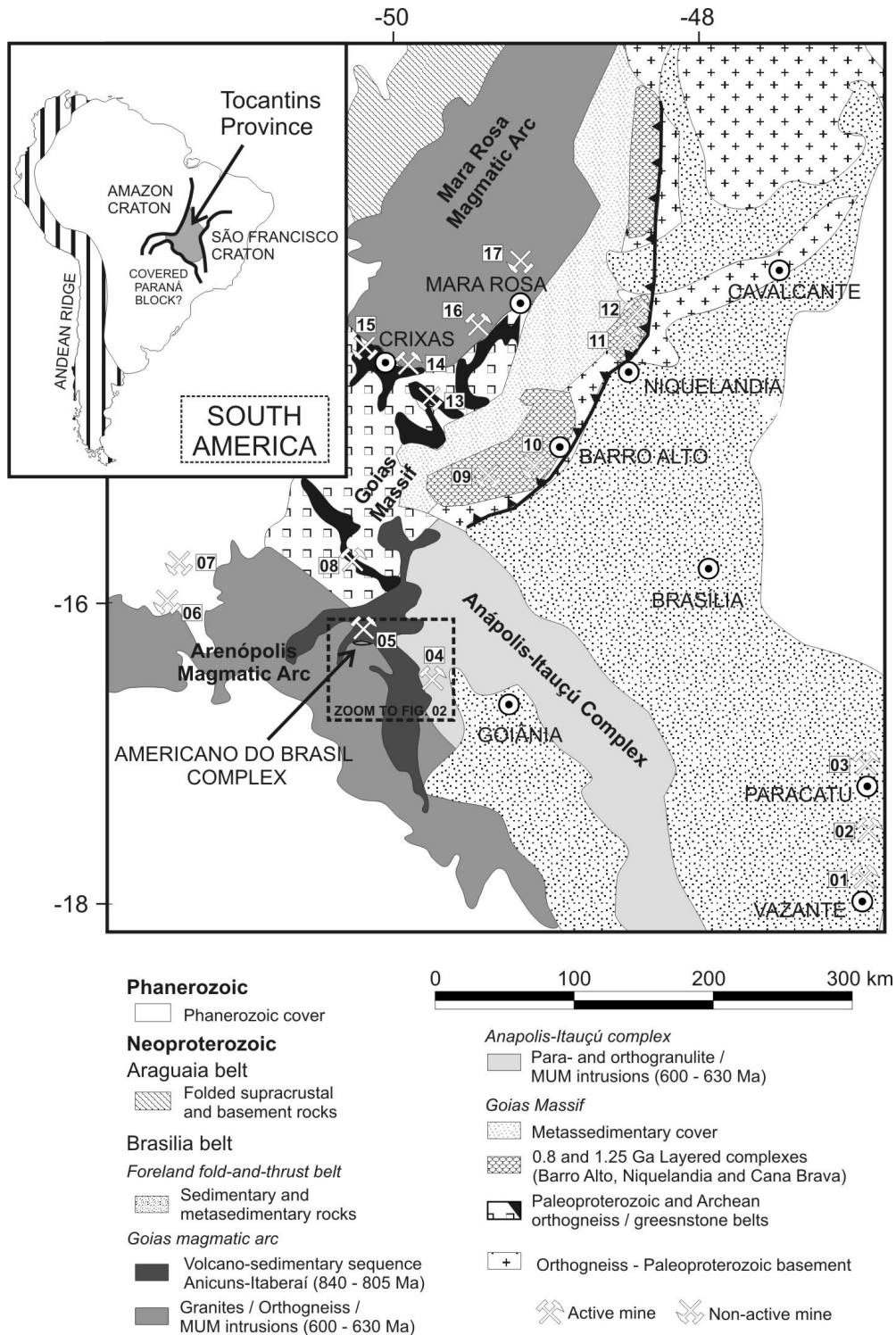
Figure 1 – Geological sketch map of the Brasília Belt, Tocantins Province, Central Brazil (after Fuck, 1994). The mineral deposits are: (1) Zn silicate - Vazante Mine; (2) Zn-Pb sulfide - Morro Agudo Mine; (3) Au - Morro do Ouro Mine; (4) Magmatic Fe-Ti - Titânio de Goiás Mine; (5) Ni-Cu-Co sulfide - Americano do Brasil Mine; (6) Lateritic Ni Montes Claros de Goiás Deposit; (7) Lateritic Ni Santa Fé Deposit; (8) Au - Sertão Mine; (9) Bauxite Deposit - Barro Alto; (10) Lateritic Ni Deposit – Barro Alto; (11) Lateritic Ni - Caron Mine; (12) Lateritic Ni - Codemin Mine; (13) Au - Pilar de Goiás Deposit; (14) Au - Anglo Gold Mine; (15) Ni - Boa Vista Komatiitic Hosted Deposit; (16) Cu-Au - Chapada Mine; (17) Au-Ba - Zacarias Deposit.

18
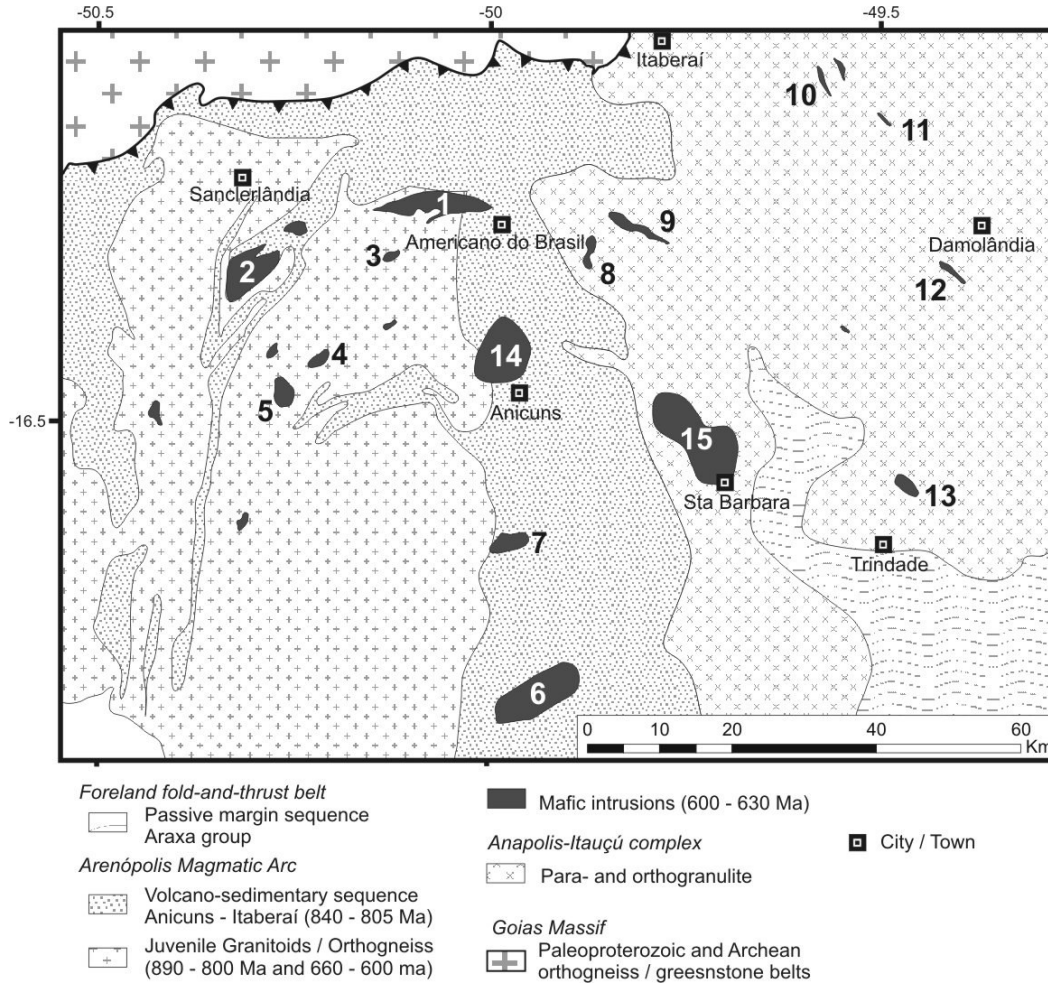
Figure 2 – Simplified geological map showing the orogenic 600 – 630 Ma mafic and mafic-ultramafic (MUM) intrusions (modified from CPRM, 2001). The intrusions 1-7 are MUM intrusions in the Arenópolis Magmatic Arc (1-Americano do Brasil*, 2-Mangabal I and II*, 3-Água Fria, 4-Adelândia, 5-Fronteira Norte, 6-Palmeiras, 7-Mata Rica and Palmito); 8-13 are MUM intrusions in the Anápolis-Itauçú Complex (8-Água Claras*, 9-Capelinha, 10-Taquaral*, 11-Sta Rosa, 12-Damolândia, 13-Goianira-Trindade*); 14-15 are gabbro-dioritic intrusions (14-Córrego Seco*, 15-Santa Bárbara*). The (*) marks the intrusions with geochronological data.
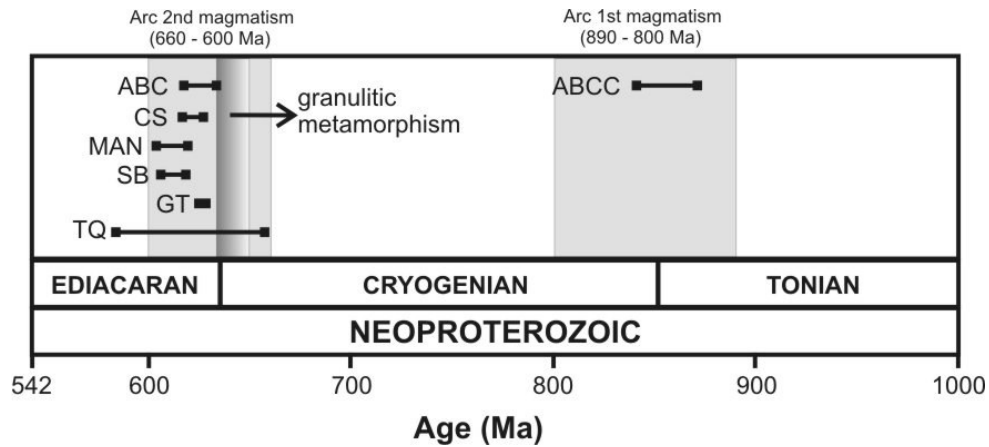
Figure 3 – Schematic geochronological timeline showing the mafic and mafic-ultramafic intrusions ages throughout the Neoproterozoic Brasiliano orogenic cycle in the Goiás Magmatic Arc and Anicúns-Itaberaí metamorphic complex. ABC = Americano do Brasil Complex; CS = Córrego Seco; MAN = Mangabal; SB = Santa Bárbara; GT = Goianira-Trindade; TQ = Taquaral; ABCC = Americano do Brasil Complex country rock.
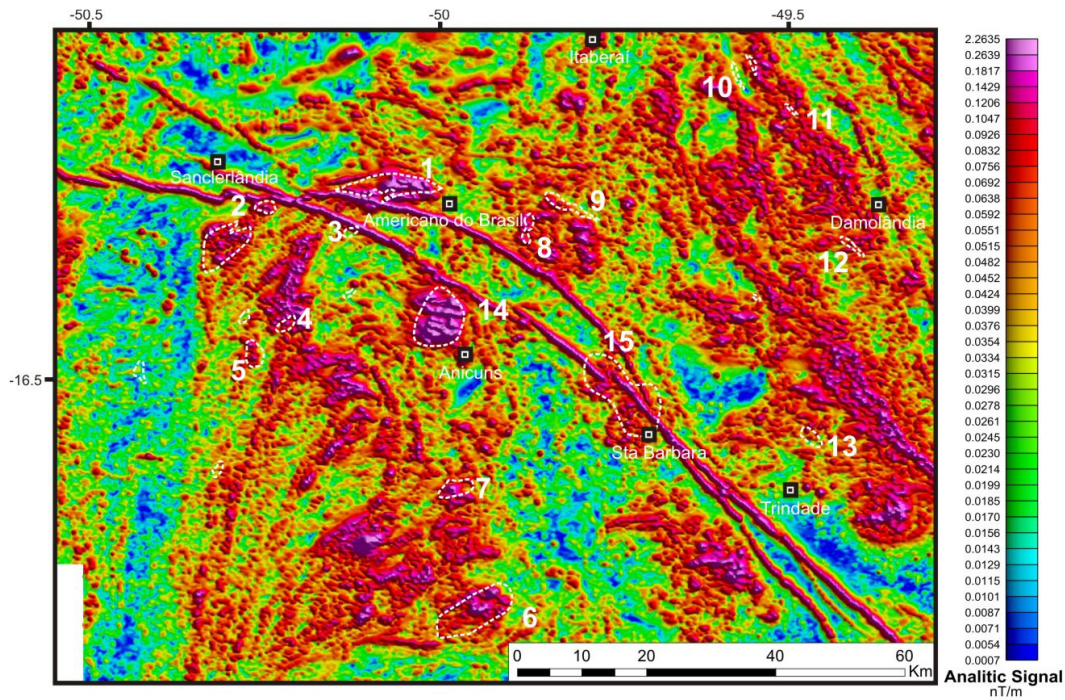
Figure 4 – Analytical signal amplitude (nT/m) image from the aeromagnetic survey delineating the 600-630 Ma mafic and mafic-ultramafic intrusions limits.

Sampling and analytical procedures

Geological mapping identified more than 1,000 outcrops of the ABC and its country rocks, and logging was done on about 25 exploration and mining drill holes.

Based upon former mapping projects of METAGO and new mapping projects of Votorantim Metais Ltd. and Prometalica Ltd., drill hole data, geophysical data (magnetometry, gamaspectometry and eletromagnetometry surveys) and soil geochemistry information, the geological map and profile section of the central part of the ABC were prepared. Along a representative geological profile across the complex, 16 outcrop samples and 60 half-drill core samples from 4 different drill holes were taken. The sample size was selected according to the grain size of the rock, with a minimum of *ca.* 2 kg weight for coarse-grained rocks.

All chemical analysis and samples preparation for major, minor and trace elements and REE was carried out at ALS Chemex, Toronto, Canada.

The major elements of whole rocks were analysed using an inductively coupled plasma atomic emission spectrometer (ICP-AES) on dissolved lithium metaborate fusion disks. The minor, trace and rare earth elements (REE) were analysed by inductively coupled plasma mass spectroscopy (ICP-MS) of dissolved samples, prior fused with lithium metaborate. The concentrations of S in whole rock samples were determined by the LECO induction furnace-titration method. The high-grade Ni or Cu ore samples were analysed by atomic absorption spectroscopy (AAS), including HF-HNO_3-$HClO_4$-HCl digestion. There were also extras Cr and Ca analyses, taken from the Americano do Brasil Mine database. These last analyses were carried out by ALS Chemex, Toronto, Canada using ICP-AES.

The analyses of the six platinum-group elements and Au were carried out by Becquerel Laboratories, Missisauga, Canada using Neutron Activation Analysis (NAA), where a nickel-sulfide fire assay pre-concentration was followed by irradiation and analysis of the sulfide precipitate. There were also used Pt, Pd and Au assays results from the AB mine routine that were carried out by ALS Chemex, Toronto, Canada using fire assay and ICP-AES finish.

For sulfur isotope analysis of pyrrhotite, pentlandite, chalcopyrite and pyrite polished sections of the samples were prepared, and cleaned in an ultrasonic bath. The laser equipment employed was a New Wave UP 213 laser with 213 μm wave length, coupled to a Finnigan-Neptune multi-collector inductively coupled plasma mass spectrometer (LA-MC-ICPMS). The laser was run at 9 Hz frequency and 36 % energy. The laser spot size was 65 μm, run is a raster scheme mode. The He gas flux through the sample chamber was 0.35 l/min . The MC-ICPMS was run in medium resolution, a forward power of 930 W and an Ar gas flux of 0.857 l/min, using the procedures

described in Bender *et al.*, 2007. Analytical precision was better than ± 0.4 ‰ 1 sigma standard deviation. The external reproducibility (accuracy) measured against a second standard was ±0.3 ‰ 1s SD. Sulfur isotope compositions are reported in the δ notation relative to CDT given by S34/S32 = 0.044994 (Ferreira *et al.*, 2007).

The Sm-Nd analyses were carried out at the Universidade of Brasília / Instituto de Geociências, according to the procedures described by Gioia and Pimentel (2000). Circa 40 mg of whole-rock powders were mixed with a 149Sm–150Nd spike solution and dissolved in Savillex capsules. Sm and Nd extraction of whole-rock samples followed conventional cation exchange techniques, using teflon columns containing LN-Spec resin (HDEHP—di-ethylhexil phosphoric acid supported on PTFE powder). Sm and Nd samples were loaded on Re evaporation filaments of double filament assemblies and the isotopic measurements were carried out on a multi-collector Finnigan MAT 262 mass spectrometer in static mode. Uncertainties on 147Sm/144Nd and 143Nd/144Nd ratios are better than ±0.3% (2σ) and ±0.005% (2σ) respectively, based on repeated analyses of international rock standards BHVO-1 and BCR-1. 143Nd/144Nd ratios were normalised to 146Nd/144Nd of 0.7219 and the decay constant (λ) used was $6.54 \times 10{-}12$.

Geology of the Americano do Brasil Complex

The geology of the "Americano do Brasil" complex (ABC) was previously described by Metago (1978) and Nilson *et al.* (1986) who give a comprehensive geological description for the complex and its country rocks. Extensive mapping and drilling data developed by Votorantim-Prometalica for mining or brownfield exploration purposes provided new significant constraints on the geology and stratigraphy of the layered sequence. The ABC consists of a 12 km-long and 3 km-wide EW trending sequence of layered mafic-ultramafic rocks (Figure 5). Even though the limits and continuity of the complex are well established by exploration data, including soil geochemistry and geophysical surveys, outcrops of the layered sequence are mainly restricted to the better exposed central area.

The ABC is limited to south and north by tectonic contacts represented by steep dipping shear zones (Figure 5). Sheared mafic or ultramafic layered rocks form a narrow, less than 200 meters wide and poorly exposed zone along the contact. The ABC

host rocks consist of highly foliated gneiss of granitic composition in the north, and muscovite-biotite mylonitic gneiss in the south. Both of them probably make part of the Arenópolis arc first magmatic event between 890 - 800 Ma, subsequently metamorphosed during the Neoproterozoic Brasiliano orogenic cycle. To the southeastern, the ABC shows tectonic contact with metasedimentary rocks classified as part of the Anicuns-Itaberaí volcano-sedimentary sequence (Nilson, 1981).

Two distinct E-W trending mafic-ultramafic sequences are juxtaposed along the Salgado's fault (Figure 5). The Northern sequence consists of interlayered ultramafic cumulates (dunite, wehrlite, lherzolite and websterite – Figure 5) and minor gabbronorite, and is exposed as steep layers dipping to the south. The Southern sequence is composed of gabbronorite and interlayered ultramafic cumulates (mainly websterite and lherzolite); the layered sequence dips gently to the north. These sequences are separated by the Salgado's fault that is an E-W 15 m thick zone with several brittle structures dipping *ca.* 80º to the north with normal dip-slip kinematic indicators. Another group of subvertical faults trending NW-SE shows dextral strike-slip (or oblique-slip), with tens or hundred of meters displacement of the ore bodies and the layered sequence. The two distinct layered sequences to the north and south of Salgado´s fault are, hereafter, treated as individual stratigraphic sequences.

Northern sequence

Extensive drilling data provided a consistent stratigraphy for the Northern sequence (Figure 6). This sequence has a minimum thickness of 400 meters and may be broadly divided into three major zones, dunite-peridotite, pyroxenite and gabbronorite. Distinctions between these zones are based upon the predominant rock types (Figure 6), without any formal stratigraphic meaning. Based upon facing criteria the steep-dipping Northern sequence is considered to be tectonically inverted. These criteria are provided by structures of the layered rocks and repeated characteristic sequences of cumulates, features that are presented in the following sections. The dunite-peridotite zone is therefore considered to represent the basal zone of the exposed layered sequence, whereas the gabbronorite zone represents the upper part.

The dunite-peridotite zone consists mainly of interlayered dunite and peridotite. These rock types are heterogeneously distributed through this zone, but dunite predominates toward the exposed base of the layered sequence. Dunite is a

medium-grained mesocumulate rock composed of cumulus olivine and chromite (Figure 7c) with minor intercumulus orthopyroxene, clinopyroxene, amphibole and plagioclase. Peridotites are compositionally variable coarse-grained meso- to orthocumulate rocks, including wehrlite and lherzolite. These lithotypes contain varying amounts of interstitial amphibole (up to 60 vol. % - Figure 7a,b), plagioclase (up to 10 vol. %) and phlogopite (up to 5 vol. %). Peridotites include rocks with cumulus olivine and chromite enclosed into large oikocrysts of clinopyroxene, orthopyroxene and/or amphibole, as well as minor interstitial plagioclase in few samples. They also include rocks with cumulus olivine and orthopyroxene (± chromite) enclosed into large oikocrysts of amphibole, clinopyroxene and, less commonly, plagioclase. The dunite-peridotite zone hosts the S2 orebody, a layer of massive to semi-massive sulfide concordant with the host rocks. Olivine crystals are partially serpentinized in dunite and peridotite. Serpentinization is heterogeneous, and both slightly and highly altered dunite (more than 90 vol. % of olivine replaced by serpentine and magnetite) may occur.

The pyroxenite zone consists of medium- to coarse-grained websterite and minor interlayered peridotites. The lower contact with the dunite-peridotite zone is gradational and defined by the predominance of pyroxenite over peridotite. Websterite is mainly composed of cumulus orthopyroxene and clinopyroxene with variable amounts of interstitial amphibole (up to 60 vol. %), plagioclase (up to 20 vol. %) and phlogopite (up to 10 vol. %). Samples with cumulus orthopyroxene and interstitial clinopyroxene, amphibole, plagioclase and phlogopite indicate that orthopyroxene is the first pyroxene to crystallize in the Northern sequence. Websterite textures vary from mesocumulate to orthocumulate, the latter consisting of large amphibole oikocrysts enclosing several pyroxene crystals (Figure 7).

The gabbronorite zone is only exposed in drill holes extending below the S2 orebody (Figure 5). The lateral continuity of the gabbronorite zone is controlled by extensive drilling extending below the S2 orebody, but its continuity away from the ore zone is largely unconstrained. Gradational change from websterite with interstitial plagioclase (orthopyroxene + clinopyroxene cumulate) to gabbronorite (orthopyroxene + clinopyroxene + plagioclase cumulate) characterizes the transition from the lower pyroxenite zone to the upper gabbronorite zone. Even though the drilled section of the gabbronorite zone is less than 30 meters thick, this zone shows a systematic transition from gabbronorite at the base to ilmenite-magnetite-bearing gabbronorite (orthopyroxene + clinopyroxene + plagioclase + magnetite + ilmenite cumulate) at the

top. Typical gabbronorite is a medium-grained mesocumulate rock, consisting of cumulus orthopyroxene, clinopyroxene and plagioclase, together with variable amounts of interstitial amphibole and phlogopite (Figure 7). Ilmenite-magnetite-bearing gabbronorite has 3-5 vol. % of cumulus ilmenite and magnetite.

The Northern sequence is locally disturbed by irregular cross cutting bodies of hornblende diorite (Figure 7g). These bodies are more abundant in the Southern sequence, which is described in the following section. A sheared contact with the granitic gneiss is exposed on the northern part of this sequence. This shear structure dips between 45° and 80° to south and also affects the ABC rocks, overprinting the igneous textures with a tectonic/metamorphic foliation on the pegmatoid diorite and pyroxenite rocks.

Southern sequence

The stratigraphy of the Southern sequence is exposed in layers with gently dip to the north (Figure 5). The sequence has a minimum thickness of about 600 meters and is divided into a lower pyroxenite-peridotite zone and an upper gabbronorite-pyroxenite zone (Figure 6). The stratigraphy is well constrained by extensive drilling in the area close to the Salgado's Fault, along the stratigraphic interval of the S1 orebody, and close to the southern contact, along the stratigraphic interval of the G2 orebody. The stratigraphy of the Southern sequence is frequently disturbed by cross cutting bodies of hornblende diorite, especially in the central zone and in the southern contact with the country rocks. It is also disrupted by large bodies of gneiss, interpreted as fragments of country rocks. Despite significant differences in the stratigraphic sequences, the rock types and characteristic sequence of cumulates of the Southern sequence are very similar to what was described for the Northern sequence.

The pyroxenite-peridotite zone consists mainly of medium- to coarse-grained websterite and interlayered peridotites. Websterite, the dominant rock type, is composed of cumulus orthopyroxene and clinopyroxene with variable amounts of interstitial amphibole (up to 60 vol. %), plagioclase (up to 20 vol. %) and phlogopite (up to 10 vol. %). The texture varies from mesocumulate to orthocumulate, the latter consisting of large amphibole oikocrysts enclosing several pyroxene crystals. Peridotites occur mainly in the southernmost area. In the Southern sequence the peridotites are identical to similar lithotypes described for the Northern sequence. Coarse-grained textures

consisting of large oikocrysts of amphibole (up to 60 vol. %) or pyroxenes predominate. The upper contact with the pyroxenite-gabbronorite zone is gradational and is defined by the appearance of abundant gabbronorite.

The gabbronorite-pyroxenite zone consists mainly of interlayered gabbronorite and websterite. The gradational transition from websterite (orthopyroxene + clinopyroxene cumulate) to gabbronorite (orthopyroxene + clinopyroxene + plagioclase cumulate) is usually marked by an intermediate facies containing interstitial plagioclase (plagioclase-bearing websterite and/or mela-gabbronorite). Typical gabbronorite is a medium-grained mesocumulate rock, consisting of cumulus orthopyroxene, clinopyroxene and plagioclase, together with variable amounts of interstitial amphibole and phlogopite. Ilmenite-magnetite-bearing gabbronorite has 3-5 vol. % of cumulus ilmenite and magnetite. Norite (orthopyroxene + plagioclase cumulate with intercumulus amphibole and phlogopite) and ilmenite-magnetite bearing gabbronorite with accessory quartz and apatite, occur locally in the gabbronorite-pyroxenite zone.

Cross-cutting bodies of hornblende diorite consist mainly coarse-grained, pegmatoidal or vari-textured rocks (Figure 7g). They consist mainly of hornblende, orthopyroxene, clinopyroxene and plagioclase. Orthopyroxene and clinopyroxene are frequently partially to extensively replaced by green hornblende, and varieties consisting mainly of hornblende and plagioclase are frequent. These irregular cross-cutting bodies range from few centimeters up to hundreds of meters wide.

Irregular and heterogeneous bodies of gneiss, interpreted as fragments of country rocks, occur within the upper gabbronorite-pyroxenite zone, adjacent to the Salgado's fault in the central part of ABC. They consist mainly of pyrite-magnetite-biotite gneiss, with tonalitic composition, that has homogeneous metamorphic foliation and blue quartz (Figure 7h). This unit has its primary mineralogy partly overprinted by hydrothermal alteration, marked by a secondary mineral assemblage formed by magnetite, pyrite (up to 2 vol. %), chlorite, epidote, pyrophyllite and sericite. This alteration is stronger in some particular clusters, but is registred in all gneiss occurrences as pervasive alteration.

A sheared contact with the biotite-muscovite mylonitic gneiss is exposed on the southern part of this sequence. This shear structure dips ~ 80º to north and also affects the ABC rocks, overprinting the igneous textures with a tectonic/metamorphic foliation on the pegmatoid diorite, pyroxenite and peridotite rocks.
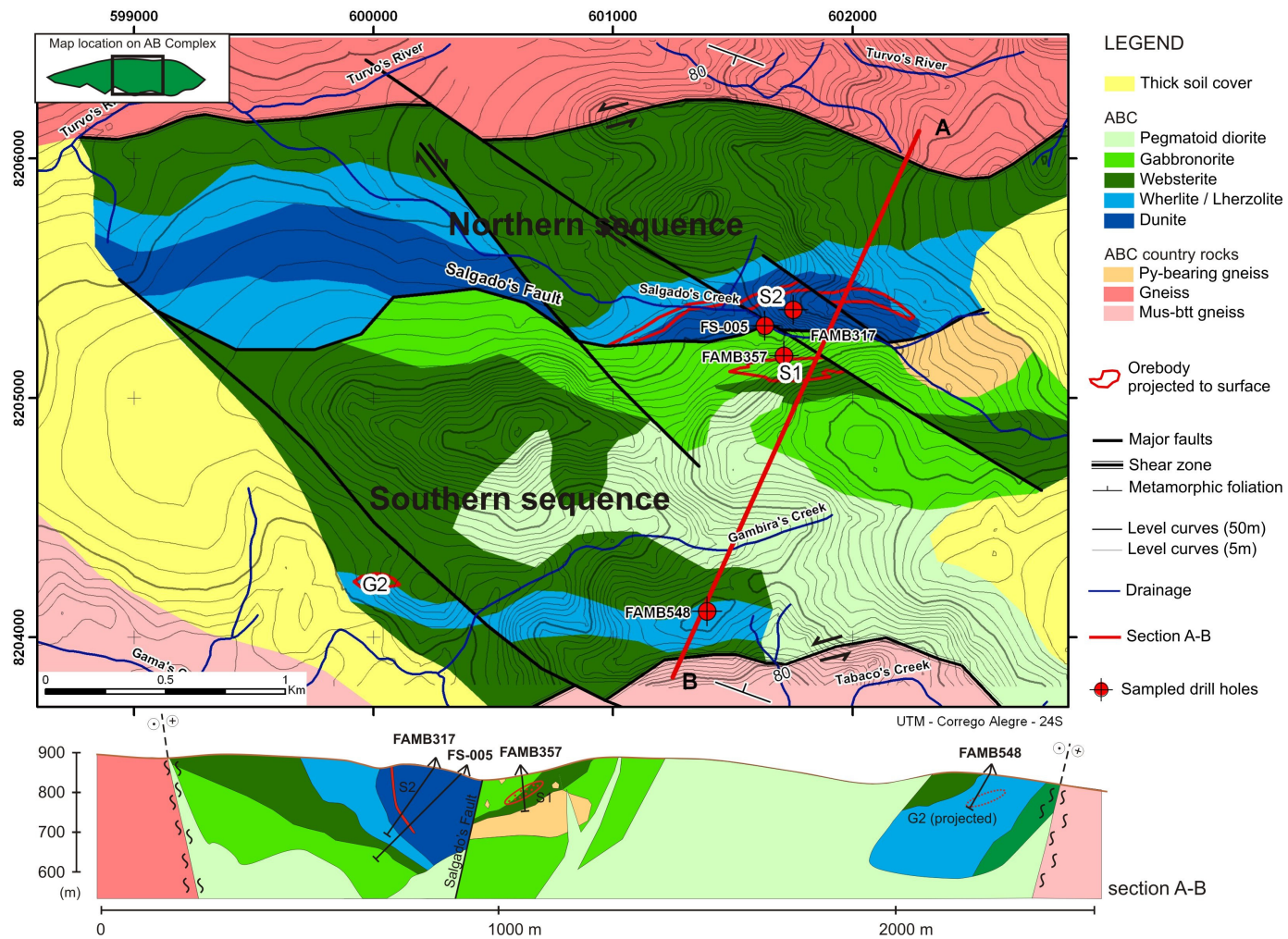
Figure 5 – Geological map and section on central part of the ABC.

"Americano do Brasil" Complex stratigraphic column
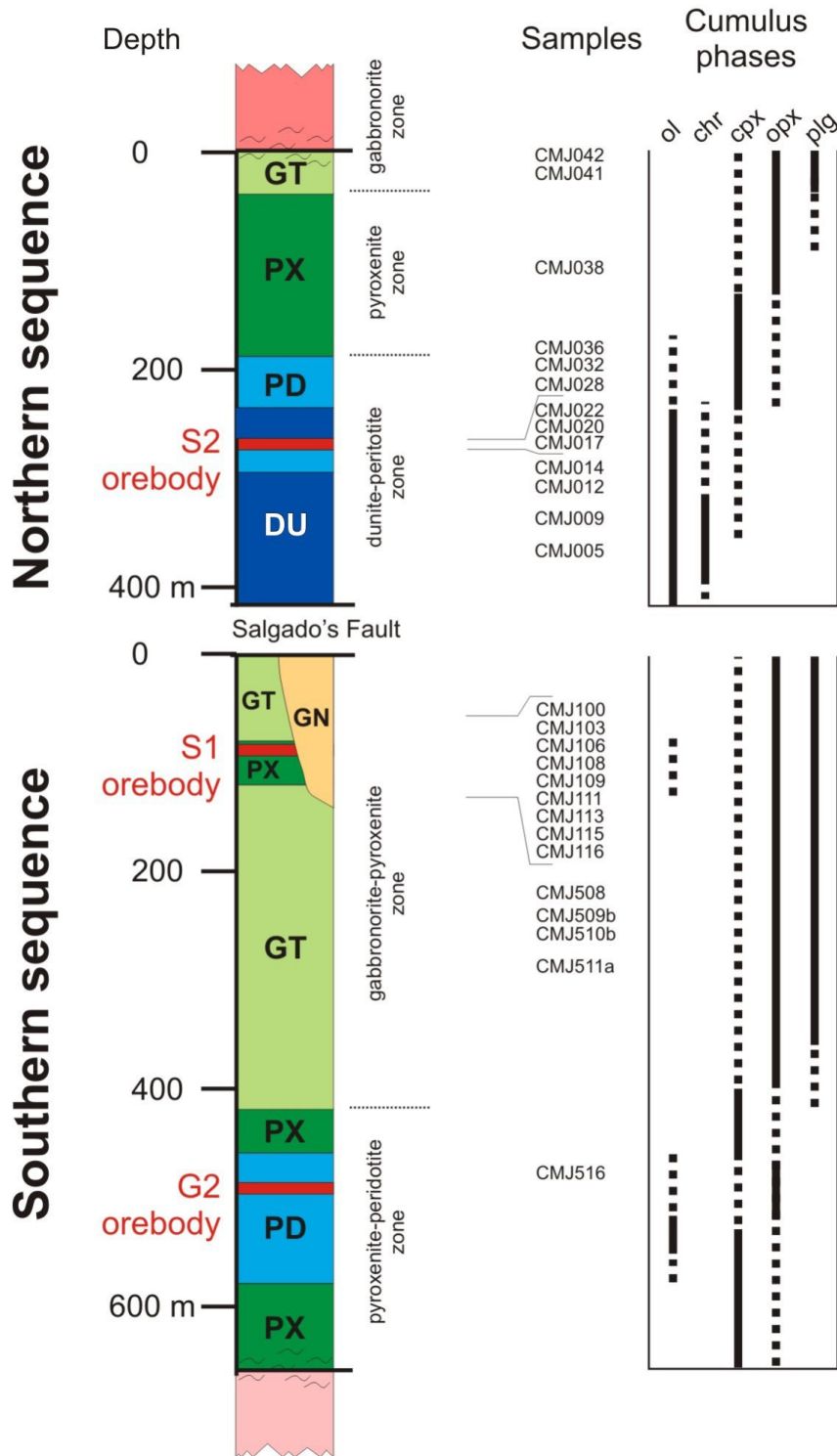
Figure 6 –Schematic stratigraphic column for the central part of the ABC. DU = dunite; PD = peridotite (wehrlite and lherzolite); PX = pyroxenite (websterite); GT = gabbronorite; GN = pyrite-bearing gneiss, ol = olivine, chr = chromite, cpx = clinopyroxene, opx = orthopyroxene and plg = plagioclase.
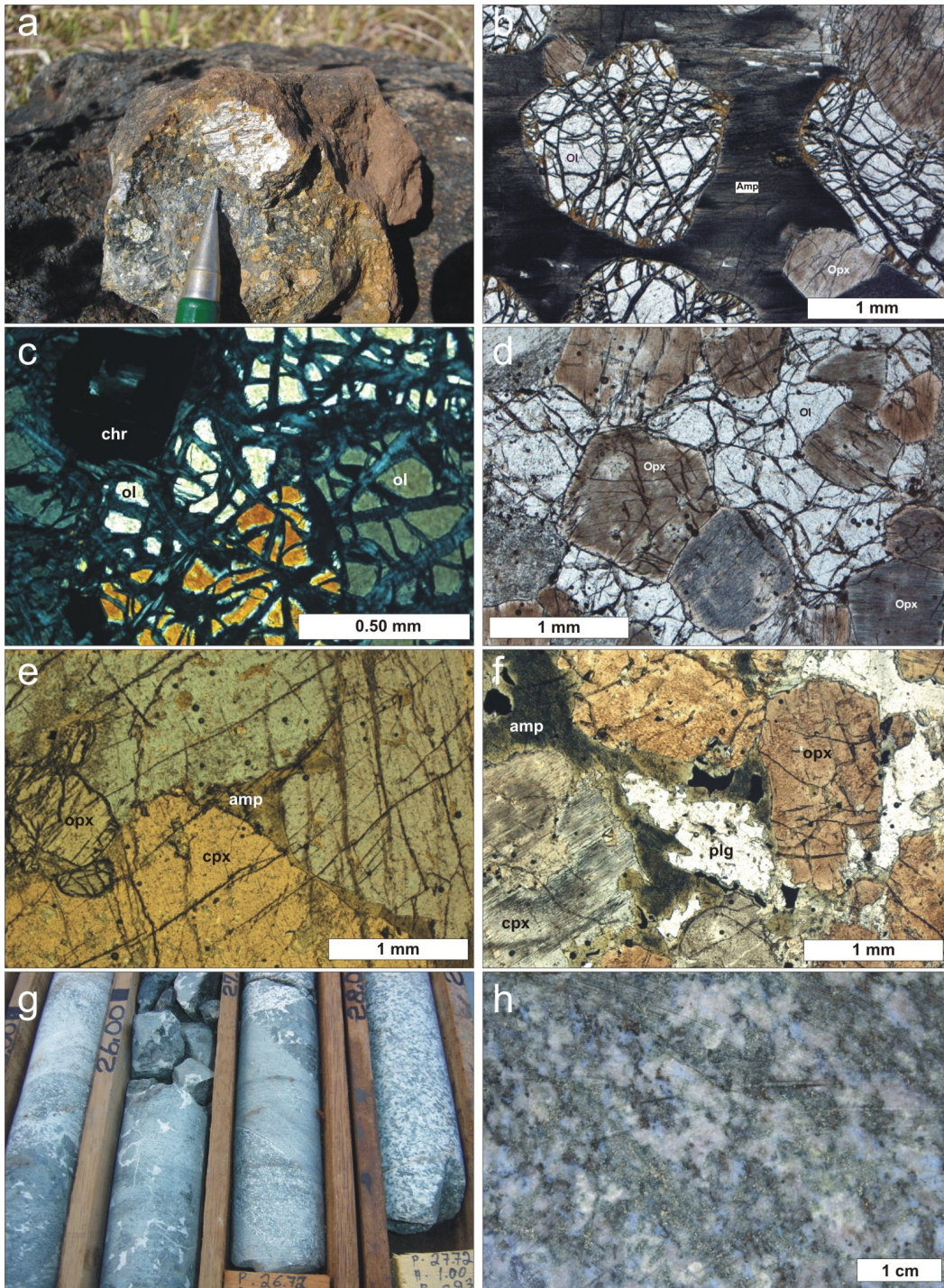
Figure 7 – a) Grab sample from outcrop showing amphibole oikocryst with orthopyroxene inclusions in websterite; b) Amphibole oikocryst with olivine and orthopyroxene inclusions (plane polarized light); c) Adcumulus olivine and chromite from dunite of the Northern sequence (cross polarized light); d) Adcumulus olivine and orthopyroxene from the Northern sequence lherzolite (plane polarized light); e) Intercumulus amphibole in websterite from the Northern sequence (plane polarized light); f) Typical gabbronorite with intercumulus plagioclase and amphibole (plane polarized light); g) Drill cores showing the vary-textured diorite that crosscut the complex units; h) The country rock gneiss, exposed on the topmost part of Southern sequence, with typical blue quartz and chlorite, sericite, epidote, pyrophyllite and pyrite as hydrothermal alteration assemblage. Mineral abbreviations: (amp) amphibole, (chr) chromite, (ol) olivine, (opx) orthopyroxene, (cpx) clinopyroxene and (plg) plagioclase.

29

Orebodies

The ABC orebodies were first described by Metago (1978) and Nilson *et al.* (1986). Measured reserves for the different orebodies indicated by Metago (ca 5.0Mt@0.62%Ni and 0.65%Cu) were recently re-evaluated by Prometalica-Votorantim at 3.1 Mt @ 1.12 %Ni and 1.02 %Cu (Table 2). The orebodies envelopes and their field relationships with their enclosing rocks were better defined by detailed drilling, underground mining and 3-D modeling developed for mining production. Three distinctively different orebodies (S1, S2 and G2) are currently in exploitation (Table 2). Underground mining uses the "sub-level" method for the S2 orebody hosted in the Northern sequence, and the "pillars and chambers" method for S1 and G2 orebodies hosted in the Southern sequence.

The S2 orebody is a steep-dipping EW trending tabular body extending for 1.2 km along strike and 250 meters deep. It was previously considered to be an orebody discordant with the layered sequence (Nilson *et al.*, 1986). However, detailed drilling and underground exposures unveiled a thin (0.5 to 4.0 meter-thick) layer of mainly massive sulfides concordant with the host rocks (Figures 8 and 9). Host rocks are partially serpentinized dunite (olivine + chromite cumulate) and wehrlite (olivine + chromite cumulate with interstitial cpx and amphibole). A typical section through the orebody shows a sharp contact of massive sulfides (> 75 vol. % sulfides) and dunite-wehrlite in the hanging wall, and a gradational contact from massive sulfide, to net-textured sulfide and barren dunite-wehrlite in the footwall (Figure 10). This asymmetric distribution of sulfides, also described in several nickel sulfide orebodies, provides facing criteria (the billiard ball of Naldrett, 1973). For the S2 orebody this criteria indicates an inverted stratigraphy, corroborating facing criteria provided by the hosting layered sequence. Net-textured ore consists mainly of olivine crystals and minor cpx, amphibole and chromite enclosed in sulfides. Olivine crystals enclosed in massive sulfides have rounded faces and rare embayed sulfides. The S2 orebody has high Ni and Cu contents, as well as the highest Ni/Cu ratio among the ABC orebodies (Table 2). The orebody has particular chalcopyrite-rich (or Cu-Pt-Pd-rich) portions, which usually occur as thin veins (usually between 0.5 and 5 centimeters-thick), sometimes crosscutting the pyrrhotite-pentlandite-rich ore, as well as small (usually between 5-20 centimeters-thick) irregular zones between the latter and barren rocks.
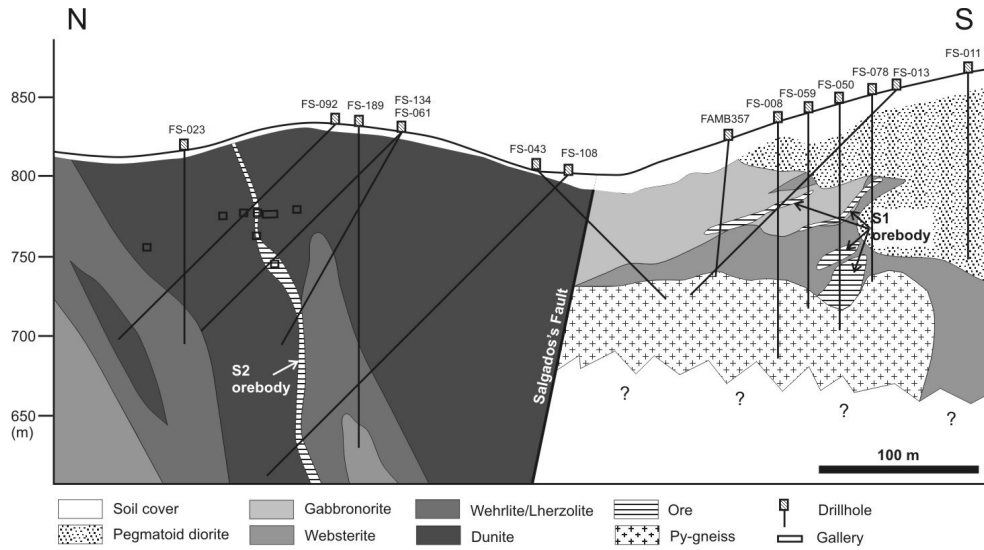
Figure 8 - Representative cross section of the S2 and S1 ore bodies.
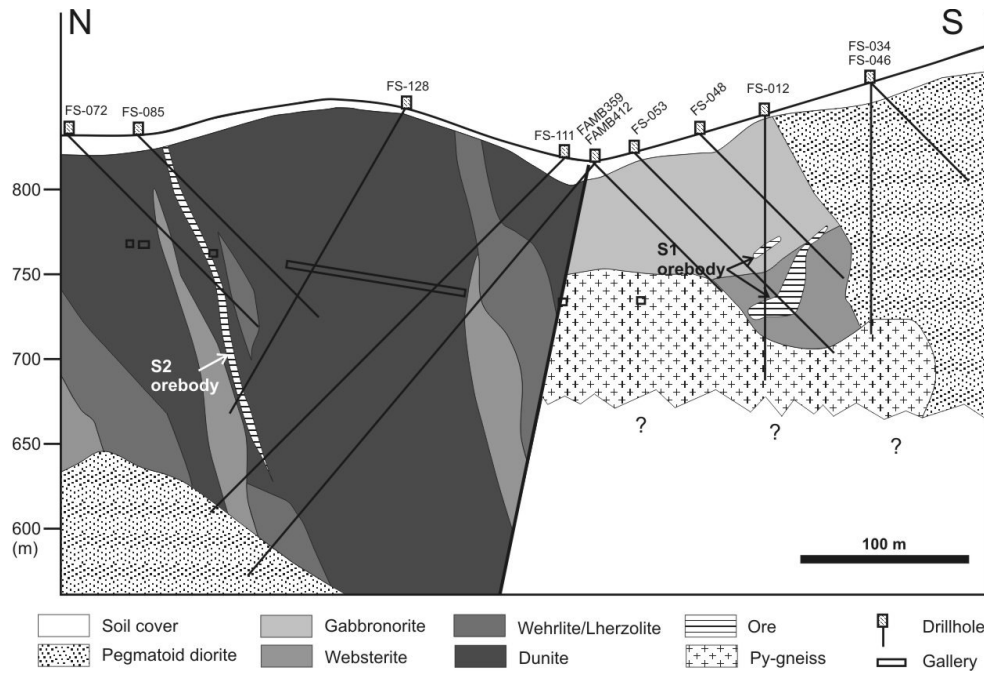
Figure 9 - Representative cross section of the S2 and S1 orebodies.

Table 2. Measured resources and grades of ABC orebodies (Votorantim Metais, 2007). Mineral abbreviations: (po) pyrrhotite, (py) pyrite, (cpy) chalcopyrite and (pn) pentlandite.

orebody	Mass (Mt)	Ni (wt.%)	Cu (wt.%)	Co (ppm)	Ni/Cu	host rock	ore type	sulfide minerals
S1	1.94	0.55	0.69	392	0.80	Websterite, gabbronorite	Disseminated and minor massive	po>py>cpy>pn
S2	0.82	2.60	1.83	1392	1.42	Dunite, wehrlite	Massive and minor net-textured	po>pn>cpy
G2	0.32	0.83	0.96	427	0.86	Lherzolite, websterite	Net-textured and minor massive	po>cpy>pn
TOTAL	3.09	1.12	1.02	662	1.10			

The S1 orebody is the largest Ni-Cu sulfide body in the ABC, but has the lowest Ni and Cu contents of 0.55 and 0.69 wt.% respectively, as well as Ni/Cu ratio of 0.8 (Table 2). This orebody is concordant with the Southern sequence layering; following the EW strike and dipping gently to the north. The S1 orebody consist of a cluster of several irregular discontinuous small ore bodies (Figures 8 and 9). This cluster has an irregular and roughly cylindrical shape, about 50 to 100 meters in diameter and extending for 500 meters along strike. Host rocks are mainly gabbronorite and coarse-grained plagioclase-amphibole bearing websterite, the latter characterized by several cumulus opx and cpx crystals enclosed into large amphibole oikocrysts (Figure 7). Rare olivine-bearing websterites are just distinct from typical websterites by the presence of few olivine crystals, usually largely replaced by opx. Sulfide contents and textures are homogeneous through the S1 orebody, and contacts with barren host rocks are gradational and diffuse. These contacts are characterized by progressively lesser amounts of sulfides toward the host rocks, lacking any significant change in the mafic or ultramafic rocks. At the bottom and at the eastern end, the orebody is limited by xenoliths of pyrite-bearing gneiss (Figures 8 and 9). The orebody becomes distinctively enriched in sulfides towards the pyrite-bearing gneiss. The texture of sulfides is homogeneous, with dominant coarse-grained disseminated sulfides (5-15 vol. % - Figure 10) and eventually some more massive portions. Sulfides are interstitial to cumulus silicates, mainly opx and cpx with rare olivine, and intermixed with intercumulus minerals, mainly amphibole and plagioclase (Figure 11a,b,c,d).
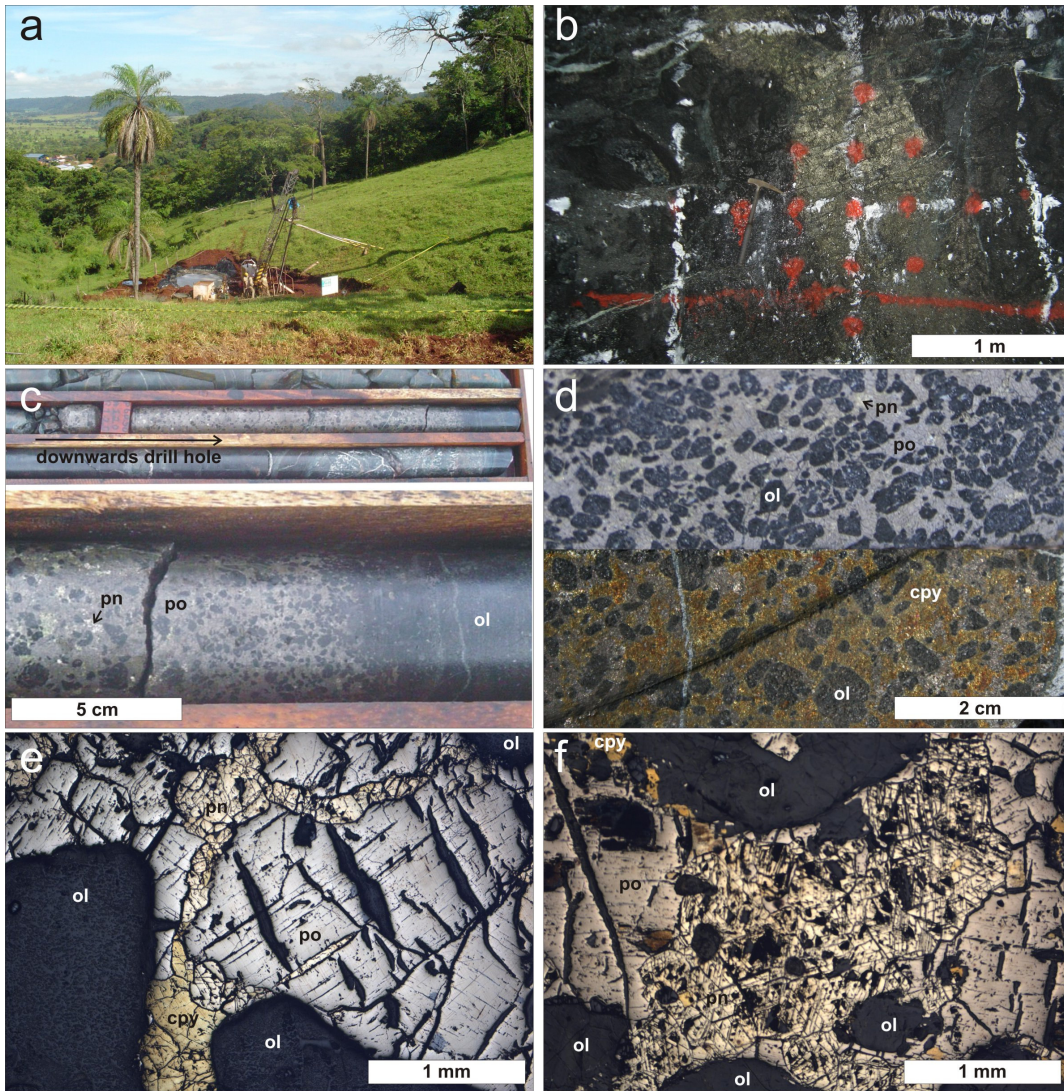
Figure 10 – a) Drilling site through the S2 orebody with ABC and the country rocks hill on landscape; b) The massive sulfide reef type ore of the S2 orebody in the underground mine; c) Typical S2 orebody intersection in drill cores, with a detail of the gradational transition from massive to disseminated sulfide to barren dunite on the footwall of S2; d) Detail of the typical S2 orebody texture, comparing the pyrrhotite- and chalcopyrite-rich portions; e) S2 sulfides in typical intercumulus texture around serpentinized olivine grains (reflected light); f) Typical coarse grain (*ca.* 4 mm) of pentlandite in S2 orebody (reflected light). Mineral abbreviations: (pn) pentlandite, (po) pyrrhotite, (cpy) chalcopyrite and (ol) olivine.
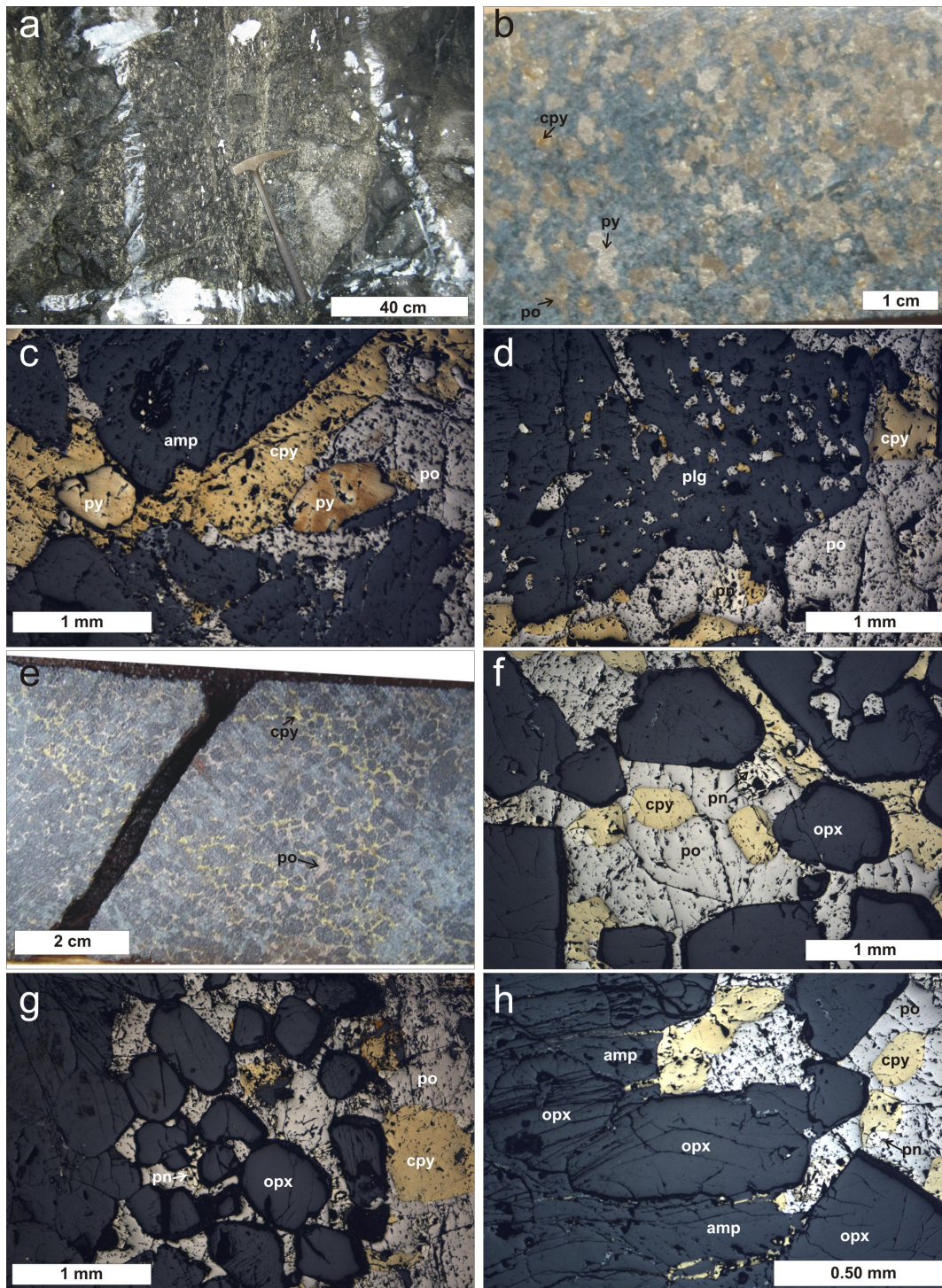
Figure 11 – a) Homogeneous disseminated sulfide of the S1 orebody in underground mine; b) Detail of the S1 orebody disseminated sulfide texture, showing large (*ca.* 4 mm) pyrite grains; c) Rounded grains of pyrite surrounded by pyrrhotite and chalcopyrite in the S1 orebody (reflected light); d) Silicates and sulfides displaying anhedral shapes in the S1 orebody (reflected light); e) Typical G2 net-textured ore in drill core; f) Intercumulus sulfide mass in the G2 orebody showing MSS composition between euhedral cumulus orthopyroxenes grains (reflected light); g) Sulfide mass in contact with orthopyroxene grains, more massive on the left hand side and grading to barren towards the right side (reflected light); h) Sulfide mass in contact with silicate minerals, showing sulfide small veinlets towards the amphibole grain (reflected light). Mineral abbreviations are the same as in Figures 7 and 10.

34

The G2 orebody is a very small and yet poorly investigated body, thus providing better perspectives for increasing resources during brown field exploration. Compared to the S1 and S2 orebodies, G2 has intermediate Ni and Cu contents of 0.83 and 0.96 wt.% respectively, as well as moderate Ni/Cu ratio of 0.86 (Table 2). Similar to the S1 orebody, G2 is concordant with the Southern sequence layering, following the EW strike and dipping gently to the north. The G2 orebody also has an irregular and roughly cylindrical shape, about 20 to 70 meters in diameter and extending for 200 meters along strike (Figure 12). At the bottom of the G2 orebody, a thin (<2 meters-thick) chalcopyrite-rich (or Cu-Pt-Pd-rich) sulfides layer occurs (Figure 12). This Cu-Pt-Pd-rich zone is restricted to the larger eastern zone of the deposit. Host rocks are mainly coarse-grained websterite and lherzolite, both lithotypes characterized by orthocumulate textures and large amphibole oikocrysts (Figure 11e,f,g,h).

Frequently, the orthopyroxene cumulus phase shows preserved olivine nuclei. This relation is probably a result of olivine crystals that has accumulated rapidly, possibly having nucleated close to the floor of the magma chamber. This olivine was then transformed to form orthopyroxene, mainly after accumulation, through reaction with intercumulus liquid, a process similar to the one observed by Boyd and Mathiesen (1979) in the Rana mafic intrusion, in Norway.

Net-textured sulfides (about 20-30 vol. %) predominate in the G2 orebody, with minor disseminated and massive sulfides. The latter predominates in the lower zone of the body, with an irregular gradation to net-textured and disseminated sulfides toward the upper zones.
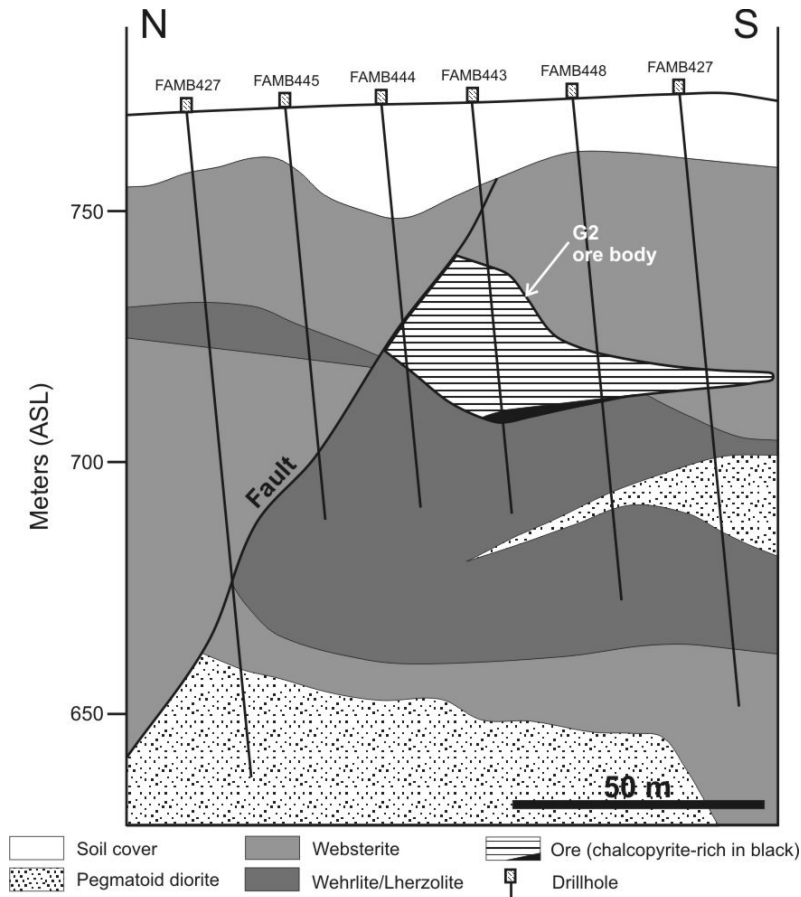
Figure 12 - Representative cross section of the G2 orebody.

The three orebodies show magmatic textures typical of sulfide liquid segregated from mafic-ultramafic magmas. They do not seem to be located in feeder zones or at the base of the intrusion, but rather placed in different stratigraphic horizons of the layered sequence. Significant differences in host rocks and metal contents between these three orebodies seem to be linked to processes occurring within the magma chamber, a subject to be addressed in the following discussions.

Petrography and Mineralogy of Sulfides

Systematic descriptions and compositions obtained by electron microprobe (EMP) of sulfide minerals from Ni-Cu ore bodies of the ABC are provided by Nilson (1981). The author emphasizes the primary magmatic origin of the sulfide assemblage, consisting mainly of pyrrhotite, chalcopyrite and pentlandite, as well as extensive lower temperature re-equilibrations. The mineralogy and textures of sulfides are typical of magmatic sulfides segregated as immiscible sulfide liquids from mafic-ultramafic magmas (Naldrett, 2004). The following description mainly deals with sulfides showing

primary magmatic textures, focusing in the distinct compositions between different orebodies and/or stratigraphic intervals.

Sulfides are not restricted to individual orebodies, but occur frequently as small droplets or minor interstitial masses throughout the complex stratigraphy. These droplets are up to 1 mm in size, and are encoutered more frequently in the ultramafic units in the lower parts of the Northern sequence. They show typical MSS (monosulfide solid solution, for a review see Naldrett, 2004) mineralogy with pyrrhotite dominating over pentlandite and chalcopyrite. However, the gabbroid rocks from the Southern and Northern sequences contain pyrite which is locally predominant relative to the other sulfides. A secondary assemblage formed by pyrite, pentlandite and ribbons of magnetite occurs on droplets surrounded by the strongly serpentinized dunites and peridotites of Northern sequence.

The S2 orebody consists mainly of pyrrhotite with associated pentlandite and chalcopyrite. Pentlandite dominates over chalcopyrite, occurring in coarse grains (usually between 0.5 and 5 mm, but up to 1 cm in diameter) and also as exsolutions consisting of ribbons and flames in pyrrhotite (Figure 10). Chalcopyrite is minor, except for chalcopyrite-rich portions where it is the dominant sulfide.

The S1 orebody consists mainly of pyrrhotite with associated pentlandite, chalcopyrite and pyrite. Chalcopyrite predominates over pentlandite while pyrite is unevenly distributed, from absent to the dominant sulfide. Pyrite occurs in medium- to coarse-grained crystals (up to 1 cm), usually in rounded grains, eventually embayed with finer aggregates of pyrrhotite-chalcopyrite-pentlandite. Moreover, frequently the sulfide and silicate phases show both rounded anhedral shapes, suggesting cristallyzation during the interaction between sulfide and silicate liquids interaction, with no cumulus phases present (Figure 11).

The G2 orebody consists mainly of pyrrhotite with associated medium- to coarse-grained pentlandite and chalcopyrite. Chalcopyrite predominates over pentlandite, occurring both associated with the dominant pyrrhotite-rich zones and in chalcopyrite-rich portions. The latter are commonly concentrated at the bottom of the orebody in massive to net-texture sulfides. This chalcopyrite-rich zone also forms small veins crosscuting the pyrrhotite-rich ore (usually between 0.5 and 3 centimeters-thick), moreover at microscopic scale this portion shows small veinlets surrounding and included in amphibole grains (Figure 11).

Whole Rock Geochemistry

Major elements

Whole-rock chemical compositions of the ABC samples are given in Tables 3 and 4. In sulfide-poor samples, variable amounts of loss-on-ignition (LOI) reflect not only variable amounts of replacing minerals, like serpentine and talc in peridotites, but also the presence of primary amphibole oikocrysts. Hence the presented data is not recalculated to anhydrous 100% compositions. Whenever necessary, compositional varations related to different amounts of altered silicates, which impact primary magmatic features, are indicated and commented. Except for the ore samples, which are treated separately, all samples are S-poor (S < 0.5 wt.%). In these samples the amount of sulfides do not impact the Mg# and the interpretations. This assumption was also verified by simulations with the monosulfide calculation method of Naldrett and Duke (1980).

The Figure 13 illustrates the variations of selected major elements oxides through the ABC. The oxides and elements are plotted against the Mg# = $MgO/(MgO+Fe_2O_3t)$, an index for fractionation in layered intrusions. In general, the Northern sequence exhibits much more distinct and continuous geochemical trends than the Southern sequence. The Northern sequence is characterized by a wide range of MgO concentrations (Figure 13a) from 37.7 wt.% on serpentinized chromite-bearing dunite to 14.2 wt.% on amphibole gabbronorite. On the other hand, the Southern sequence displays a narrower range from 26.3 wt.% in talc-serpentine lherzolite to 11.7 wt.% on amphibole gabbronorite. The contents of MgO and Cr_2O_3 (Figure 13e) fall with decreasing Mg# towards the gabbronorite in both sequences. This tendency is expected on mafic layered intrusion fractionation due to the fractionation of the cumulus phases olivine, chromite and clino- and orthopyroxene.

The oxides Al_2O_3 (Figure 13b), alkalis ($Na_2O + K_2O$ – Figure 12d) and TiO_2 (Figure 13f) display an increase along fractionation. Aluminium and alkalis are concentrated in plagioclase, while Ti forms part of the magnetite structure. The CaO (Figure 13c), however, shows an inverted "U-shape", essentially because of two factors: (i) the plagioclase compositions change from Ca-rich to Ca-poor with fractionation; and

(ii) the orthopyroxene (Ca-poor) dominates over clinopyroxene (Ca-rich) on advanced stages of the ABC fractionation.
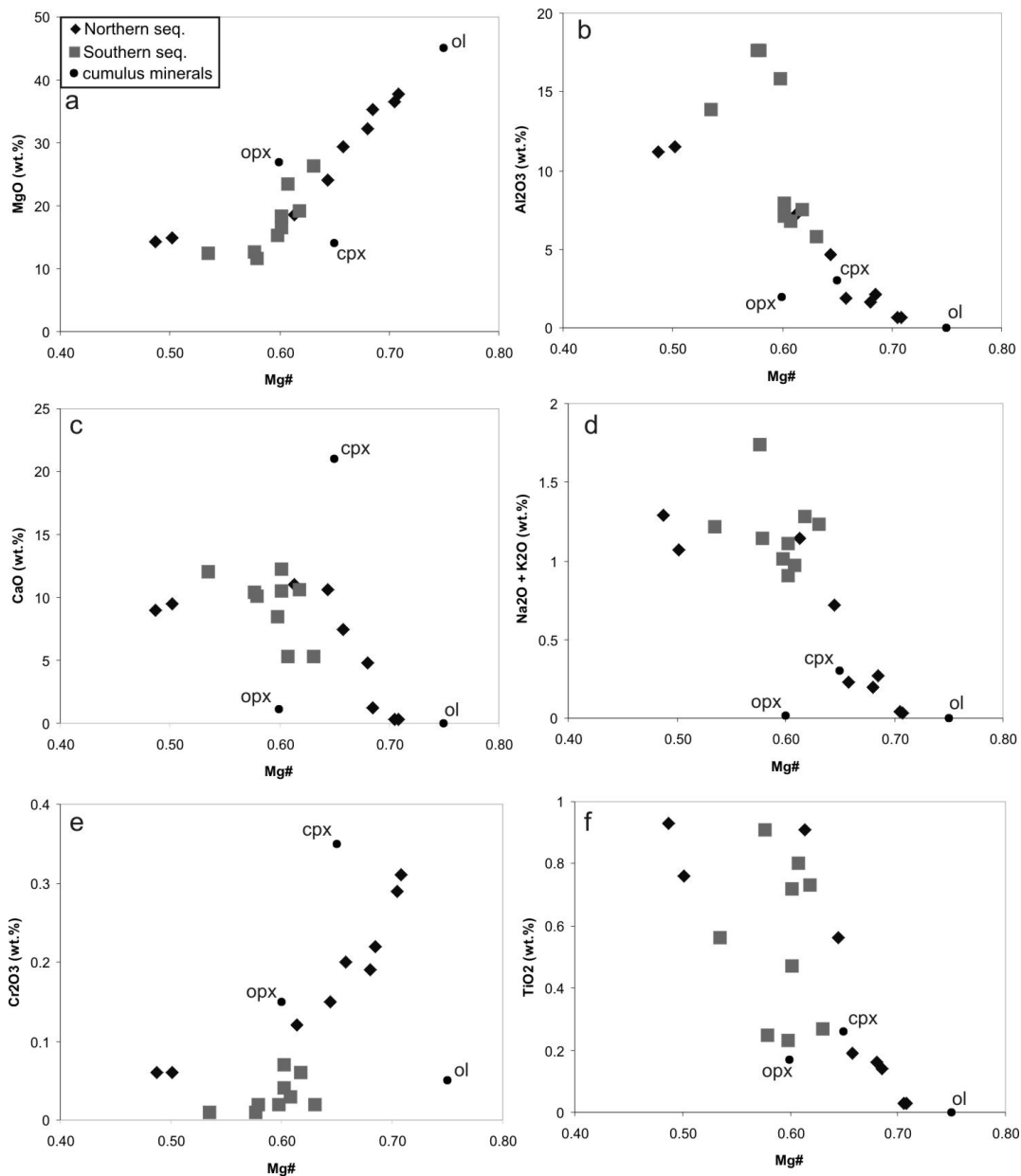
Figure 13 - Variations of MgO (a), Al_2O_3 (b), CaO (c), $Na_2O + K_2O$ (d), Cr_2O_3 (e), and TiO_2 (f) with Mg# for the Northern and Southern sequences from the ABC. The composition of the plotted cumulus minerals were calculated using the mean of the several microprobe analyses of Nilson, 1981. Mineral abbreviations: (ol) olivine, (cpx) clinopyroxene and (opx) orthopyroxene.

The trends are generally comparable or overlapping for the Southern and the Northern sequence, but the former shows a more narrow range of compositions and more fractionated rocks compared to the Northern one. The exceptions to this are the Cr2O3 (Figure 13e) and CaO (Figure 13c) plots, which display lower oxides

concentrations in the Southern sequence compared with the same Mg# range in the Northern sequence. In order to explore this feature on a larger data base, the Tables 5 and 6 and Figure 14 apply the entire mine drilling assay database with a total 395 analyses of the Southern and Northern sequences.
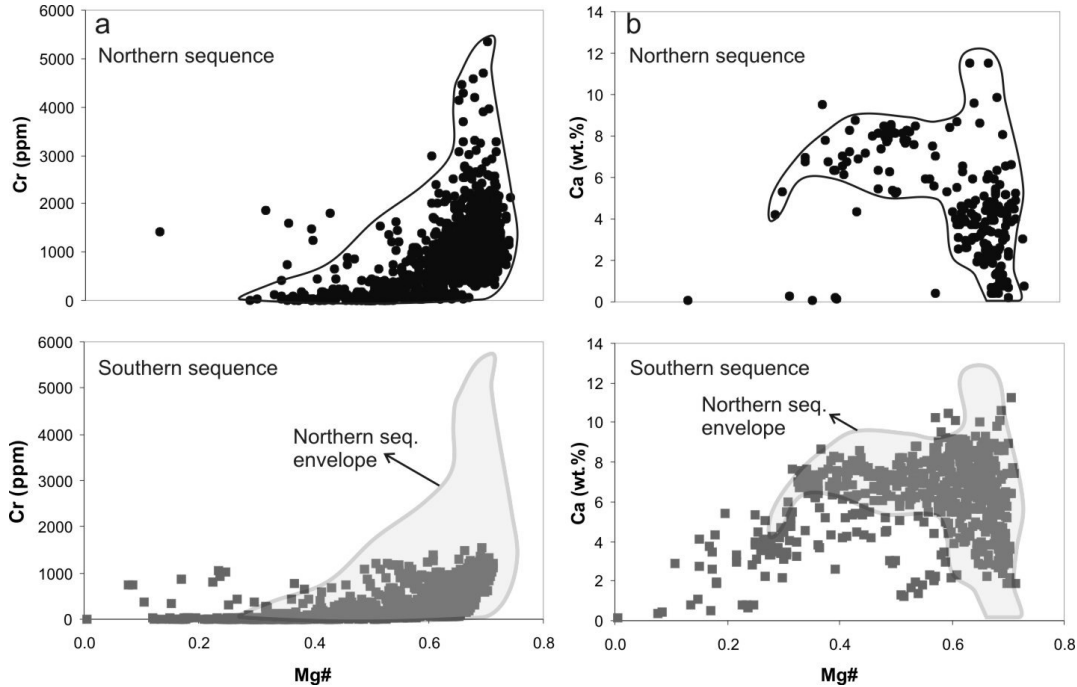
Figure 14 – Variations of Cr (a) and Ca (b) for the two distinct sequences from the ABC.

In the plot of Figure 14a the Cr increases towards more primitive rocks (higher Mg#), exactly the same tendency as displayed in Figure 13e. However, the plot illustrated more clearly that the Northern and Southern sequences have differences in the Cr contents. The Southern sequence does not contain the most primitive and Cr-rich rocks as observed in the Northern sequence. Figure 14b displays the Ca versus Mg# plot and, compared to the Figure 13c, it reveals more clearly the overlapping data ranges between Southern and Northern sequences.

The Mg# index (Figure 15a) shows a distinct decrease from 0.71 to 0.49, from the base to the top parts in the Northern sequence, mainly controlled by the olivine fractionation. The two sequences above and below the S2 orebody, respectively, show two separated trends of decreasing Mg#, with an increase of Mg# above the S2 horizon forming a reversal trend. In the Southern sequence, the Mg# plots with more constant values from the basal lherzolite (0.61 Mg#) to the top olivine websterite (0.63 Mg#). In the same sequence, the rocks nearby the S1 orebody have the lowest values of up to 0.54 Mg# and the pyrite-bearing gneiss has Mg# of 0.3.

The distribution of S (Figure 15b) in the Northern sequence seems to be divided into two distinct intervals, one in the lower part of the sequence with S > 0.3 wt.%, and the other with S < 0.1 wt.% in the top, directly above the S2 orebody. The Southern sequence shows a more scattered distribution. The semi-massive to massive mineralization of the S2 orebody shows the highest values with S ranging from 4.84 to 18.8 wt.%. On the other hand, the disseminated sulfide mineralization of the Southern sequence, entitled of S1 orebody, shows values from 1.69 to 6.64 wt.% S. The pyrite-bearing gneiss adjacent to the S1 orebody has 1.1 wt.% S.
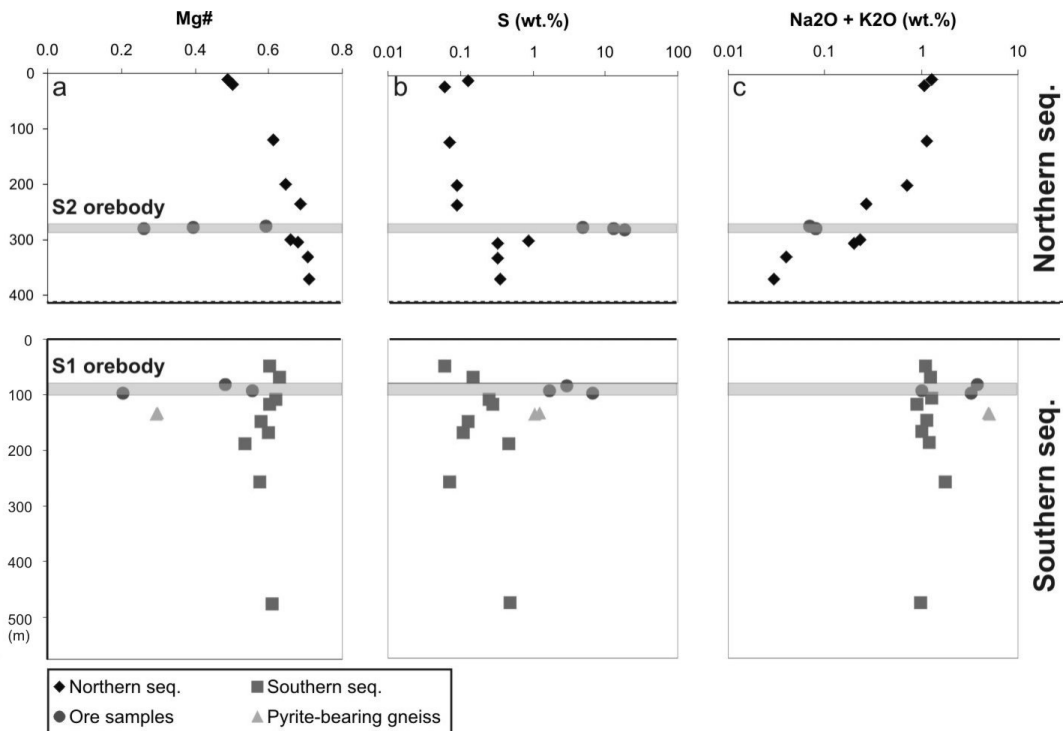
Figure 15 – Variantions of Mg# (a), S (b) and $Na_2O + K_2O$ (c) with stratigraphy from ABC.

The alkalis $Na_2O + K_2O$ are plotted on Figure 15c, and show a clear increase from the base towards the top of the Northern sequence. The Southern sequence displays a much less distinguished trend with values varying around 1 wt.% $Na_2O + K_2O$. While the S2 orebody has an alkali content within the trend, the S1 orebody reaches up to 3.83 wt.% $Na_2O + K_2O$. This alkali concentration is close to that of the pyrite-bearing gneiss with 5.09 wt.% $Na_2O + K_2O$. The high alkali content may be related to alkali-bearing mineral phases such as phlogopite observed in the S1 orebody rocks, and biotite observed in the pyrite-bearing gneiss samples.

Minor and trace elements

The geochemical evolution of Cr in the Northern sequence follows the fractionation trend, showing a distinct decrease from the basal dunite towards the top gabbronorite (2190 ppm to 410 ppm Cr, Figure 16a). However, comparing the trends above and below the S2 orebody, a reversed trend increases the Cr concentration. There is no such trend in the Southern sequence, where the Cr values are generally low between 100 and 490 ppm. Chromium is predominantly concentrated in chromite $Fe^{2+}Cr_2O_4$ with stoichiometrically 46 wt.% Cr, and in pyroxenes of the ABC with up to 2361 ppm Cr (see Nilson, 1981).

The concentration of Ni (Figure 16b) strongly decreases in the Northern sequence from the S2 orebody upward (from 1430 to 233 ppm Ni), but it is constant at *ca.* 1800 ppm Ni below it. Contrasting with the Northern, the Southern sequence reveals a more constant data from the basal lherzolite (917 ppm Ni) to the top olivine webstrite (781 ppm Ni). The country rock represented by the pyrite-bearing gneiss shows the lowest values, varying between 16 and 98 ppm Ni.
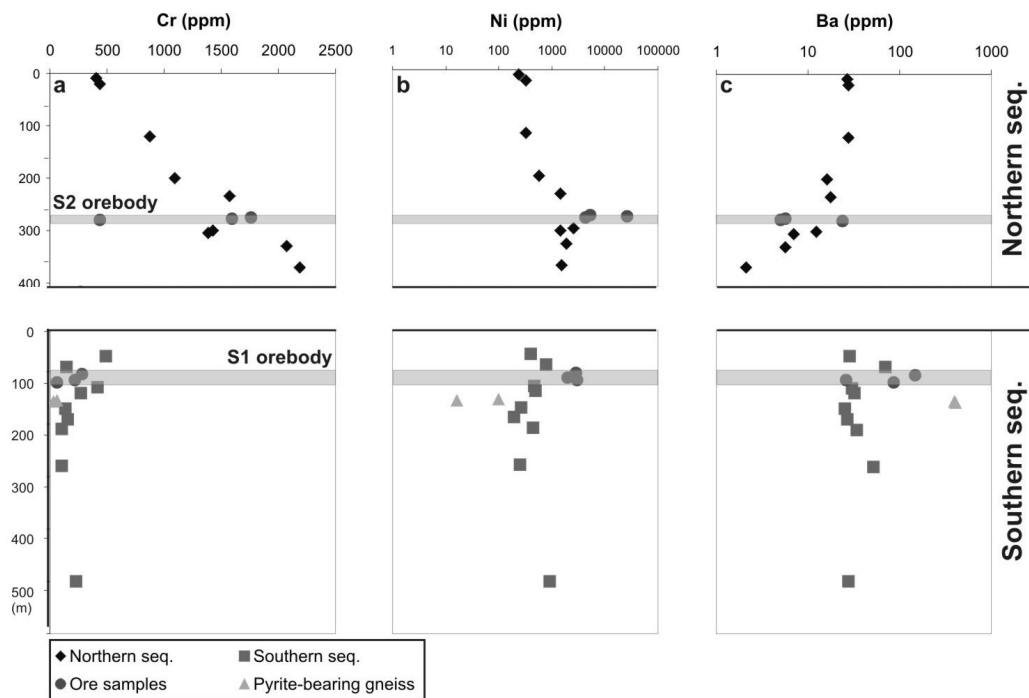
Figure 16 – Variantions of Cr (a), Ni (b) and Ba (c) with stratigraphy from ABC.

Barium behaves generally incompatible in the Northern sequence (Figure 16c), with a strong enrichment from 2.1 ppm in basal dunite towards 12.3 ppm in the S2 orebody, and a weak increase from the last to the top gabbronorite (17.9 ppm to 27.2 ppm Ba). The Southern sequence shows more constant values around 30 ppm Ba, except for the S1 orebody which has up to 147 ppm Ba. High values of about 400 ppm Ba are restricted to the pyrite-bearing gneiss.

Figure 17 illustrates primitive mantle-normalized trace element patterns, the raw data are given in Tables 3 and 4. The Northern sequence (Figure 17a) has generally low trace element concentrations, specially its most primitive rocks. The basal chromite dunite and the S2 orebody samples reveal anomalous concentrations of Zr and Hf, moreover the S2 orebody samples have high Rb and Th concentrations. On the other hand, the Southern sequence (Figure 17b) reveals higher values of trace element concentration, suggesting a more fracitonated nature than the Northern sequence. The S1 orebody samples (e.g. CMJ106) and some other adjacent samples (e.g. CMJ103) of the Southern sequence show anomalous high concentrations of Ba, Rb, Th, K, Nb, La, Ce, Sr and Nd elements, showing a tendency to overlap the pyrite-bearing gneiss curve.
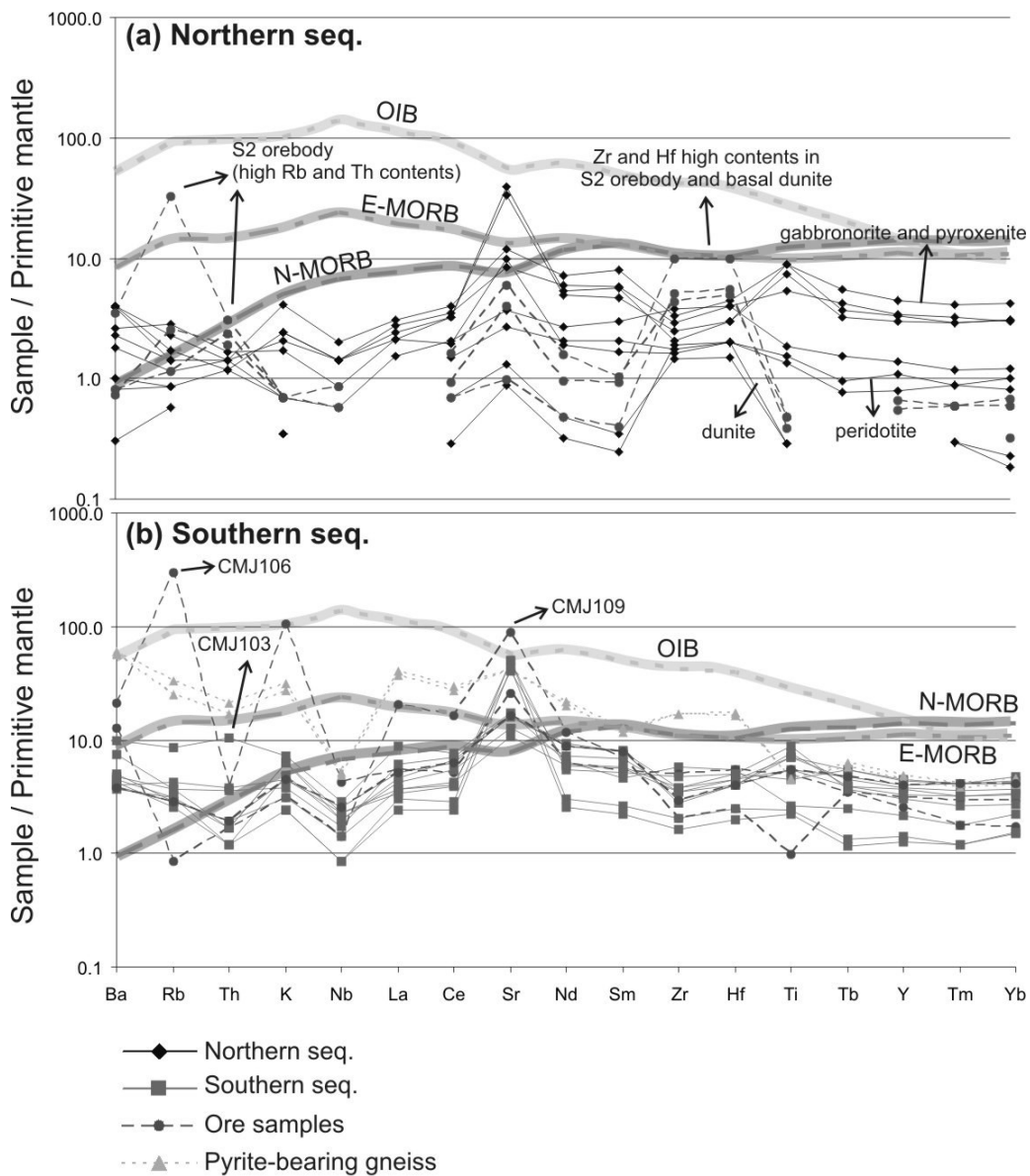
Figure 17 – Primitive mantle normalized trace element patters of the Northern sequence (a) and the Southern sequence (b) for the ABC samples. Missing data points are analyses below detection limits. The ocean island basalt (OIB), N-MORB (depleted mantle) and E-MORB (enriched mantle) trace elements values are from Sun and McDonough (1989). The values for primitive mantle are from Thompson (1982).

Rare earth elements

Whole-rock rare-earth element (REE) concentrations of the ABC are listed in Tables 3 and 4. The Northern sequence (Figure 18a) shows almost flat patterns, reflecting rocks essentially composed of olivine, pyroxenes, amphibole and plagioclase. The REE concentrations on these rocks are not far from chondrite values, thus indicating an uncontaminated signature. All samples from Northern sequence plot with

lower values compared to the N-MORB (depleted mantle), moreover the chromite-bearing dunite samples (e.g. CMJ005 and CMJ009) from the basal parts of the Northern sequence plot below the chondrite values, showing the primitive nature of this cumulate rock. As for the trace elements, the Southern sequence (Figure 18b) suggests a more fractionated nature than the Northern sequence, represented by higher light rare-earth element (LREE) concentrations. The S1 orebody (e.g. CMJ109) and the adjacent samples CMJ103 show a more LREE-enriched pattern similar to that of the gneiss samples and the ocean island basalt (OIB) curve. Figure 19 shows REE ratios representing the slopes for all REE [ratio $(La/Yb)_N$] and the LREE [ratio $(La/Sm)_N$]. The ABC samples show a linear trend from the lowest values of La/Yb and La/Sm, closer to the N-MORB, towards higher ones, closer to the OIB. The pyrite-bearing gneiss shows the highest ratios, followed by S1 orebody (e.g. CMJ109) and others adjacent samples in the Southern sequence (e.g. CMJ103). One isolated sample from the Northern sequence (CMJ028) plots close to these higher ratios of La/Yb and La/Sm group.
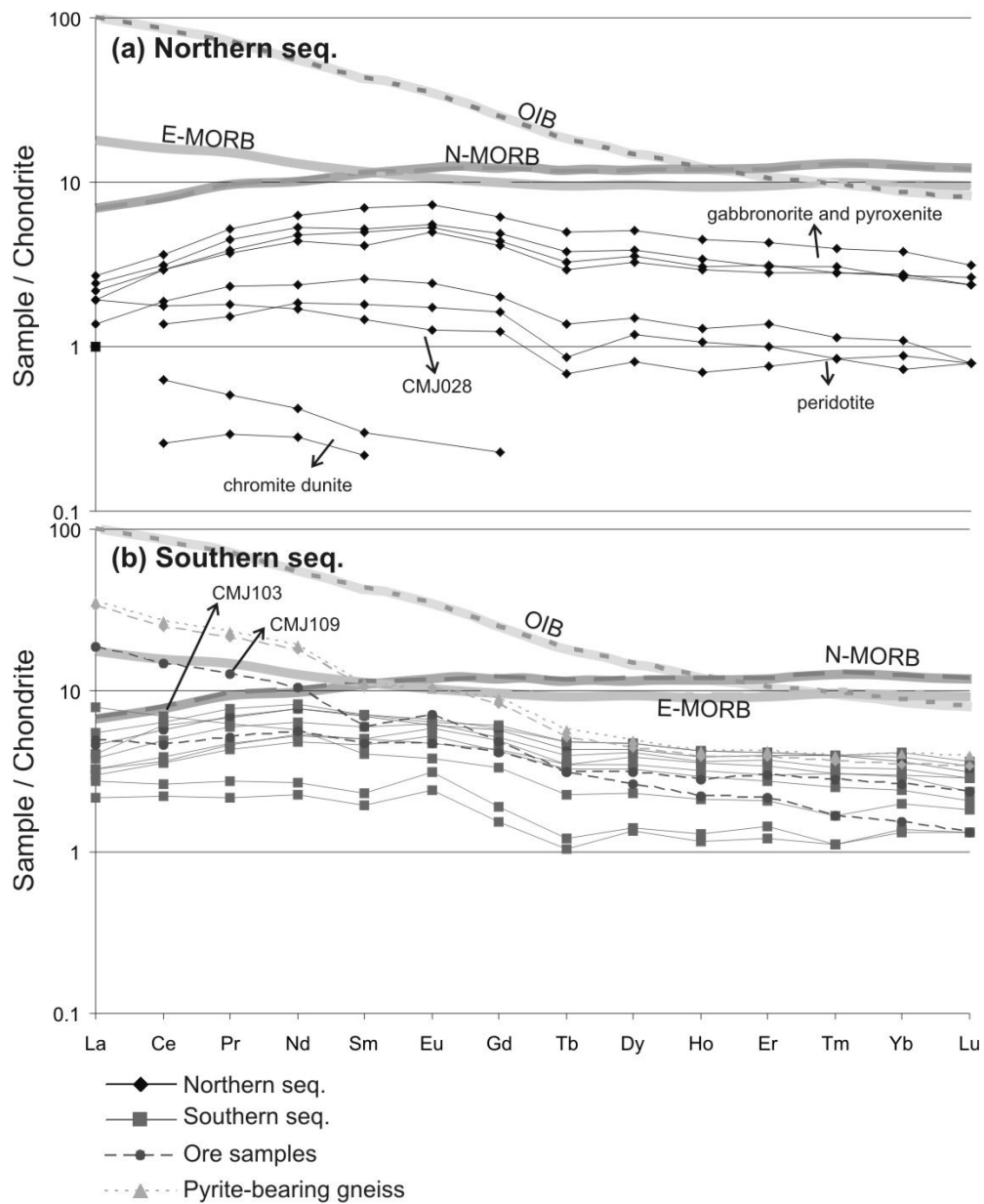
Figure 18 – Chondrite normalized REE patters on Northern sequence (a) and on Southern sequence (b) for the ABC samples. The missing or interrupted plots have reached the assay equipment lower detection limit. The ocean island basalt (OIB), N-MORB (depleted mantle) and E-MORB (enriched mantle) REE values are from Sun and McDonough (1989). The values for chondrite are from Evensen *et al.* (1978).

Table 3 – Compositions of whole-rock samples from the ABC.

Sample	CMJ042	CMJ041	CMJ038	CMJ036	CMJ028	CMJ022	CMJ020	CMJ017	CMJ014	CMJ012	CMJ009	CMJ005	CMJ100	CMJ103	CMJ106	CMJ108	CMJ109
Stratigraphy	10	20	120	200	235	275	278	280	300	305	330	370	470	490	505	515	520
Sequence	N	N	N	N	N	N	N	N	N	N	N	N	S	S	S	S	S
Rock code	GT	GT	PX	PD	DU	DS	MS	MS	PD	PD	DU	DU	PX	PX	PX	PX	PX
SiO_2	46.90	46.20	47.60	45.50	37.40	32.60	24.90	19.45	39.90	39.50	35.80	33.20	48.10	44.60	42.80	47.50	43.50
Al_2O_3	11.15	11.55	7.30	4.62	2.16	0.83	0.70	0.77	1.90	1.66	0.69	0.65	7.89	5.79	8.19	7.18	18.75
Fe_2O_3 total	14.95	14.90	11.65	13.30	16.25	22.50	36.10	46.50	15.25	15.15	15.30	15.55	12.15	15.40	16.20	15.35	12.80
MnO	0.22	0.22	0.19	0.19	0.20	0.18	0.15	0.10	0.18	0.19	0.18	0.19	0.21	0.19	0.17	0.21	0.05
MgO	14.20	15.00	18.50	24.10	35.40	32.60	23.50	16.30	29.40	32.30	36.60	37.70	18.40	26.30	15.00	19.15	3.30
CaO	8.93	9.48	11.00	10.60	1.24	0.27	0.21	0.57	7.40	4.83	0.33	0.30	10.55	5.27	7.56	8.20	11.45
Na_2O	1.22	1.00	1.02	0.66	0.22	0.05	0.06	0.06	0.21	0.18	0.03	0.02	0.97	1.02	0.79	0.87	3.15
K_2O	0.07	0.07	0.12	0.06	0.05	0.02	0.02	0.02	0.02	0.02	0.01	0.01	0.14	0.21	3.04	0.13	0.09
TiO_2	0.93	0.76	0.91	0.56	0.14	0.05	0.04	0.05	0.19	0.16	0.03	0.03	0.72	0.27	0.50	0.57	0.10
P_2O_5	<0.01	<0.01	<0.01	<0.01	<0.01	0.05	<0.01	<0.01	<0.01	<0.01	<0.01	<0.01	<0.01	0.06	<0.01	0.04	0.01
Cr_2O_3	0.06	0.06	0.12	0.15	0.22	0.33	0.27	0.29	0.20	0.19	0.29	0.31	0.07	0.02	0.03	0.03	0.01
LOI	0.68	0.51	1.44	0.15	6.64	10.15	12.25	13.65	5.32	6.20	10.30	12.00	0.71	0.79	5.01	0.93	5.26
Total	99.31	99.75	99.85	99.89	99.92	99.63	98.20	97.76	99.97	100.38	99.56	99.96	99.91	99.92	99.29	100.16	98.47
S	0.13	0.06	0.07	0.09	0.09	4.84	13.10	18.80	0.87	0.33	0.33	0.36	0.06	0.15	2.99	1.69	6.64
Se	0.5	0.6	0.6	0.5	0.5	17.2	39.3	54.7	5.6	1.4	1.8	0.5	0.6	0.6	8.9	5.4	4.4
V	350	378	300	206	36	35	<5	22	84	66	16	18	246	93	168	208	47
Cr	410	440	880	1090	1570	1760	1590	440	1430	1390	2070	2190	490	150	280	220	60
Co	77	87	76	111	178	320	840	708	177	168	184	181	75	149	302	169	182
Ni	233	326	332	577	1430	5270	26800	4380	2510	1440	1860	1540	397	781	2890	1980	3030
Cu	112	238	75	78	128	8650	3660	3140	3460	1100	1410	56	205	185	2650	1130	3480
Rb	0.5	0.6	0.8	0.5	1.0	0.4	0.9	11.4	0.4	0.3	0.3	0.2	0.9	3.0	104.5	1.0	0.3
Sr	457	396	140	101	117	47	12	70	43	32	16	10	186	207	306	193	1040
Y	6.6	5.9	9.0	6.8	1.6	1.1	<0.5	1.3	2.8	2.2	<0.5	<0.5	8.9	4.3	6.3	8.1	5.1
Zr	14	17	23	20	11	67	35	30	26	12	10	13	19	39	34	20	14
Nb	0.5	0.5	0.7	0.5	0.3	0.2	<0.2	0.3	0.2	<0.2	<0.2	<0.2	0.7	1.0	1.5	0.9	0.5
Ba	27.2	27.6	27.6	16.0	17.9	5.6	5.0	23.9	12.3	7.0	5.6	2.1	28.9	68.9	147.0	26.1	87.2

Table 3 – (continued)

Sample	CMJ042	CMJ041	CMJ038	CMJ036	CMJ028	CMJ022	CMJ020	CMJ017	CMJ014	CMJ012	CMJ009	CMJ005	CMJ100	CMJ103	CMJ106	CMJ108	CMJ109
Stratigraphy	10	20	120	200	235	275	278	280	300	305	330	370	470	490	505	515	520
Sequence	N	N	N	N	N	N	N	N	N	N	N	N	S	S	S	S	S
Rock code	GT	GT	PX	PD	DU	DS	MS	MS	PD	PD	DU	DU	PX	PX	PX	PX	PX
La	0.7	0.8	1.0	0.9	0.7	<0.5	<0.5	<0.5	0.5	<0.5	<0.5	<0.5	1.5	2.9	1.8	1.7	6.8
Ce	2.8	2.8	3.5	3.0	1.7	0.8	0.6	1.4	1.8	1.3	0.6	0.3	5.8	6.7	4.4	5.5	14.1
Pr	0.53	0.51	0.71	0.61	0.25	0.13	0.08	0.17	0.32	0.21	0.07	0.04	0.94	0.86	0.70	0.96	1.75
Nd	3.4	3.1	4.5	3.8	1.2	0.6	0.3	1.0	1.7	1.3	0.3	0.2	5.5	4.1	4.0	5.5	7.4
Sm	1.14	0.95	1.63	1.19	0.34	0.19	0.08	0.21	0.60	0.42	0.07	0.05	1.64	0.94	1.09	1.61	1.37
Cs	0.02	0.02	0.05	0.02	0.03	0.01	0.04	0.67	<0.01	0.01	0.01	<0.01	0.03	0.06	6.45	0.03	0.01
Eu	0.46	0.43	0.63	0.48	0.11	0.03	0.03	0.08	0.21	0.15	<0.03	<0.03	0.58	0.33	0.41	0.53	0.62
Gd	1.33	1.25	1.89	1.49	0.38	0.19	0.07	0.23	0.62	0.50	0.07	<0.05	1.80	1.03	1.27	1.76	1.48
Tb	0.19	0.17	0.29	0.22	0.04	<0.01	<0.01	<0.01	0.08	0.05	<0.01	<0.01	0.28	0.13	0.18	0.25	0.18
Dy	1.35	1.24	1.92	1.47	0.31	0.20	0.08	0.22	0.57	0.45	0.07	0.05	1.80	0.88	1.20	1.66	1.00
Ho	0.26	0.25	0.38	0.29	0.06	0.04	0.01	0.05	0.11	0.09	0.01	0.01	0.36	0.18	0.24	0.33	0.19
Er	0.78	0.70	1.07	0.77	0.19	0.13	0.06	0.13	0.34	0.25	0.04	0.03	1.03	0.52	0.74	0.98	0.54
Tm	0.10	0.10	0.14	0.11	0.03	0.02	<0.01	0.02	0.04	0.03	0.01	0.01	0.14	0.06	0.10	0.14	0.06
Yb	0.67	0.68	0.94	0.66	0.18	0.13	0.07	0.15	0.27	0.22	0.05	0.04	0.97	0.49	0.65	0.90	0.38
Ga	13.8	14.1	10.5	6.8	3.3	3.5	1.9	3.0	3.4	2.9	1.9	1.8	10.5	7.1	9.9	9.9	16.5
Lu	0.10	0.09	0.12	0.09	0.03	0.02	0.01	0.01	0.03	0.03	0.01	0.01	0.13	0.07	0.09	0.12	0.05
Hf	0.6	0.6	0.9	0.8	0.4	2.0	1.1	1.0	0.8	0.4	0.3	0.4	0.8	1.1	1.1	0.8	0.5
Ta	<0.1	<0.1	<0.1	<0.1	<0.1	<0.1	<0.1	<0.1	<0.1	<0.1	<0.1	<0.1	<0.1	<0.1	<0.1	<0.1	<0.1
Th	<0.05	0.05	0.06	0.06	0.07	0.10	0.08	0.13	0.06	0.05	<0.05	<0.05	0.05	0.44	0.16	0.08	0.07
U	<0.05	<0.05	<0.05	<0.05	<0.05	0.05	<0.05	<0.05	<0.05	<0.05	<0.05	<0.05	0.63	0.11	0.07	<0.05	<0.05

Note: major element oxides and S in wt.%; total iron reported as Fe_2O_3; trace elements in ppm.
LOI: Loss on ignition.
Rock code: (DU) dunite, (PD) peridotite, (PX) pyroxenite, (GT) gabbronorite, (MS) massive sulfide, (DS) disseminated sulfide, (GN) gneiss.
Sequence: (N) Northern sequence; (S) Southern sequence.

Table 4 - Compositions of whole-rock samples from the ABC.

Sample	CMJ111	CMJ113	CMJ115	CMJ116	CMJ508	CMJ509b	CMJ510b	CMJ511a	CMJ516
Stratigraphy	530	540	555	557	570	590	610	680	900
Sequence	S	S	S	S	S	S	S	S	S
Rock code	PX	PX	GN	GN	GT	GT	GT	GT	PD
SiO_2	48.00	50.80	63.50	64.20	48.20	48.60	47.10	46.50	41.40
Al_2O_3	7.49	7.08	15.90	15.80	17.65	15.80	13.85	17.60	6.76
Fe_2O_3 total	11.90	10.95	5.60	5.26	8.51	10.35	10.90	9.28	15.10
MnO	0.17	0.19	0.08	0.07	0.14	0.17	0.18	0.11	0.18
MgO	19.25	16.55	2.36	2.21	11.70	15.40	12.55	12.65	23.40
CaO	10.65	12.20	5.42	4.69	10.15	8.48	12.00	10.40	5.29
Na_2O	1.10	0.80	4.13	4.18	1.07	0.94	1.13	1.56	0.84
K_2O	0.18	0.11	0.78	0.91	0.07	0.07	0.09	0.18	0.13
TiO_2	0.73	0.47	0.48	0.46	0.25	0.23	0.56	0.91	0.80
P_2O_5	<0.01	<0.01	0.08	0.09	<0.01	<0.01	<0.01	<0.01	<0.01
Cr_2O_3	0.06	0.04	0.01	0.01	0.02	0.02	0.01	0.01	0.03
LOI	1.17	0.96	2.05	1.13	0.82	-0.19	2.12	0.74	5.18
Total	100.70	100.15	100.39	99.01	98.58	99.87	100.49	99.94	99.11
S	0.25	0.28	1.23	1.04	0.13	0.11	0.46	0.07	0.48
Se	1.0	0.9	1.4	1.2	0.9	1.0	1.6	0.6	1.5
V	240	227	101	120	123	129	228	256	246
Cr	420	270	60	30	140	160	100	100	230
Co	96	77	20	16	61	75	80	77	131
Ni	469	481	98	16	258	192	450	245	917
Cu	250	205	405	279	171	160	518	162	833
Rb	1.1	1.3	8.7	11.5	1.1	1.0	1.0	1.3	1.5
Sr	152	196	485	487	590	499	471	577	126
Y	7.6	8.8	9.0	9.7	2.8	2.5	7.3	6.0	6.6
Zr	24	26	116	116	14	11	26	32	24
Nb	0.7	0.6	1.7	1.8	0.3	0.3	0.5	0.8	0.8
Ba	30.6	32.4	391.0	412.0	25.5	27.2	34.4	51.9	27.8
La	1.4	2.0	12.2	13.2	1.0	0.8	1.2	1.1	1.2
Ce	4.7	6.1	23.8	25.8	2.5	2.1	3.5	3.4	3.7
Pr	0.81	1.05	2.94	3.16	0.38	0.30	0.63	0.59	0.65
Nd	4.5	5.9	12.6	13.5	1.9	1.6	3.8	3.4	3.7
Sm	1.39	1.62	2.39	2.57	0.53	0.45	1.17	1.06	1.15
Cs	0.02	0.03	0.15	0.25	0.02	0.03	0.07	0.03	0.06
Eu	0.54	0.55	0.90	0.88	0.27	0.21	0.51	0.46	0.41
Gd	1.56	1.85	2.50	2.74	0.58	0.47	1.49	1.30	1.33
Tb	0.23	0.28	0.30	0.33	0.07	0.06	0.20	0.19	0.20
Dy	1.56	1.81	1.69	1.88	0.54	0.52	1.47	1.25	1.33
Ho	0.31	0.36	0.33	0.36	0.11	0.10	0.30	0.25	0.27
Er	0.92	1.04	0.96	1.05	0.36	0.30	0.84	0.69	0.75
Tm	0.12	0.14	0.13	0.14	0.04	0.04	0.11	0.09	0.11
Yb	0.81	1.03	0.87	1.01	0.34	0.33	0.74	0.60	0.72
Ga	9.6	9.8	17.4	17.9	13.7	12.6	13.7	14.5	8.0
Lu	0.11	0.14	0.13	0.15	0.05	0.05	0.11	0.08	0.09
Hf	0.9	1.0	3.3	3.5	0.5	0.4	0.9	1.0	0.8
Ta	<0.1	<0.1	0.1	0.1	<0.1	<0.1	<0.1	<0.1	<0.1
Th	0.07	0.15	0.71	0.89	0.05	<0.05	0.08	0.07	0.16
U	<0.05	<0.05	0.16	0.13	<0.05	<0.05	0.05	<0.05	<0.05

Note: major oxides and S in wt.%; total iron reported as Fe_2O_3; trace elements in ppm.
LOI: Loss on ignition. Rock code: same as in Table 3. Sequence: same as in Table 3.

Table 5 – Concentrations of Ca, Cr, FeO and MgO for Northern sequence samples in ABC.

Sample	Rock code	Ca (wt.%)	Cr (ppm)	FeO (wt.%)	MgO (wt.%)	Mg#
91097	DU	3.10	383	9.47	22.47	0.70
91098	DU	0.76	745	11.35	31.67	0.74
91102	DU	1.28	791	13.38	29.10	0.69
91119	PD	4.25	772	12.20	27.69	0.69
91120	PD	5.17	753	12.08	26.20	0.68
91121	PD	5.54	572	10.00	15.99	0.62
91122	PD	4.60	1050	13.25	29.27	0.69
91123	PD	3.00	1200	13.70	31.59	0.70
91141	PD	4.38	1070	11.14	24.04	0.68
91142	PD	5.14	731	11.15	26.28	0.70
91633	GT	6.13	170	9.19	6.43	0.41
91638	GT	6.79	98	12.77	6.62	0.34
91645	GT	6.78	166	11.18	7.96	0.42
91646	GT	6.94	73	12.14	6.33	0.34
91648	GT	6.31	397	11.96	11.72	0.49
91282	DU	0.87	1695	15.18	34.49	0.69
91316	PD	6.28	285	11.14	18.57	0.63
91317	PD	7.49	52	9.53	12.70	0.57
91329	PD	4.78	601	11.63	28.86	0.71
91331	PD	3.64	806	12.68	24.71	0.66
91337	PD	1.91	1010	14.15	29.44	0.68
91340	DU	2.44	1035	12.38	29.77	0.71
91341	PD	4.40	1040	12.43	28.36	0.70
91343	PD	4.00	1015	11.37	29.27	0.72
91344	PD	4.49	1015	11.53	29.35	0.72
91345	PD	3.33	1330	13.32	30.85	0.70
91346	PD	2.22	1455	13.70	32.92	0.71
91372	PX	7.02	383	11.23	15.34	0.58
91373	PX	4.75	975	12.68	22.06	0.63
91374	PX	4.28	1050	12.62	22.39	0.64
91375	PX	4.12	1030	12.41	22.55	0.64
91376	PX	3.99	959	12.86	21.72	0.63
91377	PX	5.34	1045	12.70	18.74	0.60
91378	PX	4.36	455	13.70	21.23	0.61
91379	PX	2.23	640	15.57	34.16	0.69
91380	PX	2.81	1175	15.57	30.85	0.66
91381	PX	3.08	778	14.67	27.11	0.65
91382	PX	3.76	775	12.02	21.89	0.65
91383	PX	2.35	704	15.57	31.67	0.67
91384	PX	2.61	983	15.31	26.04	0.63
91388	PX	5.92	312	10.95	13.86	0.56
91389	PX	4.50	605	13.57	22.80	0.63
91392	PX	4.01	547	12.99	20.56	0.61
91394	PX	4.72	514	12.14	21.97	0.64
91395	PX	3.20	700	13.89	26.53	0.66
91396	PX	2.14	861	15.89	31.01	0.66
91397	PX	2.61	998	16.15	27.86	0.63
91402	PX	3.70	607	13.38	21.39	0.62
91403	PX	3.83	645	13.12	22.31	0.63
91405	PX	2.94	849	14.22	24.30	0.63
91407	PX	3.72	789	13.12	21.48	0.62
91409	PX	3.96	515	11.86	19.40	0.62

Rock code: same as in Table 3.

Table 6 – Concentrations of Ca, Cr, FeO and MgO for Southern sequence samples in ABC.

Sample	Rock code	Ca (wt.%)	Cr (ppm)	FeO (wt.%)	MgO (wt.%)	Mg#
91745	PX	7.23	132	10.43	16.35	0.61
91750	PX	5.96	169	11.50	16.91	0.60
91751	PX	3.88	197	12.93	19.74	0.60
91758	PX	7.08	149	11.87	15.66	0.57
91761	PX	5.80	175	12.25	17.50	0.59
91762	PX	5.88	199	11.27	18.81	0.63
91763	PX	6.28	182	10.57	18.75	0.64
91764	PX	6.43	185	10.64	17.59	0.62
91768	PX	6.68	185	9.34	17.00	0.65
91775	PX	7.41	200	14.02	16.84	0.55
91776	PX	6.62	215	12.65	17.91	0.59
91777	PX	5.90	227	15.31	19.15	0.56
91779	PX	7.05	212	11.27	18.75	0.62
91780	PX	6.81	302	9.93	20.90	0.68
91781	PX	7.31	472	12.03	18.32	0.60
91782	PX	6.97	430	11.03	21.49	0.66
91786	PX	8.16	521	12.61	18.16	0.59
91798	PX	6.53	509	16.27	18.07	0.53
91801	PX	6.56	441	14.15	18.25	0.56
91802	PX	6.31	456	13.38	19.06	0.59
91803	PX	7.18	334	10.90	19.81	0.65
91804	PX	6.20	280	13.64	18.81	0.58
91805	PX	4.75	255	11.09	21.90	0.66
91862	PX	4.33	173	10.09	17.41	0.63
91863	PX	6.91	168	10.02	16.30	0.62
91868	PX	7.23	199	9.83	17.91	0.65
91869	PX	7.47	210	10.18	19.56	0.66
91870	PX	6.40	168	9.85	19.65	0.67
91871	PX	6.06	179	9.58	19.31	0.67
91872	PX	5.76	180	9.29	18.81	0.67
92002	PX	6.69	180	11.66	15.66	0.57
92036	PX	3.74	266	12.09	22.31	0.65
92038	PX	5.46	198	11.28	17.41	0.61
92039	PX	7.00	247	12.85	18.50	0.59
92040	PX	6.10	304	16.79	17.25	0.51
92042	PX	7.16	410	12.16	19.81	0.62
92043	PX	4.48	273	11.00	21.31	0.66
92091	GT	6.56	186	13.25	17.25	0.57
92092	GT	6.35	123	13.25	16.20	0.55
92098	GT	3.46	51	16.47	23.21	0.58
92099	GT	4.19	51	13.64	21.58	0.61
92102	GT	7.14	106	13.64	15.31	0.53
92104	GT	6.40	143	12.36	19.65	0.61
92105	GT	6.03	118	11.80	16.05	0.58
92108	GT	6.19	176	13.06	19.15	0.59
92109	GT	5.86	179	12.43	19.00	0.60
92110	GT	5.46	175	13.57	20.31	0.60
92111	GT	6.37	157	12.41	18.66	0.60
92112	GT	9.15	221	11.59	17.34	0.60
92114	GT	8.73	239	13.25	17.41	0.57
92116	GT	5.48	117	12.68	20.63	0.62
92117	GT	5.88	72	14.28	15.71	0.52
92128	GT	6.83	156	12.58	16.34	0.56

Rock code: same as in Table 3.
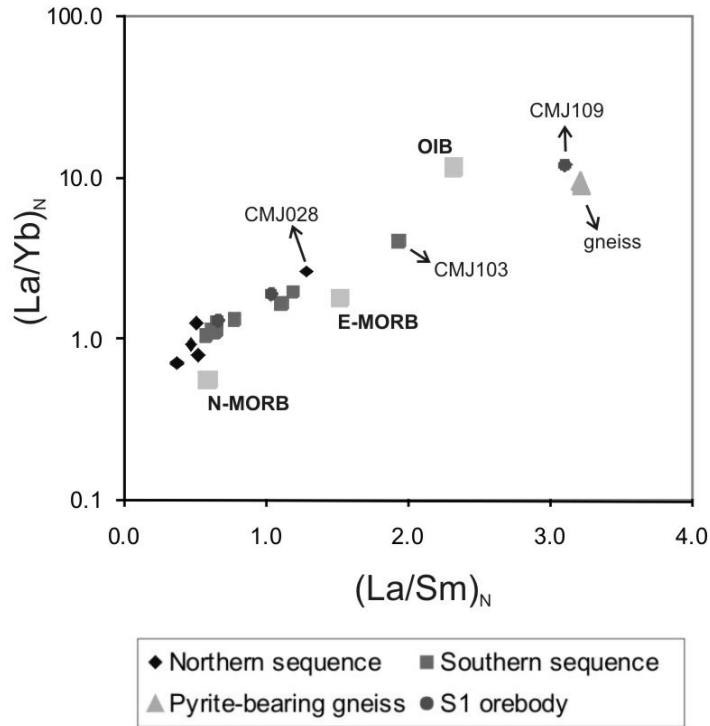
Figure 19 – Chondrite normalized REE ratios for the ABC samples. The ocean island basalt (OIB), N-MORB (depleted mantle) and E-MORB (enriched mantle) REE values are from Sun and McDonough (1989). The values for chondrite are from Evensen *et al.* (1978).

The Figure 20 displays the same REE ratios as in Figure 19 plus Gd/Yb ratio that represents the heavy rare-earth element (HREE) slope, but all of them with the stratigraphy. The HREE slope Gd/Yb shows quite constant values around 1.5 for the Northern and Southern sequences, except for one chromite-bearing dunite from the base of the Northern sequence, which has very low HREE content close to detection limit. The La/Sm and La/Yb slopes show mostly similar patterns with constant values for the Northern and Southern sequences, except to one of the S1 orebody samples (CMJ109) and the adjacent sample (CMJ103) that have more positive slopes. These last samples slopes approach that of the pyrite-bearing gneiss samples with La/Sm around 3 and La/Yb around 10. The Northern sequence sample CMJ028, from the hanging wall of the S2 orebody, also shows a moderate LREE enrichment.
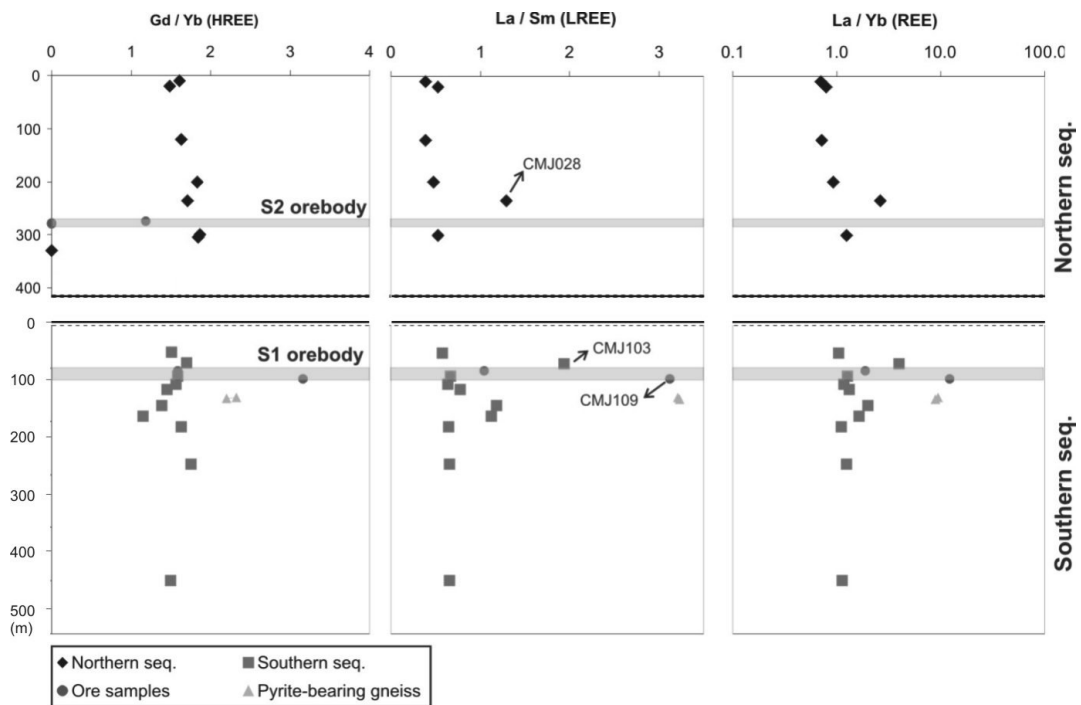
Figure 20 – Chondrite normalized REE ratios with stratigraphy for the ABC samples. The values for chondrite are from Evensen *et al.* (1978).

Ni, Cu, and platinum-group elements

Two different sources of data were used to the platinum group elements (PGE) studies. One of them is the numerous drill core assay results from the Americano do Brasil mine database, which include the Ni, Cu, S, Au Pt and Pd elements (Tables 7, 8 and 9). The other is a few whole rock samples analyzed for Ni, Co, Ir, Ru, Rh, Os, Pt, Pd, Au and Cu elements (Table 10).

Table 7 – Concentrations of Ni, Cu, S, Au, Pt and Pd of ore samples from the S2 orebody in ABC.

Sample	122058	122753	122747	121340	121343	122755	122754	122750	121342	122749	122751	121344	121345	122745	121471	122746	122818	121341	122099
Ni (wt %)	0.69	0.84	0.42	1.18	2.21	0.98	0.79	0.70	2.01	0.81	1.11	0.95	1.00	0.44	4.25	0.32	4.24	1.23	0.63
Cu (wt %)	0.70	0.86	1.01	1.63	2.83	0.73	0.67	0.75	3.15	0.89	0.84	2.08	5.62	0.94	1.03	0.77	4.08	4.35	0.48
S (wt %)	2.01	3.50	2.22	16.20	23.60	4.62	2.81	2.90	21.80	3.31	4.46	18.35	17.25	2.31	15.60	1.34	23.00	22.20	4.99
Au (ppm)	0.24	0.33	0.27	0.29	0.28	0.68	0.36	0.27	0.16	0.23	0.29	0.23	0.86	0.62	0.02	2.32	0.02	0.08	0.03
Pt (ppm)	0.57	0.42	0.96	0.42	0.32	0.24	0.64	0.66	0.38	0.48	0.52	0.26	0.07	0.42	0.07	0.56	0.00	0.81	0.07
Pd (ppm)	2.82	2.41	2.18	2.01	1.97	1.77	1.66	1.64	1.42	1.42	1.42	1.38	1.26	1.26	1.25	1.24	1.00	0.92	0.76

Sample	121175	121642	121466	122817	121623	122434	122756	122885	122905	92704	92702	121653	121478	121589	121499	121528	92598	91260	121497
Ni (wt %)	0.42	6.26	2.70	3.19	3.12	0.93	0.32	1.69	2.79	1.42	0.19	0.43	2.17	2.47	0.56	1.39	1.07	0.51	1.15
Cu (wt %)	0.62	1.84	0.19	0.72	0.57	1.45	0.69	0.52	0.54	0.19	0.01	0.30	3.03	1.99	0.48	1.26	0.31	0.29	0.42
S (wt %)	3.16	31.50	17.95	23.60	16.65	7.25	1.93	1.54	19.35	7.63	2.07	1.70	17.30	16.90	3.28	8.40	5.86	2.58	7.97
Au (ppm)	0.18	0.09	0.01	0.04	0.01	0.07	0.26	0.33	0.02	0.01	0.66	0.04	0.13	0.05	0.11	0.18	0.03	0.03	0.02
Pt (ppm)	0.47	0.78	0.09	0.00	0.08	0.33	0.93	0.24	0.02	0.49	0.29	0.03	0.00	0.00	0.12	0.02	0.10	0.08	0.17
Pd (ppm)	0.75	0.75	0.72	0.70	0.69	0.68	0.68	0.63	0.55	0.54	0.53	0.25	0.25	0.24	0.24	0.24	0.24	0.23	0.23

Table 8 – Concentrations of Ni, Cu, S, Au, Pt and Pd of ore samples from the S1 orebody in ABC.

Sample	91797	92811	121056	92282	92283	91792	121057	91784	92639	91796	92652	121030	92991	92809	91795	92653	92738	92736	92654
Ni (wt %)	0.35	0.58	1.16	0.32	0.28	0.46	0.83	0.25	0.36	0.38	0.51	0.51	1.08	1.28	0.39	0.28	0.46	0.32	0.39
Cu (wt %)	0.70	0.73	0.88	0.42	0.75	0.44	1.29	0.28	0.90	0.60	0.66	0.77	0.82	0.97	0.44	0.68	0.94	0.62	0.69
S (wt %)	3.40	4.28	7.74	2.40	2.37	3.32	9.03	1.73	13.85	3.40	2.91	5.06	8.81	9.47	3.00	2.09	2.96	2.11	2.47
Au (ppm)	0.15	0.10	0.07	0.08	0.21	0.12	0.12	0.07	0.04	0.09	0.14	0.04	0.11	0.35	0.11	0.18	0.17	0.10	0.08
Pt (ppm)	0.07	0.10	0.05	0.03	0.07	0.05	0.09	0.05	0.04	0.05	0.02	0.00	0.02	0.08	0.08	0.04	0.06	0.05	0.01
Pd (ppm)	0.20	0.16	0.16	0.12	0.11	0.10	0.10	0.09	0.08	0.08	0.08	0.08	0.08	0.07	0.07	0.07	0.06	0.06	0.06

Sample	92993	121059	92379	92625	92626	92627	92382	92218	92273	92187	92340	92281	92372	92276	92377	91785	92274	121060	92252
Ni (wt %)	0.41	0.17	0.19	0.26	0.53	0.79	0.20	0.28	0.37	0.20	0.40	0.46	0.26	0.17	0.35	0.34	0.38	0.14	0.12
Cu (wt %)	0.24	0.49	0.70	0.50	1.11	0.61	0.32	0.47	0.51	0.36	0.37	0.54	0.43	0.16	0.39	0.46	0.40	0.31	0.22
S (wt %)	3.05	1.23	2.35	5.18	6.57	6.10	1.50	2.12	3.03	1.23	3.77	3.78	2.43	1.00	2.89	2.78	2.91	0.92	3.46
Au (ppm)	0.03	0.09	0.07	0.04	0.02	0.03	0.05	0.14	0.05	0.06	0.03	0.10	0.04	0.04	0.03	0.03	0.04	0.07	0.03
Pt (ppm)	0.02	0.00	0.15	0.06	0.00	0.00	0.02	0.02	0.01	0.02	0.01	0.04	0.03	0.01	0.00	0.02	0.02	0.00	0.01
Pd (ppm)	0.04	0.03	0.03	0.03	0.03	0.03	0.03	0.03	0.03	0.03	0.03	0.03	0.03	0.02	0.02	0.02	0.02	0.02	0.02

Table 9 – Concentrations of Ni, Cu, S, Au, Pt and Pd of ore samples from the G2 orebody in ABC.

Sample	91168	91167	91170	91174	91430	91172	91961	91432	91435	91434	91196	91171	91184	91193	91177	91162	91154	91296	91183
Ni (wt %)	4.53	4.26	4.59	3.79	4.03	4.62	0.48	4.23	2.80	3.69	2.79	3.33	3.71	2.24	2.55	0.52	1.50	0.60	3.17
Cu (wt %)	0.85	1.80	0.26	0.27	0.43	0.84	0.35	0.32	0.81	0.36	0.69	0.81	0.77	0.79	1.21	0.66	0.28	0.90	1.07
S (wt %)	28.80	27.50	29.20	30.00	28.90	27.40	4.22	25.60	23.80	27.90	21.10	21.40	26.60	18.20	21.40	4.60	9.62	4.98	22.30
Au (ppm)	0.27	0.01	0.00	0.02	0.01	0.00	0.00	0.00	0.05	0.01	0.01	0.01	0.00	0.02	0.10	0.02	0.02	0.07	0.01
Pt (ppm)	0.31	0.18	0.37	0.24	0.31	0.41	0.04	0.26	0.31	0.32	0.11	0.16	0.14	0.10	0.23	0.11	0.18	0.21	0.26
Pd (ppm)	0.83	0.83	0.80	0.79	0.74	0.74	0.73	0.65	0.65	0.64	0.63	0.58	0.55	0.52	0.50	0.48	0.45	0.44	0.43

Sample	91446	91439	91682	91074	91082	91554	91684	91075	91536	91295	91696	91970	91685	91438	91687	91553	91925	91694	91924
Ni (wt %)	0.63	0.27	0.61	0.52	0.58	0.58	0.57	0.47	0.67	0.55	0.45	0.33	0.38	0.31	0.35	0.51	0.37	0.50	0.47
Cu (wt %)	1.42	0.85	0.51	0.41	0.41	0.48	0.49	0.44	0.97	0.36	0.47	0.46	0.55	0.81	0.45	1.28	0.49	1.30	0.55
S (wt %)	5.97	2.45	4.27	3.33	4.85	3.53	4.46	3.18	4.05	4.09	3.20	2.34	3.14	3.45	2.93	4.25	2.55	4.54	3.58
Au (ppm)	0.24	0.10	0.08	0.10	0.05	0.08	0.08	0.12	0.07	0.05	0.18	0.14	0.12	0.14	0.10	0.07	0.11	0.08	0.06
Pt (ppm)	0.05	0.23	0.16	0.12	0.17	0.09	0.16	0.12	0.23	0.05	0.19	0.14	0.14	2.81	0.13	0.05	0.16	0.18	0.16
Pd (ppm)	0.23	0.22	0.22	0.22	0.21	0.21	0.21	0.20	0.20	0.20	0.20	0.20	0.20	0.20	0.19	0.19	0.18	0.18	0.17

The relations between Ni, Cu, Pd and S are shown in Figure 21(a-i). The sulfur content reflects the amount of sulfides and consequently the style of mineralization. Disseminated sulfide usually has between 1 and 5 wt.% S, the net-textured ore between 5 and 20 wt.%, and the semi-massive or massive ore has between 20 and 35 wt.% S.

The Ni versus S plots (Figure 21a-c) essentially reflect the amount of pentlandite in the whole-rock, as no other Ni-sulfide has been observed or described previously (e.g. Nilson, 1981). Hence, all ore bodies display a positive correlation between Ni and S.The S2 orebody (Figure 21a) has the highest Ni content of the ABC, with a S/Ni ratio of 5. The G2 orebody (Figure 21c) has a S/Ni ratio of 7.25, and the S1 orebody (Figure 21b), has a S/Ni = 8.75. The concentration of Cu, on the other hand, should be directly related to the amount of chalcopyrite in the whole-rock. However, Cu shows a reasonable correlation with S only for disseminated sulfide samples having 1 – 5 wt.-% S, while S-rich, massive sulfide samples display a rather erratic Cu-S distribution (Figure 21d-f).

Palladium is the most abundant element of the PGE and is plotted against S in Figures 21g-i. This element shows positive correlation with S in the S2 orebody (Figure 21g), although several samples that are considerable richer in Pd, plot out of the main trend. The Pd/S ratio is 0.02 in the main trend; however, isolated anomalous samples have much higher values of up to 1.4. The G2 orebody samples (Figure 21i) show good correlation of Pd and S, forming a positive trend with a Pd/S ratio of 0.03. The S1 orebody (Figure 21h) has very low concentration of Pd (< 0.2 ppm), without a significant correlation with S.
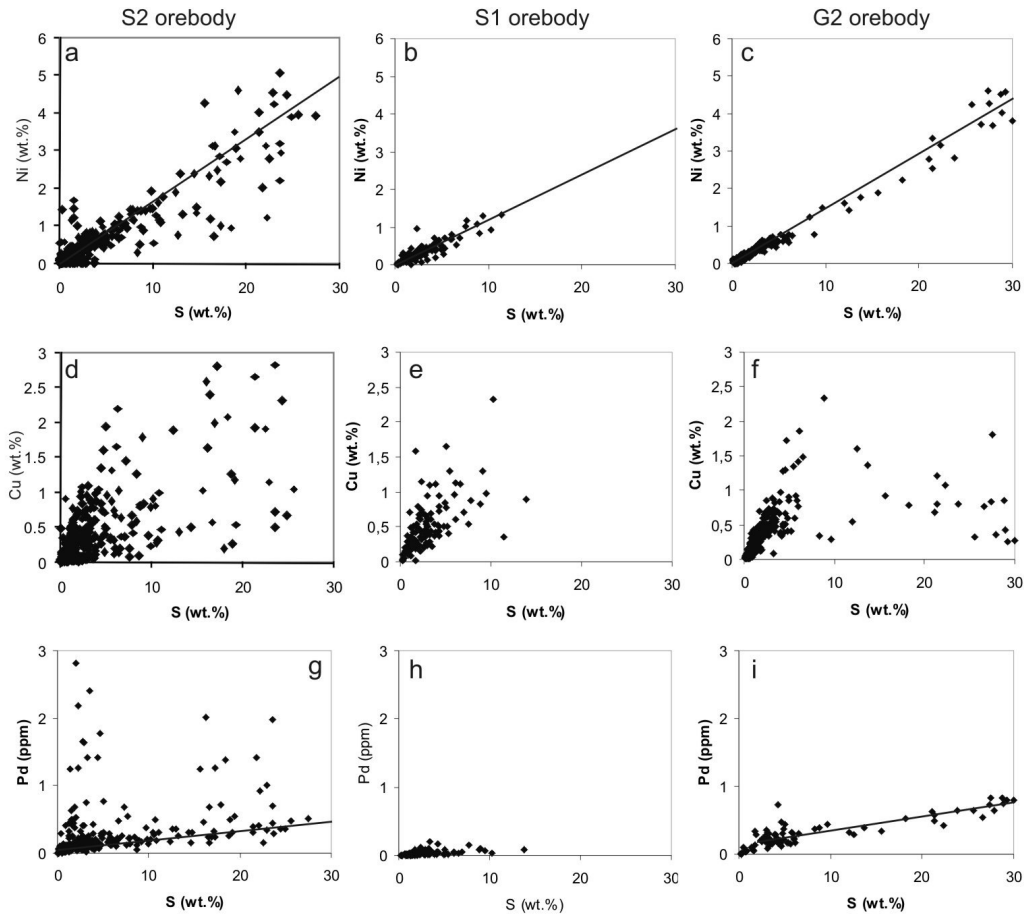
Figure 21 - Variations of Ni (a, b and c), Cu (d, e and f) and Pd (g, h and i) with sulfur (S) for the three different orebodies from the ABC. Note that on 1st column of plots is for the S2 orebody, the 2nd for S1, and the 3rd for the G2 orebody.

The relations between Pd, Pt, Au and the Ni/Cu ratio, for each orebody, are shown in Figure 22(a-c). The Ni/Cu ratio represents the composition of the sulfide fraction, comparing the amount of pentlandite with chalcopyrite. The chalcopyrite-dominant sulfide fraction can represent sulfide segregation on a fractionated magma (Ni-poor) or can be formed by the sulfide liquid fractionation. After all, the partition coefficient between the "monosulfide solid solution" (MSS) and sulfide liquid is lower for Cu (*ca.* 0.2) than for Ni (*ca.* 0.8 – Fleet *et al*., 1993; Mungall *et al.*, 2005). The Figure 22 shows plots with L-formed shape. This pattern suggests that the samples with a low Ni/Cu ratios contain the highest concentrations of Pd, Pt and Au or, alternatively, that the chalcopyrite-rich ore portions are associated with the highest Pd, Pt and Au concentrations. While the S2 and G2 orebodies reach Pd concentrations of up to 7.1 ppm, Pt = 3.4 ppm and Au = 0.7 ppm, the S1 orebody shows much lesser Pd and Pt concentrations of below 0.2 ppm each, but equivalent Au contents of up to 0.4 ppm.
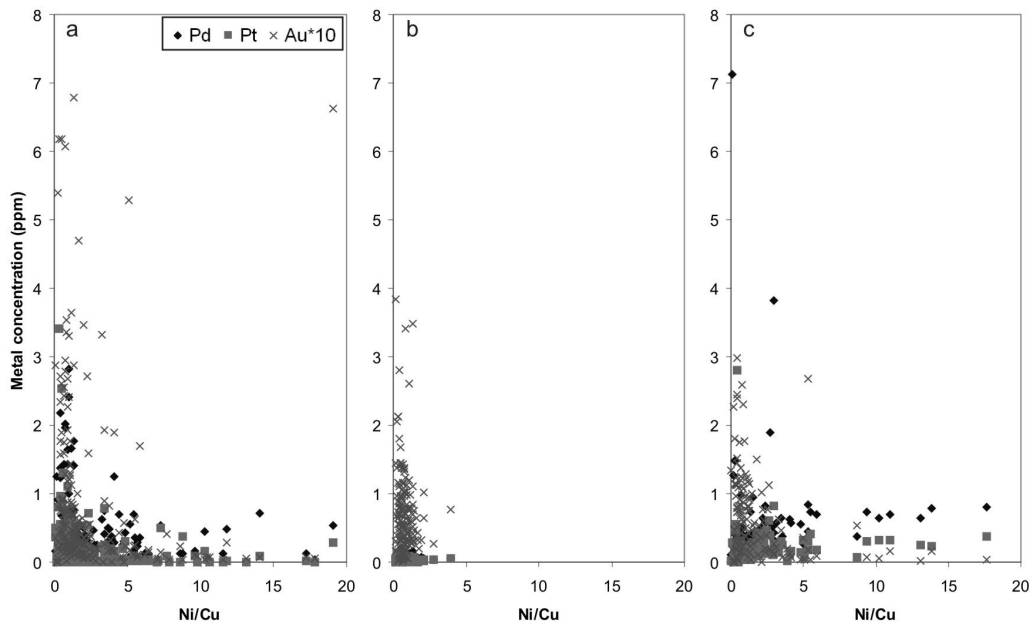
Figure 22 – Variations of three noble metals (Au, Pd and Pt) with Ni/Cu ratio, relative to S2 orebody (a), S1 orebody (b) and G2 orebody (c). Note that Au concentration is multiplied by 10.

The Ni, Co, PGE, Au and Cu variation patterns for the three orebodies are plotted in the Figure 23 and the raw data is given in the Table 10. Magmatic ores formed by imiscible sulfide liquid on basic magma chambers reflect on its PGE concentrations the silicate magma composition and the R-factor (for a review see Naldrett, 2004). The PGE content of basic and ultrabasic magmas is essentially controlled by the rate of mantle partial melting on its formation. Elements as Rh, Ru, Ir, Os and Ni act as though they are compatible in some phases in the mantle residue, being often retained into mantle in low partial melting rates magmas (Crocket, 2002).

The S2 and G2 orebodies show similar PGE variations pattern, but the S2 orebody shows a slightly more primitive signature with higher Ni, Co, Ir and Os and lower Pt, Au and Cu concentrations. The S1 orebody has a more steeply increasing tendency from Ir towards Au, thus it has the most fractionated signature. This tendencies can be expressed by the (Pt+Pd)/Ir equation. Both S2 and G2 orebodies reveal a (Pt+Pd)/Ir = 24, although the S1 orebody has a (Pt/Pd)/Ir = 120.
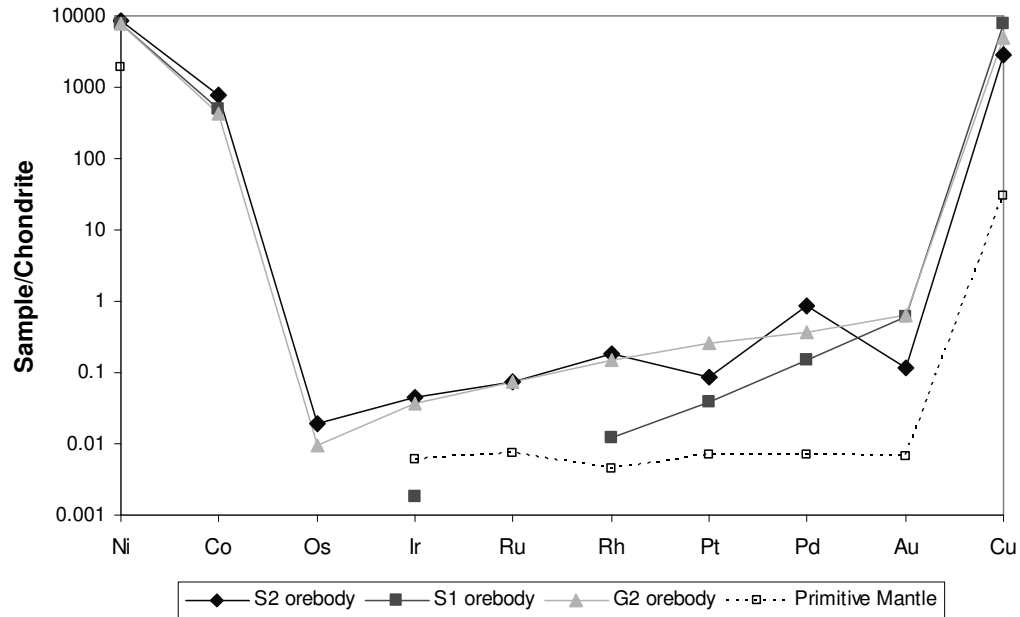
Figure 23 – Ni, Co, PGE, Au and Cu variation pattern for the three orebodies of ABC. The primitive mantle values are from McDonough and Sun (1995). Samples are normalized to the C1 chondrite concentrations values of Naldrett and Duke (1980).

The comparison between the PGE variation pattern of the pyrrhotite and the chalcopyrite-rich (po-rich and cpy-rich) portions of the S2 orebody is shown in Figure 24. The cpy-rich sample has lower values of Ni, Co, Os and Ir compared to the po-rich, however it has higher values of Rh, Pt, Pd, Au and Cu, and equivalent Ru. Consequently, the cpy-rich sample has a steep slope (more fractionated) on the increasing tendency from Os to Pd. This slope can be expressed by equations as: (Pt+Pd)/(Ru+Ir+Os) = 84.1, Cu/(Cu+Ni) = 0.98, (Pt+Pd)/Ir = 414 or simply Pd/Ir = 357.
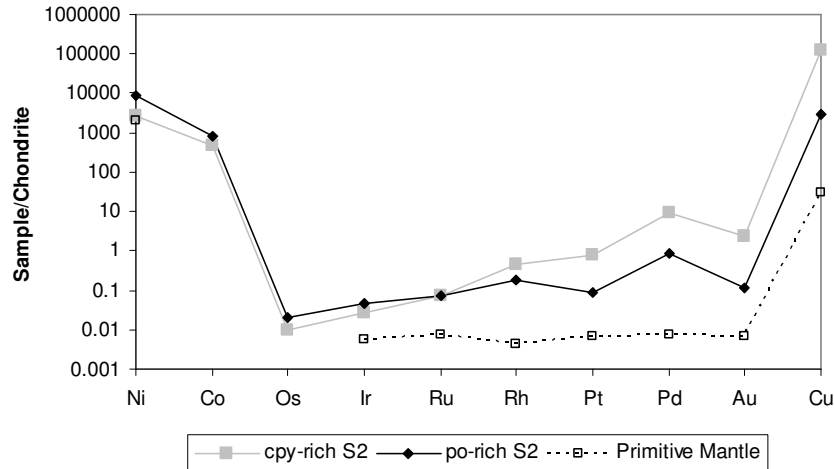
Figure 24 – Ni, Co, PGE, Au and Cu variation pattern for the pyrrhotite and the chalcopyrite-rich portions of the S2 orebody. The primitive mantle values are from McDonough and Sun (1995). All samples are normalized to the C1 chondrite concentrations values of Naldrett and Duke (1980).

Table 10 – Ni, Co, PGE, Au and Cu concentrations for the ABC orebodies samples. (*) is the primitive mantle reference of McDonough and Sun (1995).

Sample	JMT101	JMT102	JMT103	JMT106	Primitive Mantle*
Ore body	S2	S1	S2	G2	
Ni (ppm)	2570	7790	8560	7690	1960
Co (ppm)	461	490	782	430	
Os (ppm)	*<0.01*	*<0.01*	0.01	*<0.01*	
Ir (ppm)	0.014	0.001	0.024	0.02	0.0032
Ru (ppm)	0.05	*<0.05*	0.05	0.05	0.005
Rh (ppm)	0.09	0.005	0.037	0.03	0.0009
Pt (ppm)	0.8	0.04	0.09	0.27	0.0071
Pd (ppm)	5.0	0.08	0.48	0.2	0.0039
Au (ppm)	0.351	0.091	0.018	0.095	0.001
Cu (ppm)	122000	7730	2890	4870	30
(Pt + Pd)/(Ru + Ir + Os)	84.1	-	6.8	6.3	1.3
Cu/(Cu + Ni)	0.98	0.50	0.25	0.39	0.02
(Pt + Pd)/Ir	414	120	24	24	3
Pd/Ir	357	80	20	10	1

Sulfur isotopes

Sulfur isotopes have been extensively used in the past to identify crustal contamination or assimilation of mafic magmas, which then may lead to the precipitation of sulfides in magmatic sulfide ores as in the Duluth complex, the Noril'sk giant ore field or the Voisey's Bay deposit (Naldrett, 1999; Ripley and Li, 2007). The $\delta^{34}S$ data of sulfide minerals from the ABC and its country rocks (pyrite-bearing gneiss) are listed on Table 11. There is no significant evolutionary trend in S isotopic

composition along the complex lithostratigraphy. Moreover, the monosulfide solid solution (MSS) sulfides pyrrhotite, chalcopyrite and pentlandite do not show prominent differences one to the other for a particular sample. The three sulfide phases spread a range from -2.6 to at most 3.5 $^0/_{00}$ δ³⁴S (CDT) with a mean of +0.5 $^0/_{00}$, plotting all within the mantle range (Figure 25). The only exception is sample CMJ109 with +4.2 $^0/_{00}$ δ³⁴S, which comes from a locality adjacent to the pyrite-bearing gneiss. The gneiss itself shows the most homogeneous isotopic composition, with positive δ³⁴S values around +4.0 $^0/_{00}$.
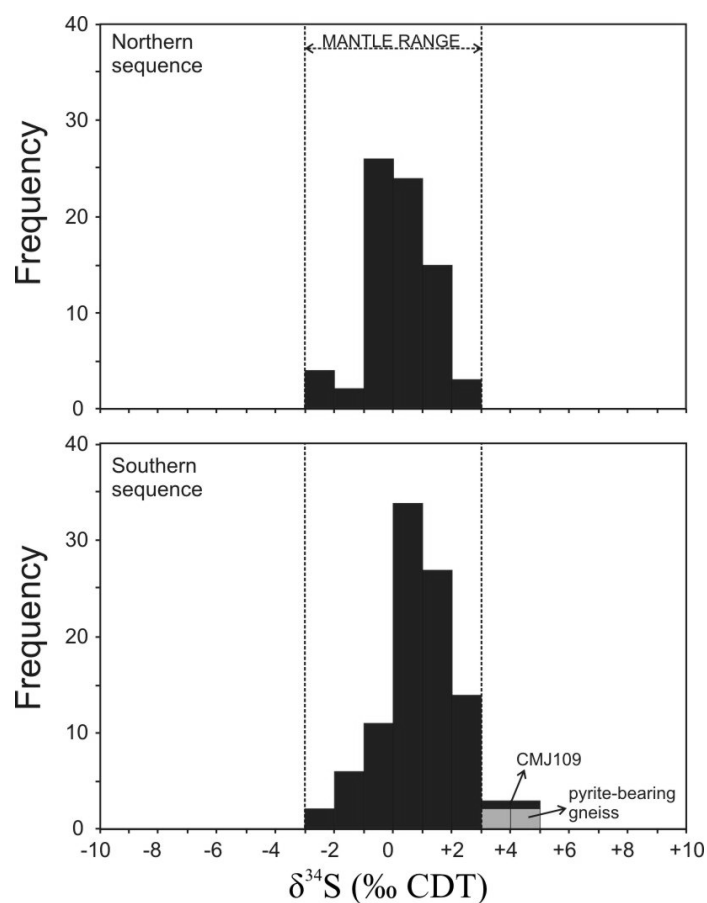
Figure 25 – Histogram of δ³⁴S values of sulfides of ABC and of the country rock pyrite-bearing gneiss.
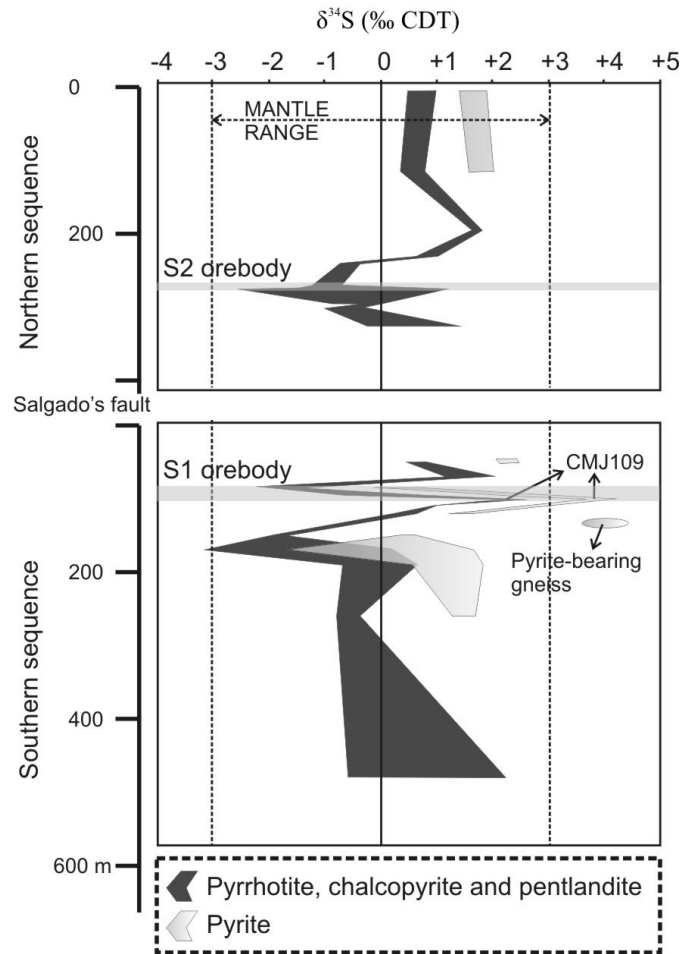
Figure 26 – Plot of the δ^{34}S values of sulfides of ABC and of the country rock pyrite-bearing gneiss with stratigraphy column. The plot range is related to the 1σ errors on precision.

However, it is most noteworthy that pyrite coexisting with the MSS sulfide always shows a distinctly heavier isotopic composition than the MSS sulfide, generally about 1.7 $^0/_{00}$ more positive than pyrrhotite or chalcopyrite (there was no analyzable pentlandite on these samples).

Nine samples from the ABC containing pyrite and the typical magmatic sulfide minerals (e.g. pyrrhotite, pentlandite, chalcopyrite) were analyzed, revealing that the pyrite has a δ^{34}S 1.7 ($^0/_{00}$ CDT) more positive than pyrrhotite or chalcopyrite (there was no analyzable pentlandite on these samples), as indicated on Figure 26.

Table 11 – Sulfur isotopic data of ABC and its coutry rock gneiss.

Sample	CMJ009	CMJ009	CMJ009	CMJ009	CMJ012	CMJ012	CMJ012	CMJ012	CMJ014	CMJ014	CMJ014	CMJ014	CMJ017	CMJ017	CMJ017	CMJ017	CMJ020
Mineral	pn	pn	Pó	pn	pn	pn	pn	pn	pn	po	po	pn	po	pn	pn	po	pn
32/34S (1σ)	22.193	22.223	22.206	22.207	22.231	22.239	22.241	22.247	22.186	22.235	22.239	22.228	22.271	22.222	22.219	22.237	22.238
1σ error (‰)	0.422	0.310	0.276	0.393	0.416	0.342	0.321	0.506	0.340	0.991	0.378	0.308	0.311	0.335	0.412	0.455	0.404
δ34S ‰ CDT	1.4	0.1	0.9	0.8	-0.3	-0.6	-0.7	-1.0	1.8	-0.4	-0.6	-0.1	-2.1	0.2	0.3	-0.5	-0.6
1σ SD unid. CDT	0.4	0.3	0.3	0.4	0.4	0.3	0.3	0.5	0.3	1.0	0.4	0.3	0.3	0.3	0.4	0.5	0.4

Sample	CMJ020	CMJ022	CMJ022	CMJ022	CMJ022	CMJ028	CMJ028	CMJ028	CMJ032	CMJ032	CMJ032	CMJ032	CMJ036	CMJ036	CMJ036	CMJ036	CMJ038
Mineral	po	cpy	cpy	cpy	cpy	cpy	cpy	cpy	pn	pn	pn	pn	po	po	po	po	py
32/34S (1σ)	22.239	22.206	22.225	22.263	22.232	22.208	22.203	22.204	22.232	22.236	22.247	22.235	22.194	22.192	22.190	22.183	22.181
1σ error (‰)	0.353	0.796	0.425	0.539	0.369	0.397	0.514	0.444	0.232	0.297	0.376	0.192	0.326	0.389	0.292	0.538	0.117
δ34S ‰ CDT	-0.6	0.9	0.0	-1.7	-0.3	0.8	1.0	0.9	-0.3	-0.5	-1.0	-0.5	1.4	1.5	1.6	1.9	2.0
1σ SD unid. CDT	0.4	0.8	0.4	0.5	0.4	0.4	0.5	0.4	0.2	0.3	0.4	0.2	0.3	0.4	0.3	0.5	0.1

Sample	CMJ038	CMJ038	CMJ042	CMJ042	CMJ042	CMJ042	CMJ042	CMJ042	CMJ042	CMJ042	CMJ100	CMJ100	CMJ100	CMJ100	CMJ103	CMJ103	CMJ103
Mineral	py	py	cpy	po	py	po	po	py	po	po	cpy	py	cpy	py	pn	cpy	pn
32/34S (1σ)	22.229	22.213	22.187	22.211	22.189	22.215	22.167	22.181	22.196	22.177	22.221	22.185	22.204	22.163	22.186	22.186	22.200
1σ error (‰)	0.673	0.382	0.277	0.260	0.204	0.346	0.353	0.426	0.258	0.294	0.329	0.150	0.697	0.193	0.371	0.359	0.349
δ34S ‰ CDT	-0.2	0.5	1.7	0.6	1.6	0.5	2.6	2.0	1.3	2.2	0.2	1.8	0.9	2.8	1.7	1.8	1.1
1σ SD unid. CDT	0.7	0.4	0.3	0.3	0.2	0.3	0.4	0.4	0.3	0.3	0.3	0.1	0.7	0.2	0.4	0.4	0.3

Sample	CMJ103	CMJ103	CMJ103	CMJ106	CMJ106	CMJ106	CMJ106	CMJ108	CMJ108	CMJ108	CMJ108	CMJ109	CMJ109	CMJ109	CMJ109	CMJ111	CMJ111
Mineral	po	po	po	py	py	cpy	cpy	cpy	po	pn	cpy	cpy	po	py	cpy	cpy	pn
32/34S (1σ)	22.164	22.217	22.173	22.215	22.223	22.258	22.260	22.225	22.218	22.225	22.236	22.175	22.172	22.131	22.168	22.205	22.196
1σ error (‰)	0.465	0.577	0.492	0.153	0.138	0.410	0.466	0.404	0.328	0.434	0.282	0.348	0.319	0.179	0.289	0.315	0.269
δ34S ‰ CDT	2.8	0.4	2.4	0.5	0.1	-1.5	-1.6	0.0	0.3	0.0	-0.5	2.2	2.4	4.2	2.6	0.9	1.3
1σ SD unid. CDT	0.5	0.6	0.5	0.2	0.1	0.4	0.5	0.4	0.3	0.4	0.3	0.3	0.3	0.2	0.3	0.3	0.3

Note: po = pyrrhotite; cpy = chalcopyrite; pn = pentlandite; py = pyrite.

Table 11 – (continued).

Sample	CMJ111	CMJ111	CMJ111	CMJ111	CMJ113	CMJ113	CMJ113	CMJ113	CMJ113	CMJ113	CMJ115	CMJ115	CMJ115	CMJ115	CMJ508	CMJ508	CMJ508
Mineral	pn	cpy	cpy	pn	py	cpy	py	py	py	py	py	py	py	py	py	cpy	py
32/34S (1σ)	22.170	22.220	22.240	22.196	22.176	22.219	22.215	22.165	22.208	22.199	22.135	22.132	22.143	22.138	22.198	22.274	22.219
1σ error (‰)	0.868	0.526	0.422	0.544	0.239	0.438	0.421	0.341	0.406	0.369	0.087	0.158	0.277	0.123	0.192	0.357	0.129
δ34S ‰ CDT	2.5	0.3	-0.7	1.3	2.2	0.3	0.5	2.7	0.8	1.2	4.1	4.2	3.7	3.9	1.2	-2.2	0.3
1σ SD unid. CDT	0.9	0.5	0.4	0.5	0.2	0.4	0.4	0.3	0.4	0.4	0.1	0.2	0.3	0.1	0.2	0.4	0.1

Sample	CMJ509	CMJ509	CMJ509	CMJ510	CMJ510	CMJ510	CMJ510	CMJ511	CMJ511	CMJ511	CMJ511	CMJ516	CMJ516	CMJ516	CMJ516
Mineral	cpy	py	cpy	py	py	py	py	cpy	cpy	py	cpy	cpy	po	po	cpy
32/34S (1σ)	22.265	22.213	22.249	22.183	22.183	22.231	22.228	22.246	22.232	22.184	22.238	22.205	22.200	22.213	22.213
1σ error (‰)	0.539	0.125	0.364	0.377	0.454	0.246	0.266	0.444	0.410	0.237	0.408	0.583	0.474	0.446	0.450
δ34S ‰ CDT	-1.8	0.5	-1.1	1.9	1.9	-0.3	-0.1	-0.9	-0.3	1.8	-0.6	0.9	1.1	0.6	0.5
1σ SD unid. CDT	0.5	0.1	0.4	0.4	0.5	0.2	0.3	0.4	0.4	0.2	0.4	0.6	0.5	0.4	0.4

Note: po = pyrrhotite; cpy = chalcopyrite; pn = pentlandite; py = pyrite.

Sm-Nd isotopes

Bulk rock analyses of various rocks types from the Northern and the Southern sequences were performed for Nd isotopic composition, whose results are given in Table 12. Epsilon recalculation of these data was done to the time of ABC intrusion cristalization (626 Ma). These values are plotted against stratigraphy in Figure 27.

Most of the samples from both sequences show εNd(626 Ma) values within the range +1 and +3. Three samples from the top part of the Southern sequence show negative values reaching εNd(626 Ma) = -2.4. The pyrite-bearing gneiss yield the most positive value with εNd(626 Ma) = +3.7. Sample CMJ109 which forms part of the S1 orebody has the most positive value in the Southern sequence with an εNd(626 Ma) of +3.1.

Table 12 – Sm-Nd isotopic data of ABC and its country rock gneiss.

sample	CMJ042	CMJ038	CMJ028	CMJ032	CMJ014	CMJ012	CMJ100	CMJ103
sequence	N	N	N	N	N	N	S	S
rock	GT	PX	DU	DU	PD	PD	PX	PX
Sm (ppm)	1.083	1.824	0.146	0.627	0.462	0.433	1.473	1.189
Nd (ppm)	3.265	5.299	0.622	2.328	1.367	1.270	4.915	4.422
147Sm/144Nd	0.2006	0.2080	0.1415	0.1628	0.2042	0.2061	0.1812	0.1625
143Nd/144Nd	0.51276	0.51283	0.51242	0.51262	0.51273	0.51276	0.51245	0.51241
2σ error	13	10	19	23	14	22	22	29
eNd (626)	+2.1	+2.8	0.0	+2.4	+1.2	+1.7	-2.4	-1.7

sample	CMJ108	CMJ109	CMJ111	CMJ113	CMJ508	CMJ509b	CMJ516	CMJ115
sequence	S	S	S	S	S	S		
rock	PX	PX	PX	PX	GT	GT	PD	GN
Sm (ppm)	1.582	1.265	1.259	1.546	0.476	0.313	1.138	2.901
Nd (ppm)	5.475	6.019	4.417	5.442	1.710	1.339	3.817	14.907
147Sm/144Nd	0.1746	0.1271	0.1723	0.1717	0.1682	0.1412	0.1802	0.1177
143Nd/144Nd	0.51265	0.51251	0.51265	0.51266	0.51263	0.51253	0.51266	0.51250
2σ error	19	7	14	10	16	10	7	9
eNd (626)	+1.9	+3.1	+2.2	+2.4	+2.0	+2.4	+1.7	+3.7

Note: Rock code same as in Table 3. Sequence classified as: (N) Northern and (S) Southern.
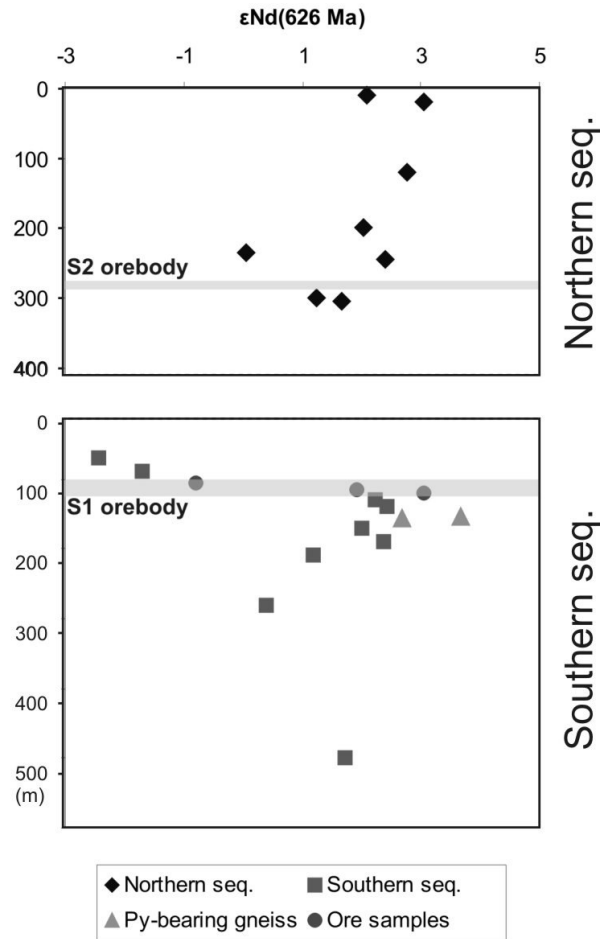
Figure 27 – The εNd(626 Ma) variation with the stratigraphy for the ABC samples and the pyrite-bearing gneiss.

Discussions

Geotectonic setting

Extensional tectonic regimes are typical geological settings where mafic and mafic-ultramafic (MUM) intrusions are encountered. However, synorogenic (e.g. formed in domain of compressive tectonic regime) MUM intrusions are described in the literature (see Naldrett, 2004). These intrusions do not share a particular geochemical or petrological signature, but they were classified as synorogenic due to their age and geotectonic position. Synorogenic intrusions are considered of lesser importance for hosting Ni-Cu deposits (Naldrett and Duke, 1980). The Rona mafic intrusion in Norway, which hosts a 43 Mt @ 0.33 % Ni deposit (Boyd and Mathiesen, 1979), is the

commonly referred example of mineralized synorogenic intrusion. This 437±0.5 Ma old intrusion (Tucker *et al.*, 1990) is related to the Caledonian orogenic belt at the closure of the Iapetus Sea (Ihlen *et al.,* 1997 apud Lamberg, 2005). Naldrett (2004) has classified the worldwide Ni-Cu deposits in several classes, fitting the orogenic ones inside the NC-5 class, that includes the Rona intrusion, Moxie intrusion in Canada, and Aberdeenshire Gabbros in Scotland. Recently, Tang *et al.* (2007) have classified the Chinese small intrusions that hosts Ni-Cu(-PGE) ore deposits in differents geologic settings. One of them includes the intrusions related to orogenic belts, which host some minor Ni-Cu ore deposits. They were interpreted to occur in the extension stage of the orogeny.

The ABC has an age of 626±8 Ma and its geotectonic position supports the interpretation that this intrusion is related to the second magmatic event of the Arenópolis Arc. This event is bracket between 600-660 Ma (Pimentel *et al.*, 1997; Junges *et al.*, 2002; Laux *et al.*, 2004) indicating that the magmatism of the ABC is coeval to the evolution of the magmatic arc. Therefore, nickel-sulfide deposits of the ABC should also be classified as synorogenic.

The Figure 18 shows that Northern and Southern sequences samples have a REE pattern more similar with the N-MORB (depleted mantle) curve, with no enrichment in LREE. In Figure 28, the samples of the ABC are compared in the Th/Yb *versus* Nb/Yb diagram with different mantle reservoirs that are typically related to particular geotectonic environments. The ABC samples form a trend from the N-MORB towards the volcanic arc array, which has more Th-rich signatures. In that manner, the ABC might have formed from the partial melt of the depleted mantle, but some specific localities of the magma chamber have partly assimilated the juvenile arc host rocks (a subject to be addressed in the following discussions of orebodies formation), generating the Th-enriched rocks displayed on Figure 28. Although depleted mantle partial melting is unlikely to occur on compressive environments due to the thick crust of orogens. During the 600 – 660 Ma magmatic event of the Arenópolis Arc (Laux *et al.*, 2004) localized extensional tensions might have caused the uplift of asthenospheric mantle, promoting the 649 to 634 Ma (Baldwin and Brown, 2008) granulitic metamorphism and the depleted mantle partial melting to generate the mafic magmatism. These link between voluminous mafic magmatism and high-grade metamorphism was previously interpreted as corresponding to a "hot orogen" for the Brasília Belt (Pimentel *et al.*, 1996, 2003; Hollanda *et al.*, 2003, Della Giustina *et al.*, 2009).
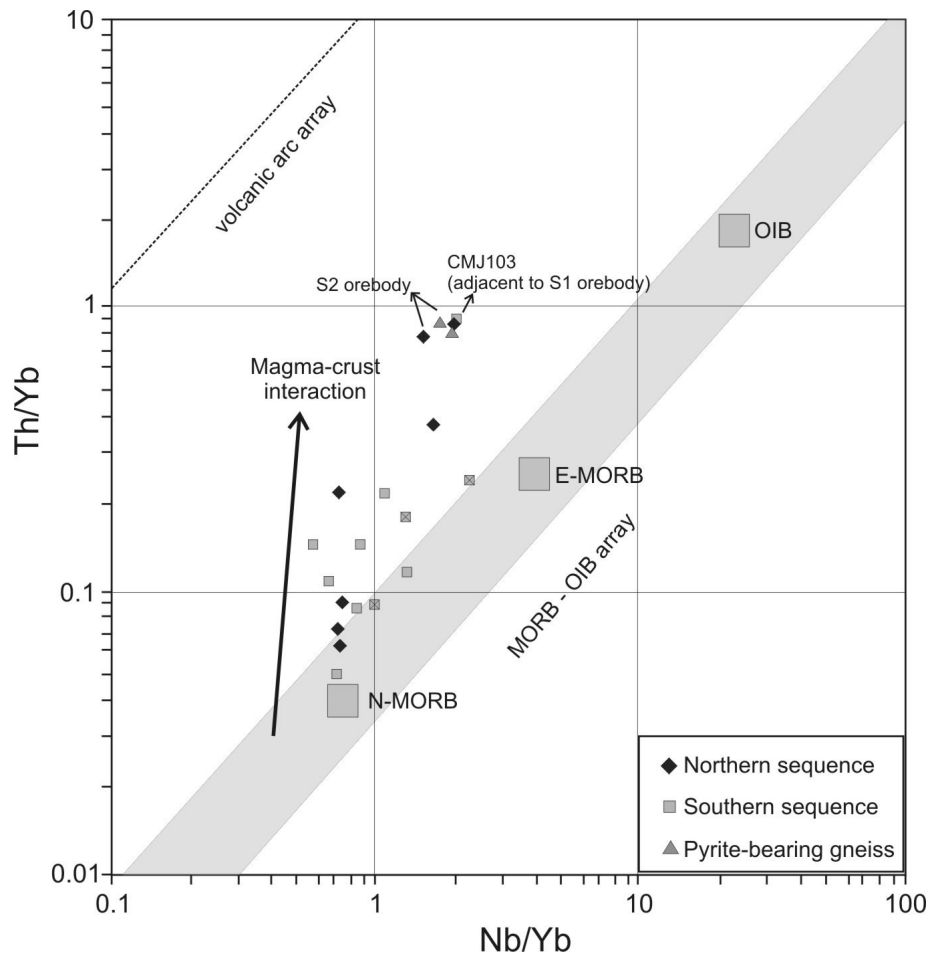
Figure 28 – Plot displaying the Th/Yb and Nb/Yb ratios of ABC samples. The N-MORB, E-MORB and OIB fields, the MORB - OIB and volcanic arc arrays and the magma-crust interaction arrow are from Pearce (2008).

Petrology of ABC

Both sequences that form the ABC have signicant amount of amphibole oikocrysts, which can represents a water-rich trapped liquid on the cumulus pile. The Northern sequence has a thicker ultramafic basal sequence exposed when compared to the "gabbronorite dominant" characteristic of the Southern sequence. However, the proposed cumulus phase's pile suggests similar fractionation trends for both sequences: ol+chr => ol+cpx+chr => ol+cpx+opx => cpx+opx => opx+plg+cpx (see Figure 6). The Northern and Southern sequences may represent different parts of the same magma chamber tectonically juxtaposed side by side, or they represent two different chambers formed from parental magmas of the same composition. We prefer the latter hyphotesis

for the following reasons: i) the disseminated and net-textured orebodies from the Southern sequence, G2 and S1, have different petrological and geochemical characteristics with regard to the massive to semi-massive reef layer of the Northern sequence, the S2; ii) the Southern sequence has a greater number of pegmatoid diorite dykes crosscutting the layered sequence compared to the Northern sequence; iii) The Northern sequence dip steeply to south, whereas the Southern one has a gentle dip to north; iv) differences in the Cr content, even on very primitive rocks, as exhibited in the Figure 14; v) several other coeval intrusions (e.g. Mangabal I and II, Água Fria, Adelandia, Fronteira Norte, Palmeiras, Palmito and Mata Rica – Figures 2 and 4) occur surrounding and adjacent to the ABC in less than dozen kilometers of distance.

The ABC does not show chilled–margin features, neither is the whole complex exposed, which would permit to infer the parental magma composition. However, there are some petrological and chemical characteristics which may be used to approximately constrain the nature of the parental magma, which they are:

i)   Olivine of the Southern and the Northern sequences has forsterite contents ranging from 62 to 81 mole % (Nilson, 1981).

ii) Assuming that the Northern and Southern sequences were formed from similar parental magmas, the compound bulk composition of the intrusion would be within the range of 40% gabbronorite, 25% pyroxenite, and 35% peridotite and dunite.

iii) Based on petrographic observations, the sequence of cumulus phase crystallization was ol+chr => ol+cpx+chr => ol+cpx+opx => cpx+opx => opx+plg+cpx (see Figure 6).

iv) The rocks of ABC show low TiO_2 (< 1 wt.%) and $Na_2O + K_2O < 1.8$ wt.%, excluded here the contaminated phlogopite-bearing rocks of top of Southern sequence.

v)   The orebodies of ABC have metal base and noble metal contents typicall of magmatic sulfides segregated from a primitive magma. These characteristics can be expressed by the Ni/Cu and Pd/Ir ratios for example.

Crystallization trends are deduced from the crystallization succession in the stratigraphic section of a layered intrusion. Distinct trends reflect different compositions of the parental magma and/or physical conditions of crystallization. Thus, the crystallization trend represents a fundamental characteristic of layered intrusions originated from similar parental magmas on specific tectonic settings. These

characteristics suggest that the parental magmas of the Northern and Southern sequences were primitive, with high Mg content, low total alkalis and TiO_2 content, indicating tholeiitic affinity. In this manner, the parental magma is probably similar to the one in the Skaergaard intrusion (McBirney, 1996), in the lower part of Bushveld Complex (Cameron, 1978) and in the Lower Series of the Niquelândia Layered Intrusion (Ferreira Filho *et al.*, 1998).

Shear zones limit the ABC to north and south, suggesting a ductile-brittle E-W tectonic activity after the complex crystallization. This activity might be responsible for the inverted position of the Northern sequence as well as to the Salgado's Fault development.

Ore genesis in ABC

The three orebodies S2, S1 and G2 show magmatic textures typical of sulfide liquid segregation from a mafic-ultramafic magma, that filled the spaces between the already crystallized cumulus phases. This process is evident from textures which exhibit intercumulus disseminated sulfides as observed in S1 orebody, intercumulus net-textured sulfides as in the G2 orebody, and a layer of massive sulfide grading to net-textured portions in the S2 orebody. Moreover, the orebodies have metal contents, specially Ni and Cu, comparable to other magmatic deposits on Earth (Figure 29). All ABC orebodies are hosted within the cumulus rocks in the layered intrusion. Apart from that, small droplets with MSS composition and sulfides included in silicate cumulus phases are present throughout the complex stratigraphy. In this manner, the orebodies formation was carried out by magmatic process within the magma chamber, during the fractionation process, and they are not related to other typical Ni-Cu deposits that are hosted in the base of intrusions or feeder zones. The orebodies of ABC have different characteristics suggesting that they were formed by different events of sulfide liquid segregation, each of them at distinct intervals of the stratigraphy.
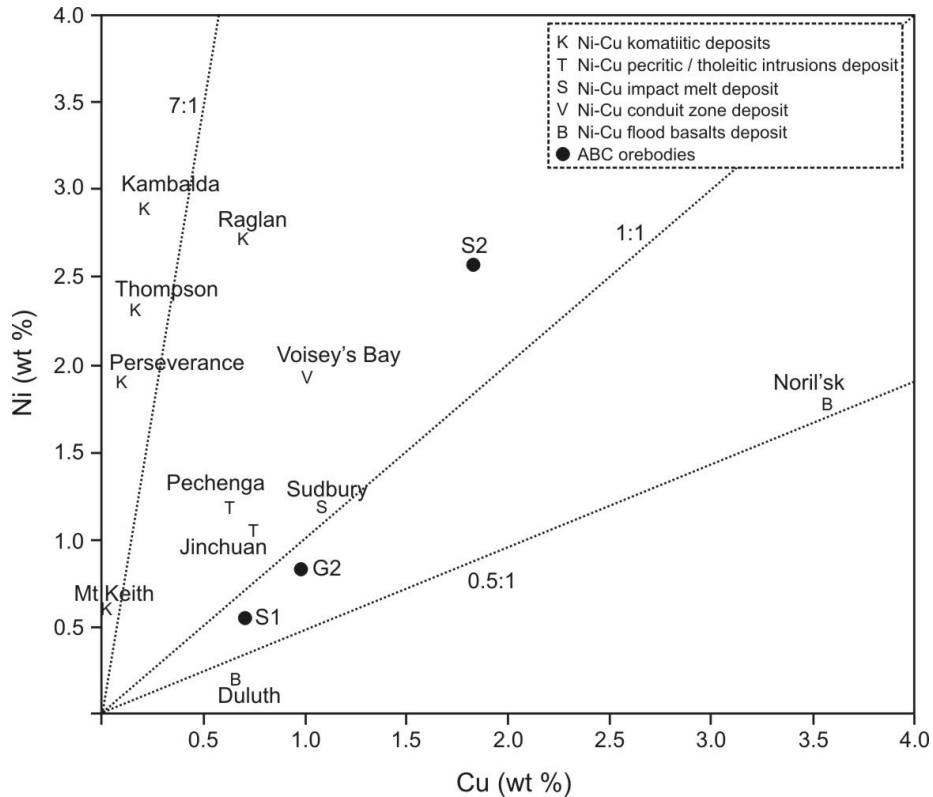
Figure 29 – Comparison of the Ni and Cu content from ABC orebodies with other world-class deposits. The Ni and Cu contents for the deposits are taken from Naldrett (2004).

The S2 Ni-Cu orebody is essentially a reef type deposit formed by a 2 meters thick layer of massive sulfide within and concordant to the stratigraphy of Northern sequence. The world's most important Ni-Cu deposits are also composed of massive sulfide masses which are located almost entirely at the base of their associated igneous bodies (Naldrett, 1999). In that manner, S2 is an uncommon orebody type, formed by very specific conditions. The lithological succession on the base of the Northern sequence exhibits homogeneous chromite dunite followed by the same rock but interlayered with metric wehrlite layers, where the S2 orebody layer occurs. To the top of it, the homogeneous chromite dunite is dominant again followed by the typical north sequence succession (e.g. wehrlite, lherzolite, websterite and gabbronorite). The whole rock geochemistry supports the proposed stratigraphy, showing reversals trends on Mg# and Cr (Figures 15a and 16a) with stratigraphy plots. This pattern might be related to a new magma influx associated with the S2 formation. This new influx is able to drive the system to sulfur supersaturation, sulfide liquid segregation and accumulation processes. This new magma influx was primitive (high-MgO), regarding the Mg# and Cr reversal trends, but probably, it was slightly contaminated with LREE (Figures 18, 19 and 20)

and incompatible elements such as alkalis (Figure 15c), Rb, Th and Ba (Figure 17a). As evident in Figure 28, it is likely that the pyrite-bearing gneiss country rock has contributed as contaminant into the new magma influx. The Figure 15b illustrates that the S content below the S2 orebody is quite constant with concentrations higher than 0.3 wt.%, and immediately above it, the S concentration in the rocks falls to S < 0.1 wt.%. This behavior suggests that the magma was S-saturated at the moment of the new magma influx, which is confirmed by the great amount of sulfide droplets in this portion. During the S2 orebody formation, the magma lost a great amount of S, and the following rocks have crystallized into a S-unsaturated environment.

The high water content of the ABC magma has probably contributed to the efficient sulfide accumulation on the chamber's base, thus to form the unusual massive to semi-massive sulfide reef type S2 orebody. The high water content of the magma lowers its viscosity (Giordanno *et al.*, 2004; Ardia *et al.*, 2008), facilitating the sulfide droplets to percolate downward.

The S2 orebody has high grade of Ni (2.6 wt.%) and Cu (1.83 wt.%), as well as high Ni/Cu ratio (Ni/Cu = 1.42), compared to other typical magmatic deposits around the world (Figure 29). The orebody plots above the Ni/Cu ratio 1:1 line, with grades of Ni and Cu higher than conduit deposits as Voisey's Bay (Li and Naldrett, 1999) or intrusion's base of Sudbury (Li *et al.*, 1992).

The Ni-Cu S1 orebody is a cluster of several irregular discontinuous orebodies adjacent to the pyrite-bearing gneiss unit, interpreted as a large fragment of country rock (e.g. pending roof) within the Southern sequence. Other smal gneiss fragments of about 20 cm in diameter are also present in the Southern sequence, showing irregular embayed contacts with the mafic and ultramafic rocks. The host rocks of this orebody are websterite and gabbronorite, both rich in amphibole oikocrysts and phlogopite-bearing and varying from meso to orthocumulate texture. In part, this is similar to the Voisey's Bay mafic magma conduit structure that hosts world class Ni-Cu deposit, which was probably formed as a result of country rock assimilation. Naldrett (1999) describes numerous partially reacted inclusions of gneiss (interbanded garnet-sillimanite and quartzo-feldspathic gneisses) in a matrix of norite or troctolite accompanied by variable amounts of sulfide and a variable texture rocks.

The S1 is the only orebody with pyrite as part of the sulfide fraction. This mineral is formed by embayed rounded crystals surrounded by the pyrrhotite-chalcopyrite-pentlandite association. This feature suggests reaction of early crystallized

72

pyrite with the later sulfides. This reaction is probably similar to the one described by Ripley (1981) as follows: $FeS_2 + 3H_2O + {}^5/_2C = FeS + CH_4 + {}^3/_2CO_2 + H_2S$. On that case the reaction proceeds at temperature less than 400°C. The geochemical data points out that the trends along the stratigraphy for several elements are interrupted on the S1 orebody portion, where the complex samples plot close to the pyrite-bearing gneiss samples. These tendencies of overlapping the gneiss field are well represented by the sum of alkalis ($K_2O + Na_2O$), LREE, Ba, Rb, Th, Nb and Sr elements (Figures 13c, 14c, 15, 16, 17 and 18). This association of elements is typical for crustally contaminated magmas (Lightfoot *et al.*, 1990. Li *et al.*, 2000). The isotopic data also shows the same tendency, displayed on the $\delta^{34}S$ and εNd plots. These data remark that the S1 orebody was formed by a restricted pyrite-bearing gneiss partial melting, assimilation and mixture with the mafic magma. This process has inputed to the mafic magma some amount of alkalis, Ba, LREE, incompatible trace elements and S. As such, the siliceous and sulfur restricted assimilation has played a role to drive the system to sulfur supersaturation and S1 orebody formation (Figure 30).
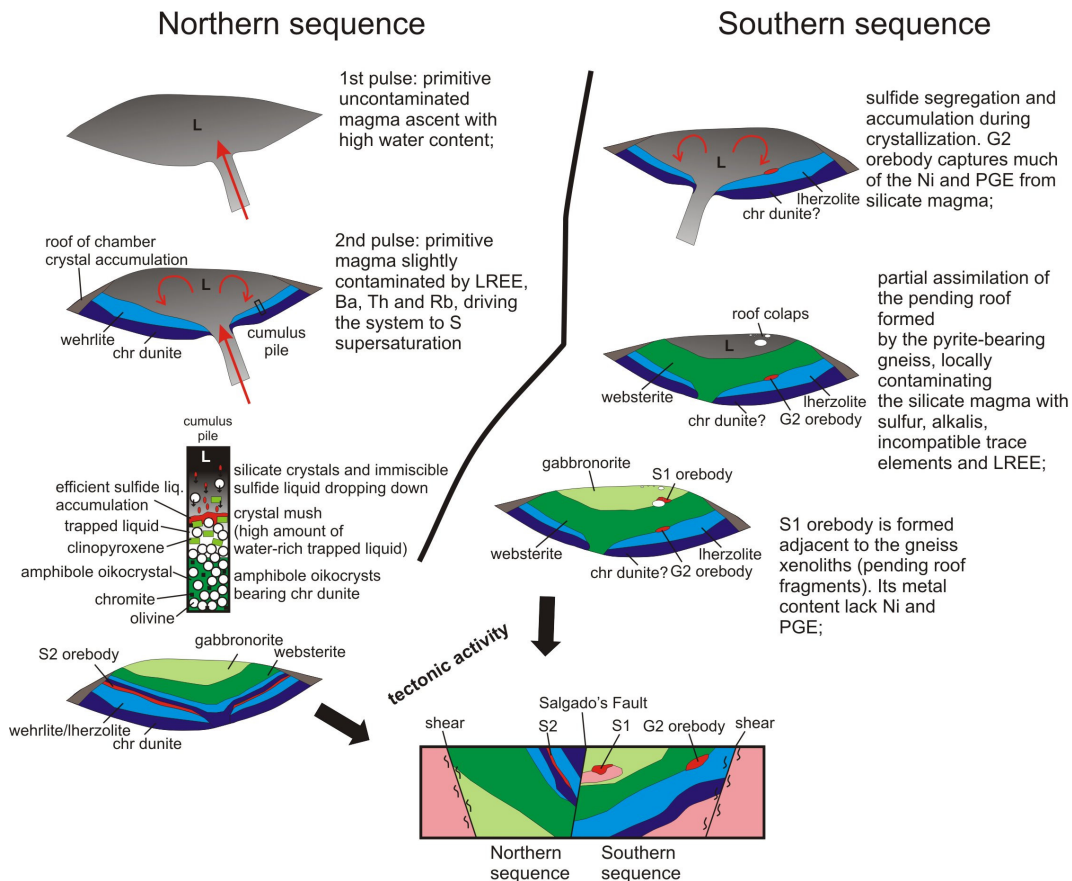
Figure 30 – Schematic evolution of ABC and its orebodies. Note that "L" means liquid.

This interpretation follows the classical Voisey's Bay intrusion, that has trace element, Re-Os and S and O isotope data, and mineralogical studies indicating that the magma pulses interacted with country gneiss, extracting SiO_2, Na_2O, K_2O and possibly sulfur from the gneiss, which accounts for the magma becoming sulfide saturate (Ryan, 1995; Naldrett, 1999); eventually leading to silicious and sulfur contaminations. Although, different from the presence of paragneiss in the Voisey's Bay's contry rocks, the S1 ore deposit country rocks are formed by juvenile island arc tonalitic gneiss.

The contamination of mafic magma by crust may play a significant role in the generation of large, sulfide-rich magmatic Cu-Ni-PGE deposits (Naldrett, 1966; Li *et al.*, 2002). The ABC shows a typical mantle derived sulfur signature, and no important contamination related to marine (meta-) sedimentary rocks could be identified. However, the S1 ore deposit shows restricted pyrite-bearing country rock assimilation, but it has not affected the whole magma chamber.

The Figure 29 shows that S1 orebody plots between the 1:1 of Sudbury and 0.5:1 of Noril'sk tie lines for Ni/Cu ratio. This is consistent with the idea that S1 orebody was formed from a more fractionated and metal depleted magma. The stratigraphic column and the proposed ABC evolution (Figure 6 and 30) show that G2 orebody was formed prior to S1 orebody during the Southern sequence crystallization. This fact was probably determinative to promote lack of Ni and PGE in the environment of the S1 orebody formation. Although, on the time of S1 orebody crystallization, the surrounding silicate magma still had regular amounts of Cu and Au, what is registred on the orebody metal contents (Figure 21 and 22).

The G2 orebody is smaller than the others and is concordant to the complex layering on the most ultramafic portion exposed of the Southern sequence. Its Ni/Cu ratio and PGE content are much higher than the S1 (Figure 21 and 22).

Apart from the regular orebodies mineralogy and textures in ABC, the S2 and G2 orebodies have chalcopyrite- and PGE-enriched zones that are usually segregated from the main ore towards the barren host rocks. These zones occur in the base of the massive sulfide portion of the G2 orebody and more often crosscutting or in the outer parts of the S2 orebody. The PGE analyses of one sample from this portion of the S2 orebody reveals lower values of Ni, Co, Os and Ir and higher values of Rh, Pt, Pd, Au and Cu compared to the regular (pyrrhotite-dominant) S2 orebody sample (Figure 24).

Aiming to understand this PGE zonation, it is worth to emphaze that PGE and Au have strong chalcophile behaviour. The coefficients governing the partition of these elements between the sulfide and silicate liquid, have a range from the order of 10^3 to 10^5 (Campbell and Barnes, 1984). Although the partition coefficient (K_D) between the monosulfide solid solution (MSS) and the sulfide liquid is different for each element. The experimental data reveal that Pt, Pd and Au have $K_{D(sulf.\ liq.\ /\ mss)}$ in the order of 10 to 10^2 counting in favor of the enrichment of these elements on the sulfide liquid phase (Fleet *et al.*, 1993; Li *et al.*, 1996; Barnes *et al.*, 2001). Rhodium, Ru, Ir and Os have the opposite behaviour, showing to be compatible with the MSS phase.

The origin of the compositional zonation is thought to be fractional crystallization of an Fe–Ni–Cu sulfide liquid, with the Fe-rich portions representing the mss cumulate and the chalcopyrite-rich portions the fractionated liquid (Distler 1994; Naldrett *et al.*, 1994; Zientek *et al.*, 1994).

The sulfide liquid fractionation has probably played a key role in S2 and G2 orebodies formation. The great amount of water-rich liquid on ABC system could promote a better fluid migration and segregation ("wetter" system – Naldrett *et al.*, 1999), allowing the formation of discordant ore clusters similar to the identified footwall deposit of the Subdury Complex (Naldrett *et al.*, 1982; Li *et al.*, 1992; Naldrett *et al.*, 1999). The Figure 31 displays the ABC orebodies and the S2 chalcopyrite-rich (or Cu-Pt-Pd-rich) portion in a Pd/Ir against Ni/Cu diagram.
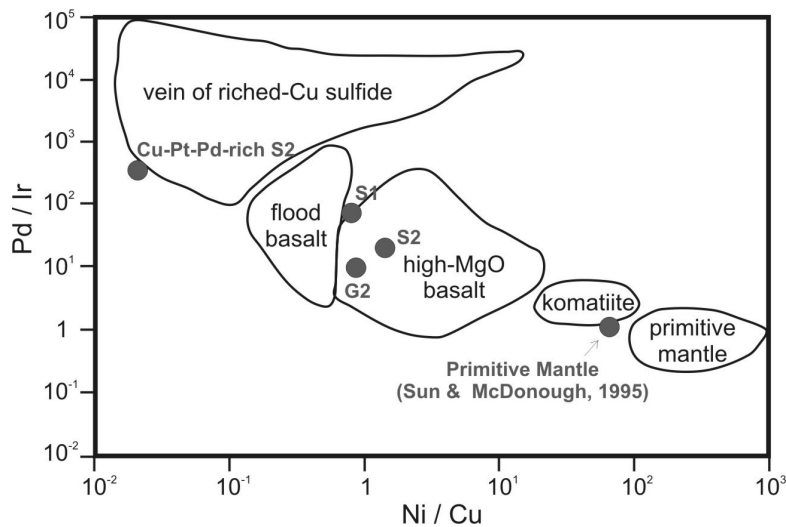
Figure 31 – Plot of Pd/Ir against Ni/Cu of the ABC orebodies and the Cu-Pt-Pd-rich portion of the S2 orebody. The outlines remark the typical magma or liquid types (Chai and Naldrett, 1992).

The ratios Cu/(Cu + Ni), (Pt + Pd)/Ir and Pd/Ir are different manners to measure the sulfide liquid fractionation (Li *et al.*, 1992; Barnes *et al.*, 1985). The G2 orebody has a Pd/Ir ratio of 10, the S2 has 20, S1 has 80 and the segregated chalcopyrite-rich portion of S2 orebody has 357 (Table 10). The PGE ore JM-reef of the Stillwater intrusion has a Pd/Ir ratio of 865 (Barnes *et al.*, 1985).

Naldrett and Duke (1980) use a different equation (Pt+Pd)/(Ru+Ir+Os) that can be applied to magmatic sulfide ores to predicted magma composition. They conclude that (Pt+Pd)/(Ru+Ir+Os) ratio <2.0 represents very primitive magmas (~ 20% MgO); ratios ~13 are more characteristic of gabbroid rocks that have crystallized from magmas containing less than 12% MgO. Finally, ratios between 5.2 and 7.3 in Ungava deposit seem consistent with magmas containing 16% MgO. On this classification, G2 (e.g. 6.3) and S2 (e.g. 6.8) orebodies fall within the Ungava deposit range where the authors conclude to be segregated from a 16 wt.% MgO magma. The S1 orebody cannot be classified by this equation, because its PGE content is too low that was not possible to determine the Ru and Os concentrations.

Conclusions

The conclusions are summarized as follows:

- The ABC makes part of a group of synorogenic mafic and mafic-ultramafic layered intrusions, hosted in a juvenile island arc of 890 – 800 Ma composed of magnetite series tonalitic rocks associated to the Neoproterozoic Brasiliano Orogeny. Quantitative age dates are available for six of the intrusions, all of them falling in the age range of 630 and 600 Ma;

- The complex can be divided into the Northern and Southern sequence. Both has similar crystallization trend, but differ from each other in several petrological characteristics. These sequences probably represent two different magma chambers tectonically juxtaposed side by side;

- The parental magma for ABC has a tholeiitic affinity, and comparing the PGE content in the ABC ore with other deposits worldwide the parental magma may contain *ca.* 16% MgO. The magma was extracted from the depleted mantle in a extensional tectonic event on the final stages of the Arenopolis Arc magmatic activity;

- ABC has three distinct magmatic Ni-Cu orebodies formed during crystallization of the magma chambers. The orebodies are hosted in different and specific stratigraphic intervals, and they are hosted within the cumulus pile, with no relation to feeder zones or intrusion's base;

- The S1 orebody, hosted in the uppermost part of the Southern sequence, was formed by localized country rock assimilation that is registered by crystallization of phlogopite in the gabbronorite and incorporation of K_2O, Na_2O, LREE, Ba, Rb, Th, Nb and Sr elements. The isotopic data register this contamination with more positive values of $\delta^{34}S$ and ϵNd;

- The S2 orebody, hosted in the bottom parts of Northern sequence, was probably formed during a new magma influx into the magma chamber. This new influx has higher anomalous content of LREE, Ba, Th and Rb, probably related to contamination by the juvenile gneiss country rocks. This massive sulfide layer might have formed in a very efficient process of sulfide accumulation. The low viscosity of the ABC magma (water-rich magma), indicated by the great amount of amphibole oikocrysts in the entire complex, has facilitated the sulfide liquid to percolate downward and accumulate efficiently in the cumulus pile;

- The G2 orebody, hosted in the bottom part of the Southern sequence, was formed during the fractionation of the Southern sequence prior to the S1 orebody formation. This process has caused that formation of the S1 orebody in a metal depleted system, with low contents of Ni, Pt and Pd;

- All the analyzed orebodies and droplets of ABC show mantle range signature for $\delta^{34}S$, indicating that none external source of sulfur related to marine sediments has contributed to the magma sulfur saturation. The only registered assimilation is related to the S1 orebody, but it is very restricted influenced by the pyrite-bearing gneiss country rock;

- The S2 orebody Cu-Pt-Pd-rich ore shoots to the outer parts of the main orebody is analogous to the footwall mineralization in Sudbury, being formed by the sulfide liquid fractionation from MSS. This sulfide liquid fractionation is also registred in the G2 orebody;

- The ABC and several other coeval intrusions of the Goias Magmatic Arc indicate that small, faulted and synorogenic mafic-ultramafic intrusions in the

region should not be overlooked for their potential to host economic Ni-Cu(-PGE) sulfide deposits.

Acknowledgements

References

Almeida FFM (1977) O Cráton do São Francisco. Revista Brasileira de Geociências 7(4):349-364

Almeida FFM, Hasui Y, Brito-Neves BB, Fuck RA (1981) Brazilian structural provinces: an introduction. Earth Sciences Review 17: 1–29

Ardia P, Giordano D, Schmidt MW (2008) A model for the viscosity of rhyolite as a function of H2O-content and pressure: A calibration based on centrifuge piston cylinder experiments. Geochim Cosmochim Acta 72(24):6103-6123

Baldwin JA, Brown M (2008) Age and duration of ultrahigh-temperature metamorphism in the Anápolis–Itauçu Complex, Southern Brasília Belt, Central Brazil – constraints from U–Pb geochronology, mineral rare earth element chemistry and trace-element thermometry. Journal of Metamorphic Geology 26:213-233

Barnes SJ, Naldrett AJ, Gorton MP (1985) The origin of the fractionation of platinum-group elements in terrestrial magmas. Chem Geol 53:303-323

Barnes SJ, Maier WD (1999) The fractionation of Ni, Cu and noble metals in silicate and sulphide liquids. In: Keays RR, Lesher CM, Lightfoot PC and Farrow CEG (eds.) Dynamic processes in magmatic ore deposits and their aplication in mineral exploration , Geological Association of Canada, Short course notes 13:69-106

Barnes S-J, Acterberg E, Makovicky E, Li C (2001) Proton probe results for partitioning of platinum-group elements between monosulphide solid solution and sulphide liquid. S Afr J Geol 104:275–286

Bendall C, Lahaye Y, Fiebig J, Weyer S, Brey GP (2006) In situ sulfur isotope analysis by laser ablation MC-ICPMS. Applied Geochemistry 21:782-787

Bender KM, Buhn BM, Mota-e-Silva J, Chaves JGS (2007) 32S/34S Isotope analyses by laser ablation MC-ICPMS: Method and application. VI South American Symposium on Isotope Geology, San Carlos de Bariloche, Argentina, 2008

Boyd R, Mathiesen CO (1979) The Nickel Mineralization of the Rona Mafic Intrusion, Norland, Norway. Can Mineral 17:287-298

Buchanan DL, Nolan J, Suddaby P, Rouse JE, Viljoen MJ, Davenport JWL (1981) The genesis of sulfide mineralization in a portion of the Potgietersrus Limb of the Bushveld intrusion. Econ Geol 76:568–579

Cameron EN (1978) The lower zone of the eastern Bushveld Complex in the Olifants river trough. Journal of Petrology 19:437-462.

Campbell IH, Barnes SJ (1984) Partition coefficients for platinum and palladium between immiscible sulfide and silicate liquids. Can Min 22:151-160

Chai G, Naldrett AJ (1992) Characteristics of Ni-Cu-PGE Mineralization and Genesis of the Jinchuan Deposit, Northwest China. Econ Geol 87:1475-1495

CPRM (2001) Mapa Geológico 1:1,000,000 do Programa de Levantamentos Básicos do Brasil, CD

Crocket JH (2002) Platinum-Group Element Geochemistry of Mafic and Ultramafic Rocks. In: Cabri LJ (ed) The Geology Geochemistry Mineralogy and Mineral Beneficiation of Platinum-Group Elements. Ottawa Ontario, Can Inst Min Met Special 54:177-210

Dardenne MA (2000) The Brasília fold belt. In: Cordani UG, Milani EJ, Thomaz Filho A, Campos DA (eds) Tectonic Evolution of South America. 31st International Geological Congress, Rio de Janeiro 231–263

Della Giustina MES, Oliveira CG, Pimentel MM, Buhn B (2009) Neoproterozoic magmatism and high-grade metamorphism in the Goiás Massif: New LA-MC-ICMPS U–Pb and Sm–Nd data and implications for collisional history of the Brasília Belt. Prec Res 172:67–79

Distler VV (1994) Platinum mineralization of the Noril'sk deposits. In: Lightfoot PC, Naldrett AJ (eds) Proceedings of Sudbury-Noril'sk symposium, Ont Geol Surv Spec 5:243–260

Evensen NM, Hamilton PJ, O'Nions RK (1978) Rare earth abundances in chondritic meteorites. Geochimica et Cosmochemica Acta 42:1199-1212

Ferreira VP, Tassinari CCG, Sial AN, Bittencourt JS, Babinski M (2007) Geoquímica isotópica e aplicações em prospecção geoquímica. In: Licht OAB, Mello CSB, Silva CR (eds) Prospecção Geoquímica: Depósitos Minerais Metálicos, Não-Metálicos, Óleo e Gás. CPRM and DEPAT Rio de Janeiro, Brazil, 780p

Ferreira Filho CF (1998). Geology and petrology of the large layered intrusions of Central Brazil: implications for PGE mineralization. In: Platinum Symposium, Rustemburg, South Africa, Extended Abstracts 107–110

Ferreira Filho CF, Naldrett AJ, Gorton MP (1998). REE and pyroxene compositional variation across the Niquelândia layered intrusion, Brazil: petrological and metallogenetic implications. Trans. Inst. Mining Metallurg. 107:B1–B21

Ferreira Filho CF, Pimentel, MM, Araújo SM, Laux JH (2009) Layered Intrusions and Volcanic Sequences in Central Brazil: Geological and Geochronological Constraints for Mesoproterozoic (1.25 Ga) and Neoproterozoic (0.79 Ga) Igneous Associations. Prec Res (submitted)

Fischel DP, Pimentel MM, Fuck RA (1998) Idade do metamorfismo de alto grau no Complexo Anápolis-Itauçu, determinada pelo método Sm-Nd. Revista Brasileira de Geociências 28(4):543-544

Fleet M, Chryssoulis SL, Stone WE, Weisener CG (1993) Partitioning of platinum-group elements and Au in the Fe–Ni–Cu–S system: experiments on the fractional crystallization of sulphide melt. Contrib Mineral Petrol 115:36–44

Fuck RA, Jardim de Sá EF, Pimentel MM, Dardenne MA, Soares ACP (1993) As faixas de dobramentos marginais do Cráton São Francisco: Síntese dos conhecimentos. In: Dominguez JML, Misi A (eds) O Cráton do São Francisco 161–185

Fuck RA, Pimentel MM, D'el Rey Silva LJH (1994) Compartimentação tectônica da porção oriental da província Tocantins. SBG, 38th Congresso Brasileiro de Geologia, Balneário Camburiú – SC 215–216

Fuck RA, Dantas EL, Pimentel MM, Junges SL, Moraes R (2001) Nd isotopes, U–Pb single grain and SHRIMP zircon ages from basement rocks from Tocantins Province. 3rd South American Symposium on the Isotope Geology, Pucón, Chile 141–144

Giblin PE (1984) Chapter 1, History of Exploration and Development, of Geological Studies and Development of Geological Concepts. In: The Geology and Ore Deposits of the Sudbury Structure, edited by EG Pye, AJ Naldrett, and PE Giblin, Ontario Geological Survey, Special Volume 1:3-23

Gioia SMCL (1997) Preparação da Metodologia Sm-Nd para Datação de Amostras Geológicas e sua Aplicação em Rochas das Áreas de Firminópolis, Fazenda Nova e Americano do Brasil – GO. Unpublished Master's Thesis

Gioia SMCL, Pimentel MM (2000) The Sm–Nd isotopic method in the Geochronology Laboratory of the University of Brasília. Ann Acad Bras Cienc 72:219–245

Giordano D, Romano C, Dingwell DB, Poe B, Behrens H (2004) The combined effects of water and fluorine on the viscosity of silicic magmas. Geochim Cosmochim Acta 68(24):5159–5168

Godlevsky MN, Grienko LN (1963) Some data on the isotopic composition of sulfur in the sulfides of the Noril'sk deposit. Geochemistry 1:335–341

Gorbachev NS, Grinenko LN (1973) The sulfur isotope ratios of the sulphides and sulphates of the Oktyabr'sk sulphide deposit, Noril'sk region, and the problem of its origin. Geokhimiya 8:1127–1136

Grinenko LN (1985) Sources of sulfur of the nickeliferous and barren gabbro-dolerite intrusions of the northwest Siberian platform. International Geology Review 28:695–708

Irvine TN (1975) Crystallization sequences of the Muskox intrusion and other layered intrusions: II. Origin of chromitite layers and similar deposits of other magmatic ores. Geochim Cosmochim Acta 39:991–1020

Junges SL, Pimentel MM, Moraes R (2002) Nd isotopic study of the Neoproterozoic Mara Rosa Arc, Central Brazil: implications for the evolution of the Brasília Belt. Prec Res 117:101–118

Keays RR, Lesher CM, Burnham OM (1997) Requirements for the formation of giant Ni–Cu–PGE sulfide deposits: the role of magma generation. EOS Trans 78:F799

Krogh TE, Davis DW, Corm F (1984) Precise U-Pb zircon and baddeleyite ages of the Sudbury Area. In: Pye EG, Naldrett AJ, Giblin, PE (eds) The Geology and Ore Deposits of the Sudbury Structure. Ontario Geological Survey, Special Volume 1:431-446

Lamberg P (2005) From genetic concepts to practice – Lithogeochemical identification of Ni-Cu mineralized intrusions and localizations of the ore. Bull of Geol Soc of Finl 402 264p

Laux JH, Pimentel MM, Dantas EL, Armstrong R, Armele A, Nilson AA (2004) Mafic magmatism associated with the Goiás Magmatic Arc in Anicuns region, Goiás, Central Brazil: Sm-Nd isotopes and new ID-TIMS and SHRIMP U-Pb data. Jour of South Amer Earth Sci 16:599–614

Laux JH, Pimentel MM, Dantas EL, Armstrong SA, Junges SL (2005) Two neoproterozoic crustal accretion events in the Brasília Belt, Central Brazil. Journal of South American Earth Sciences 18:183–198

Li C, Naldrett AJ (1999) Geology and petrology of the Voisey's Bay intrusion: Reaction of olivine with sulfide and silicate liquids. Lithos 47:1–31

Li C, Naldrett AJ, Coats CJA, Johannessen P (1992) Platinum, Palladium, Gold and Cooper-Rich Stringers at Strathcona Mine, Sudbury: Their Enrichment by Fractionation of a Sulfide Liquid. Econ Geol 87:1584-1598

Li C, Barnes S-J, Makovicky E, Rose-Hansen J, Makovicky M (1996) Partitioning of Ni, Cu, Ir, Rh, Pt and Pd between monosulfide solid solution and sulfide liquid: effects of composition and temperature. Geochim Cosmochim Acta 60:1231–1238

Li C, Lightfoot PC, Amelin Y, Naldrett AJ (2000) Contrasting petrological and geochemical relationships in the Voisey's Bay and Mushuau intrusions, Labrador, Canada: Implications for ore genesis. Econ Geol 95(4):771-799

Li C, Ripley EM, Maier WD, Gomwe TES (2002) Olivine and sulfur isotopic compositions of the Uitkomst Ni–Cu sulfide ore-bearing complex, South Africa: evidence for sulfur contamination and multiple magma emplacements. Chem Geol 188:149–159

Li C, Ripley EM, Naldrett AJ (2003) Compositional variations of olivine and sulfur isotopes in the Noril'sk and Talnakh Intrusions, Siberia: implications for ore-forming processes in dynamic magma conduits. Econ Geol 98:69–86

Lightfoot PC, Naldrett AJ, Gorbachev NS, Doherty W, Federenko VA (1990) Geochemistry of the Siberian trap of the Noril'sk area, USSR, with implications for the relative contributions of crust and mantle to flood basalt magmatism. Contrib Mineral Petrol 104: 631-644

McBirney AR (1996) The Skaergaard Intrusion. In: Cawthorn RG (ed) Layered Intrusions, Developments in Petrology, Elsevier, 15:147-180

McDonough WF, Sun S-S (1995) The composition of the earth. Chem Geol 120:223–253

Metago (1978) Complexo máfico ultramáfico de Americano do Brasil. Relatório de pesquisa DNPM, unpublished

Moraes R, Brown M, Fuck RA, Camargo MA, Lima TM (2001) The evolution of melt-bearing UHT metamorphic mineral assemblages and construction of P-T paths: an example from Central Brazil. Jour of Met Geol 43(9):1673-1705

Mungall JE, Andrews DRA, Cabri LJ, Sylvester PJ, Tubrett M (2005) Partitioning of Cu, Ni, Au, and platinum-group elements between monosulfide solid solution and sulfide melt under controlled oxygen and sulfur fugacities. Geochim Cosmochim Acta 69:4349–4360

Naldrett AJ (1966) The role of sulphurization in the gneiss of iron-nickel sulphide deposits of the Porcupine district, Ontario. Trans LXIX:147-155

Naldrett AJ (1973) Nickel Sulfide Deposits – Their Classification and Genesis, with special emphasis on Deposits of Volcanic Association. CIM Bull. 66:45-63

Naldrett AJ (1989) Magmatic Sulfide Deposits. Claredon Press. Oxford University Press 186p

Naldrett AJ (1999) World-class Ni-Cu-PGE deposits: key factors in their genesis. Mineralium Deposita 34:227-240

Naldrett AJ (2004) Magmatic Sulfide Deposits – Geology, Geochemistry and Exploration. Germany, Springer Berlin 724p

Naldrett AJ, Duke JM (1980) Platinum metals in magmatic sulfide ores. Science 208:1417-1424

Naldrett AJ, Innes DG, Sowa J, Gorton MP (1982) Compositional Variations within and between 5 Sudbury ore-deposits. Econ Geol 77(6):1519-1534

Naldrett AJ, Rao BV, Evensen NM (1986) Contamination at Sudbury and its role in ore formation. In: Gallagher MJ, Ixer R, Neary CR, Pritchard HM (eds) Metallogeny of Basic and Ultrabasic Rocks. Spec. Pub. Inst. Min. Metal., London 75–92

Naldrett AJ, Asif M, Gorbachev NS, Kunilov VYe, Stekhin AI, Fedorenko VA, Lightfoot PC (1994) The composition of the Ni-Cu ores of the Oktyabr'sky deposit, Noril'sk region. In: Lightfoot PC, Naldrett AJ (eds) Proceedings of Sudbury-Noril'sk symposium, Ontario Geol Surv Spec 5:357–373

Naldrett AJ, Asif M, Schandl E, Searcy T, Morrison GG, Binney WP, Moore C (1999) Platinum-group elements in the Sudbury ores: Significance with respect to the origin of different ore zones and to the exploration for footwall orebodies. Econ Geol 94(2):185-210

Nilson AA (1981) The nature of Americano do Brasil mafic-ultramafic complex and associated sulfide mineralization, Goiás, Brazil. PhD Thesis, University of Western Ontario 460p

Nilson AA, Santos MM, Cuba EA, Sá CMG (1986) Jazida de níquel, cobre e cobalto de Americano do Brasil, Goiás. In: Schobbenhaus C, Coelho CES (eds) Principais Depósitos Minerais do Brasil II:257-273

Pearce JA (2008) Geochemical fingerprinting of oceanic basalts with applications to ophiolite classification and the search for Archean oceanic crust. Lithos 100:14–48

Pimentel MM, Fuck RA (1992) Neoproterozoic crustal accretion in Central Brazil. Geology 20:375–379

Pimentel MM, Heaman L, Fuck RA (1991) Zircon and sphene Pb–U geochronology of Upper Proterozoic volcanic-arc rock units from southwestern Goiás, Central Brazil. Journal of South American Earth Sciences 4:329–339

Pimentel M.M., Fuck RA, Silva JLH (1996). Dados Rb–Sr e Sm–Nd da região de Jussara-Goiás-Mossâmedes (GO), e o limite entre terrenos antigos do Macicço de Goiás e o Arco Magmático de Goiás. Rev Bras Geociências 26:61–70

Pimentel MM, Whitehouse MJ, Viana MG, Fuck RA, Machado N (1997) The Mara Rosa arc in the Tocantins Province: further evidence for Neoproterozoic crustal accretion in Central Brazil. Prec Res 81:299–310

Pimentel MM, Fuck RA, Jost H, Ferreira Filho CF, Araújo SM (2000). The basement of the Brasília Fold Belt and the Goiás Magmatic Arc. In: Cordani, UG, Milani EJ, Thomaz Filho A, Campos DA (eds) The Tectonic Evolution of South America, Rio de Janeiro. Proceedings of the 31st International Geological Congress 195–229

Pimentel MM, Laux JH, Hollanda MHBM, Gioia SMCL (2003). The Brasília Belt as a "HotOrogen": new SHRIMP and conventional U–Pb data and Sm–Ndisotopic constraints from terminal mafic

magmatism in central-western Goiás. In: Proceedings of the III International Symp. on Tectonics, Búzios, Brazil, Anais 21-23.

Pimentel MM, Ferreira Filho CF, Armstrong SA (2004) SHRIMP U–Pb and Sm–Nd ages of the Niquelândia layered complex: Meso- (125 Ga) and Neoproterozoic (079 Ga) extensional events in Central Brazil. Prec Res 132:133–153

Pimentel MM, Ferreira Filho CF, Armele A (2006). Neoproterozoic age of the Niquelândia Complex, Central Brazil: further ID-TIMS and Sm–Nd isotopic evidence. J South Am Earth Sci. 21:228–238

Piuzana D, Pimentel MM, Fuck RA, Armstrong RA (2003) Neoproterozoic granulite facies metamorphism and contemporaneous granite magmatism in the Brasília Belt, Central Brazil: regional implications of new SHRIMP U–Pb and Sm–Nd data. Prec Res 125: 245–273

Ripley EM (1981) Sulfur isotopic studies of the Dunka Road Cu–Ni deposit, Duluth intrusion, Minnesota. Econ Geol 76:610–620

Ripley EM, Park Y-R, Li C, Naldrett AJ (1999) Sulfur and oxygen isotopic evidence of country rock contamination in the Voisey's Bay Ni–Cu–Co deposit, Labrador, Canada. Lithos 47:53–68

Ripley EM, Li C (2007) Applications of Stable and Radiogenic Isotopes to magmatic Ni-Cu-PGE Deposits: Examples and Cautions. Earth Science Frontiers 14(5):124–132

Ryan B, Wardle R, Gower C, Nunn G (1995) Nickel–copper sulfide mineralization in Labrador: the Voisey Bay discovery and its exploration implications. Current Research Newfoundland Department of Natural Resources, Geological Survey Report 95-1:177–204

Song X-Y, Zhou M-F, Wang CY, Qi L (2006) Role of crustal contamination in formation of the Jinchuan intrusion and its world-class Ni-Cu-(PGE) sulfide deposit, NW China. Int. Geol. Rev. 48:1113–1132.

Sun SS, McDonough WF (1989) Chemical and isotopic systematics of oceanic basalts: implications for mantle composition and processes. In: Saunders AD, Norry MJ (eds) Magmatism in the Ocean Basins, Geological Society Special Publication 42:313-345.

Tang Z, Yan H, Jiao J, Pan Z (2007) Regional Metallogenic Controls of Small-intrusion-hosted Ni-Cu (PGE) Ore Deposits in China. Earth Science Frontiers 14(5):92–103

Thompson RN (1982) British Tertiary Volcanic Province. Scot J Geol 18:49-107

Tucker RD, Boyd R, Barnes S-J (1990) A U-Pb zircon age for Rona intrusion, N Norway: New evidence of basic magmatism in the Scandinavian Caledonides in Early Silurian time. Norsk Geologisk Tidsskrift 70:229-239

Votorantim Metais (2007) Geological model of Americano do Brasil ore deposits. Unpublished internal report

Zientek ML, Ripley EM (1990) Sulfur isotope studies of the Stillwater intrusion and associated rocks, Montana. Econ Geol 85:376–391

Zientek ML, Likhachev AP, Kunilov VE, Barnes S-J, Meier AL, Carlson RR, Briggs PH, Fries TL, Adrian BM (1994) Cumulus processes and the composition of magmatic ore deposits: examples from the Talnakh district, Russia. In: Lightfoot PC, Naldrett AJ (eds) Proceedings of the Sudbury-Noril'sk Symposium. Ontario Geological Survey, Spec. 5:373–392

CONCLUSÕES

A pesquisa realizada chegou a um conjunto de conclusões, que incluem o que já foi exposto de forma detalhada no artigo, que podem ser sintetizadas nos seguintes tópicos:

1. O complexo AB é uma das 15 intrusões identificadas como provavelmente associadas a um único grupo de intrusões sinorogênicas maficas e maficoultramáficas acamadadas com idades entre 600 e 630 Ma no Arco Magmático de Arenópolis (porção sul do Arco Magmático de Goiás) e Complexo Anápolis-Itauçú, na Faixa Brasília. Essas intrusões são principalmente intrusivas nos magnetita tonalitos da fase arco de ilha oceânico do arco (800 – 890 Ma). Essas 15 intrusões conformam um atrativo prospecto no que diz respeito ao potencial para depósitos magmáticos (e.g. Ni-Cu, PGE-Ni, Fe-Ti-V e Cu-Au);

2. O complexo AB é subdividido em 2 seqüencias: a norte e a sul. Na sequência sul afloram, majoritariamente, as unidades máficas e websteritos, enquanto que na norte, principalmente as unidades ultramáficas, apesar de ambas apresentarem o mesmo sequênciamento na cristalização das fases cúmulus. Uma série de características petrologicas e metologenéticas que distinguem as duas seqüencias, nos faz acreditar que as seqüências representam duas câmaras magmáticas distintas. Todavia, a hipótese de tratar-se de diferentes porções de uma mesma câmara tectonicamente colocadas lado-a-lado, não pode ser descartada. Estudos posteriores, utilizando-se a variação críptica das diferentes fases cúmulus ao longo da estratigrafia, poderão elucidar melhor essa questão;

3. O complexo AB é marcado, em suas duas sequências e por todas as suas camadas, por constantes e grandes quantidades de anfibólio intercúmulus com inclusões, conhecidos na literatura por *oikocrysts*. Este tipo de textura evidencia a grande quantidade de líquido intercúmulus com água existente no processo de cristalização deste complexo. Na literatura existem inúmeros trabalhos evidenciando que a presença de água faz com que a viscosidade do magma seja diminuída;

4. A sequência norte apresenta camadas com forte mergulho para sul, deste modo com dunito no topo e gabronorito na base. Além disso, texturas que gradam de sulfeto maciço a dunito estéril (comparáveis ao "billiard ball" de Naldrett, 1973 – referência citada no artigo da dissertação) na base do corpo de minério S2

reforçam a hipótese de que a sequência apresenta-se invertida. A sequência sul, por sua vez, mostra-se em posição normal com suave mergulho para norte;

5. Todos os 3 corpos de minério do complexo AB apresentam texturas magmáticas claras: sulfeto maciço com rara olivina e agregados de olivina, net-textured (sulfeto intercúmulus > 20%) e disseminado (sulfeto intercúmulus <20%). Além disso, ocorrem no complexo, pequenas porções arredondadas de sulfetos (*droplets*) formados por pirrotita, calcopirita e pentlandita, interpretados como gotas imiscíveis, e pequenas inclusões dessas em fases cúmulus. Essas características associadas à geometria de camada do S2 e às características geoquímicas dos corpos mostram que todos eles estão localizados dentro da câmara magmática, formados durante o fracionamento magmático e posicionados em diferentes níveis estratigráficos da pilha cumulática;

6. Nas adjacências do corpo de minério S1, ocorre por centenas de metros um bloco de gnaisse hidrotermalizado e com pirita. Este gnaisse também ocorre como xenólitos decimétricos nesta porção do complexo AB. Conforme mostrado pela geoquímica de rocha total esta rocha foi parcialmente assimilada pelo magmatismo básico, exercendo papel de fornecedor de K_2O, NaO, Ba, LREE e S para o magma básico. Este processo tem a condição de saturar o magma básico em S e assim promover a segregação de sulfetos. O corpo de minério S1 foi formado neste contexto, conforme reforçado pelos dados de isótopos de S;

7. Os isótopos de S mostram assinatura de origem mantélica para os sulfetos do Complexo AB, com δ^{34}S entre -3 e +3 ‰ (CDT). Deste modo, o único processo de assimilação de fonte externa de S foi a interação com rochas encaixantes na região do corpo de minério do S1;

8. O corpo de minério S2 é formado por típica associação de sulfetos MSS com pirrotita > pentlandita > calcopitira. O corpo de minério G2, também apresenta típica associação de sulfetos MSS, porém menos rica em Ni com pirrotita > calcopirita > pentlandita. Já o corpo de minério S1 apresenta composição diferente com pirrotita > pirita > calcopirita > pentlandita. Neste caso a pirita aparece como grandes cristais arredondados e com golfos de corrosão, sugerindo uma formação anterior à de outras fases sulfetadas. Os isótopos de enxofre reforçam essa idéia, evidenciando valores de δ^{34}S sistematicamente +1.5 ‰ (CDT) em relação à pirrotita, pentlandita e calcopirita. A presença de pirita no

corpo S1 deve estar ligada à alta fS$_2$ no momento da assimilação do gnaisse encaixante com pirita;

9. A geoquímica de rocha total, principalmente no que diz respeito ao índice Mg# e ao elemento Cr marca na seqüência norte um claro *trend* de fracionamento partindo de dunitos até gabronoritos. Todavia, o corpo de minério do S2 marca um nível da câmara com um restrito *trend* reverso, que pode estar ligado ao processo de reinjeção de um novo magma primitivo no sistema. Este processo pode ter levado a câmara à saturação em S e deposição do corpo de minério do S2. Este novo influxo de magma apresenta assinatura geoquímica com contaminação por elementos terras raras leves, Ba, Th e Rb. Estudos posteriores, utilizando-se de variação críptica das diferentes fases cúmulus ao longo da estratigrafia, poderão confirmar essa hipótese;

10. O corpo de minério S2 é um tipo *reef* maciço, com geometria de camada, o que não é típico em outros depósitos magmáticos Ni-Cu. Esta particularidade do S2 pode ser conseqüência da segregação de sulfetos em condições de reinjeção de magma primitivo, somada à grande presença de líquidos e água, que é característica do complexo AB. Dentro deste cenário, a acumulação de sulfetos no fundo da câmara pode ter sido facilitada, uma vez que poucas fases cúmulus estavam formadas e assim permitindo a eficiente "descida" das gotículas (do inglês *droplets*) de sulfeto através de um líquido de baixa viscosidade;

11. O corpo de minério S1 tem uma quantidade de Ni, Pt e Pd muito menor que S2 ou G2. O S1 ocorre nas porções de topo da seqüência sul, onde provavelmente o magma já estava empobrecido em metais nobres, uma vez que corpos de minério como o G2 devem ter "sequestrado" estes elementos nas porções mais basais. A falta de níquel explica-se pela grande quantidade de olivina cristalizada também nas porções mais basais desta seqüência;

12. O corpo de minério S2 apresenta porções ricas em calcopirita nas bordas do corpo de minério principal ou segregada em meio às rochas hospedeiras. Este tipo de minério assemelha-se ao *offshot* de Sudbury, Canadá, onde durante o fracionamento do líquido sulfetado, uma porção de líquido migra para fora do corpo principal deixando para trás o MSS (*Monosulfide Solid Solution*). Esta porção de líquido que migra é enriquecida em elementos incompatíveis. Nas porções ricas em calcopirita do S2, vê-se um enriquecimento em Rh, Pt, Pd, Au e Cu, em detrimento ao empobrecimento em Ni, Co, Os e Ir;

13. A implantação de análises de isótopos de S *in-situ* no equipamento LA-MC-ICPMS (ver Anexo II) no Laboratório de Geocronologia do IG/UnB foi conduzido pela doutoranda Karin M. Bender, pelo autor e, principalmente, pelo Prof. Dr. Bernhard Buhn. Vale ressaltar, que a primeira comunicação científica a respeito desse feito é de Bender, K.M., Buhn, B.M., Mota-e-Silva, J., Chaves, J.G.S (2008). Foram estabelecidos dois padrões internos, calcopirita e pirita, com erros 1σ (‰) de 0,23 e 0,26 no $\delta^{34}S$ respectivamente em acurácia e precisão. A aplicação deste método encontra-se detalhada em anexo ao corpo principal deste trabalho;

14. A experiência com utilização de ataque brando (ou seletivo – ver Anexo I) para abertura exclusiva da fração sulfetada teve sucesso parcial. O método tem uma grave limitação no que diz respeito a abertura da estrutura da pirita, dificultando o estudo geoquímico de depósitos minerais que contenham este mineral. Caso a pirita não esteja presente na fração sulfetada, o ataque brando torna-se uma ferramenta eficiente para estudo da geoquímica de gotículas de sulfeto ou da fração sulfetada de rochas com pequenas quantidades de sulfetos. Este estudo pode contribuir para o melhor entendimento da evolução do magma silicático durante o fracionamento magmático em complexos máficos acamadados.

Desta maneira, o presente trabalho procurou contextualizar o complexo AB dentro de uma geologia mais regional e, mais localmente, contribuir para o entendimento de sua gênese, evolução e metalogênese. A dissertação abordou, mais fortemente, a questão econômica, destacando a origem e as características dos corpos de minério. Trabalhos futuros utilizando-se de microssonda eletrônica nas fases cúmulus ao longo da estratigrafia, certamente trarão à luz mais elementos sobre a evolução magmática desta intrusão.

Fica destacado também o grande potencial metalogenético para depósitos magmáticos desta região do Estado de Goiás. Este grande conjunto de rochas MUM ainda carece de estudos mais sistemáticos, visando gerar um arcabouço de conhecimento que nos permita fazer correlações mais claras entre cada uma dessas intrusões. Com o incremento das pesquisas e do conhecimento geológico nesta região, certamente mais potenciais para prospecção de riquezas minerais irão surgir, e assim, quem sabe diminuir o risco de estarmos fechando os ouvidos para aquilo que a Terra, através das rochas, está tentando nos dizer.

ANEXOS

Anexo 1 - Análise Seletiva de Sulfetos

Análise seletiva de sulfetos é uma ferramenta amplamente utilziada por empresas que trabalham com depósitos minerais magmáticos Ni-Cu de baixo teor. Depósitos deste tipo têm teores de Ni sulfetado (recuperável) usualmente entre 0,2 e 1,0 (% peso). A soma do Ni contido nas fases minerais silicáticas (não recuperável) da rocha hospedeira pode chegar a um teor ~ 0,3 (% peso), o que pode ser significativo comparado a ordem de grandeza dos teores de depósitos de baixo teor. Por esse motivo, um método que abra somente a estrutura dos sulfetos para posterior análise química pode ser muito útil.

Neste trabalho realizado no complexo AB, foi separada uma fração de ~ 0,5 kg, a partir das mesmas amostras utilziadas pelos outros métodos analíticos, para análise seletiva de sulfetos. O objetivo central da utilização deste método, foi determinar a composição química dos *droplets* (gotas) de sulfeto nas rochas estéreis, ou seja, fora dos corpos de minério. Os *droplets* representam a química da fração sulfetada que estava em equilíbrio com o magma silicático, uma vez que, eles conformam um corpo muito pequeno frente à grande quantidade de magma silicático no entorno (para uma revisão veja Naldrett, 2004). Essas rochas estéreis possuem quantidades muito pequenas de sulfeto (~ 1 % vol.) e certamente possuem quantidades significativas de Ni contido nos silicatos, de forma que seria muito difícil, e provavelmente irreal, fazer um balanço de massa para recalcular o Ni, Cu, Fe e Co contidos na fração sulfetada.

A análise seletiva de sulfetos deste trabalho foi realizada pelo laboratório Labtium Oy, Finlândia. A abertura das amostras foi dada através de lixiviação utilizando-se do solvente orgânico bromo-metanol (*bromine-methanol* – em inglês). Esta lixiviação dissolve totalmente os sulfetos deixando os silicatos intocados, com exceção da pirita que, em média, tem apenas 7 % de sua massa dissolvida. Por fim, a solução com os sulfetos dissolvidos foi analisada em por espectômetria de absorção atômica em chama (FAAS - *Flame Atomic Absorption Spectrometry*), que determinou as concentrações de Ni, Cu, Fe e Co. Esses metais são os principais constituintes de sulfetos magmáticos, sendo que através de suas concentrações, é possível montar a composição modal mineralógica da fração sulfetada. O método de abertura e análise seletiva de sulfetos através do bromo-metanol foi descrito por Penttinen *et al.* (1977).

A Tabela 13 mostra a composição típica dos sulfetos que comumente formam a assembléia sulfetada de sistemas magmáticos máficos ou ultramáficos. Nesta tabela o

cobalto não é parte constituinte de nenhuma das quatro fases minerais, afinal ele funciona como elemento traço neste sistema. Nilson (1981) mostra que o cobalto contribui com até 2,1 (% peso) na estrutura das pentlanditas do complexo de AB.

Tabela 13 – Principais minerais constituintes da fração sulfetada de origem magmática (dados de www.webmineral.com, acesso em 01/02/2009). Notar que os dados estão em % de peso atômico.

	S	Ni	Cu	Fe	Co	TOTAL
pirrotita	37,67			62,33		100,00
calcopirita	34,94		34,63	30,43		100,00
pentlandita	33,23	34,21		32,56		100,00
pirita	53,45			46,55		100,00

Vale lembrar que a pirita não é um típico mineral da associação magmática em sistemas máficos, estando ela relacionada a processos secundários ou de contaminação crustal (revisão em Naldrett, 2004). Este mineral foi incluído nesta lista devido a sua forte presença nos porções de topo da Sequencia Norte do complexo AB, inclusive no corpo de minério S1.

Os resultados relativos às análises com ataque seletivo estão listados na Tabela 14, enquanto que os resultados das análises feitas em rocha total sem ataque seletivo estão expostos na Tabela 15. Para efeito de comparação do método bromo-metanol com a convencional geoquímica de rocha total, foi plotado na Figura 01 gráfico comparativo. O elemento Cu foi escolhido para tal comparação, pois este se comporta como elemento exclusivamente calcófilo, estando portanto somente relacionado à quantidade de calcopirita na rocha.

Tabela 14 – Concentração de metais em rocha total em análise de ataque seletivo com método bromo-metanol (Penttinen *et al.*, 1997).

Field_code	CMJ042	CMJ041	CMJ038	CMJ036	CMJ028	CMJ032	CMJ014	CMJ012	CMJ009
Rock	GT	GT	PX	PD	DU	DU	PD	PD	DU
orebody sequence	N	N	N	N	N	N	N	N	N
Ni (wt %)	0.006	0.006	0.009	0.014	0.221	0.054	0.140	0.034	0.099
Cu (wt %)	0.012	0.015	0.008	0.008	0.455	0.031	0.367	0.077	0.160
Co (wt %)	0.001	0.001	0.001	0.002	0.013	0.007	0.008	0.004	0.010
Fe (wt %)	0.306	0.355	0.235	0.291	2.150	0.388	1.110	0.334	0.521

Field_code	CMJ005	CMJ100	CMJ103	CMJ106	CMJ108	CMJ109	CMJ111	CMJ113	CMJ115
Rock	DU	PX	PX	PX	PX	PX	PX	PX	GN
orebody				S1	S1	S1			
sequence	N	S	S	S	S	S	S	S	S
Ni (wt %)	0.040	0.008	0.019	0.365	0.110	0.263	0.019	0.049	0.002
Cu (wt %)	0.003	0.019	0.019	0.604	0.137	0.431	0.028	0.098	0.036
Co (wt %)	0.004	0.001	0.002	0.005	0.005	0.009	0.001	0.004	0.001
Fe (wt %)	0.436	0.154	0.293	1.780	1.480	5.140	0.309	1.600	0.341

Field_code	CMJ508	CMJ509b	CMJ510b	CMJ511a	CMJ516
Rock	GT	GT	GT	GT	PD
orebody					
sequence	S	S	S	S	S
Ni (wt %)	0.007	0.004	0.020	0.004	0.037
Cu (wt %)	0.012	0.010	0.049	0.006	0.053
Co (wt %)	0.001	0.001	0.001	0.001	0.004
Fe (wt %)	0.149	0.214	0.163	0.136	0.248

Tabela 15 – Concentração de metais e enxofre em rocha total.

Field_code	CMJ042	CMJ041	CMJ038	CMJ036	CMJ028	CMJ032	CMJ022	CMJ020	CMJ017	CMJ014
Stratigraphy	10	20	120	200	235	245	275	278	280	300
Lito	GT	GT	PX	PD	DU	DU	DS	MS	MS	PD
S (wt.%)	0,13	0,06	0,07	0,09	0,09	1,23	4,84	13,10	18,80	0,87
Co (ppm)	77	87	76	111	178	233	320	840	708	177
Cu (ppm)	112	238	75	78	128	3660	8650	3660	3140	3460
Ni (ppm)	233	326	332	577	1430	3140	5270	26800	4380	2510

Field_code	CMJ012	CMJ009	CMJ005	CMJ100	CMJ103	CMJ106	CMJ108	CMJ109	CMJ111	CMJ113
Stratigraphy	305	330	370	470	490	505	515	520	530	540
Lito	PD	DU	DU	PX	PX	PX	PX	PX	PX	PX
S (wt.%)	0,33	0,33	0,36	0,06	0,15	2,99	1,69	6,64	0,25	0,28
Co (ppm)	168	184	181	75	149	302	169	182	96	77
Cu (ppm)	1100	1410	56	205	185	2650	1130	3480	250	205
Ni (ppm)	1440	1860	1540	397	781	2890	1980	3030	469	481

Field_code	CMJ115	CMJ116	CMJ508	CMJ509b	CMJ510b	CMJ511a	CMJ516
Stratigraphy	555	557	570	590	610	680	900
Lito	GN	GN	GT	GT	GT	GT	PD
S (wt.%)	1,23	1,04	0,13	0,11	0,46	0,07	0,48
Co (ppm)	20	16	61	75	80	77	131
Cu (ppm)	405	279	171	160	518	162	833
Ni (ppm)	98	16	258	192	450	245	917

No *plot* da Figura 32 fica claro uma tendência mais forte na correlação linear de razão 1:1 entre os dois métodos. No entanto, ao menos três amostras estão distantes da tendência principal, configurando pontos fora da reta, ou, *outliers*. Este fenômeno pode estar relacionado ao efeito pepita embutido em análises de elementos erraticamente

disseminados em amostras de baixo volume (~ 0,5 kg). Todavia, a maioria das amostras sugere coerência entre os métodos de análise.
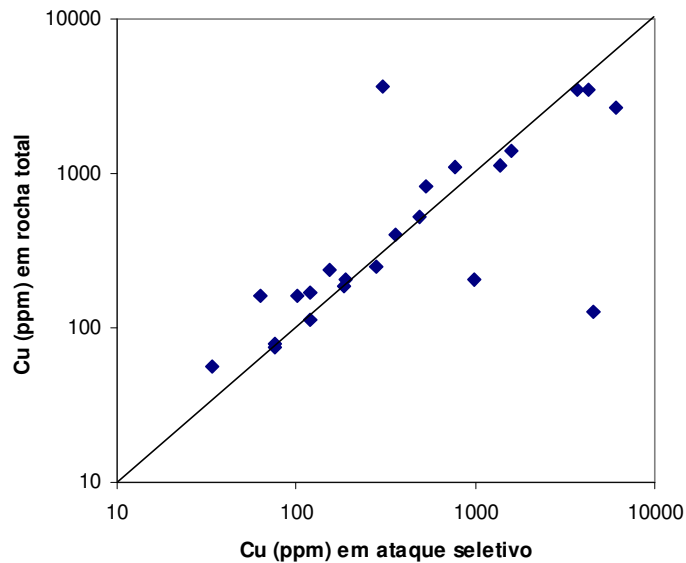

Figura 32 – Gráfico comparativo entre concentração de Cu entre o ataque seletivo bromo-metanol e a análise convencional de rocha total.

A Figura 02 utiliza-se da razão Ni/Cu contra a estartigrafia, objetivando vislumbrar a evolução química do magma ao longo do fracionamento magmático, através da composição dos *droplets* de sulfeto. Logo a primeira vista, fica evidente, através da curva comparativa *plotada* na Figure 02b, que as amostras analisadas pelo ataque seletivo apresentam razões Ni/Cu sempre menores que as amostras analisadas como rocha total. Todas as amostras da Sequencia Sul apresentam razões Ni/Cu =< 1 ao ataque seletivo, porém na analise de rocha total mostra-se frequentemente com valores Ni/Cu > 1, atingindo um máximo de 4,2 nas adjacências do corpo de minério S1. Esta diferença forte está ligada ao Ni contido nas fases silicáticas que foi contabilizada pela análise em rocha total, mas não no ataque seletivo. A amostra CMJ005 apresenta um valor Ni/Cu exageradamente alto (11,8 no ataque seletivo e 27,5 em rocha total) em ambas as análises, fator que deve estar ligado a um reequilíbrio secundário dos *droplets* com as olivinas ao redor.

Segundo relatório da Votorantim Metais (2007) onde foram utilizados critérios estatísticos consistentes (e.g. código JORC) para modelagem geológica dos corpos de minério do complexo AB, o corpo de minério S2 possui razão Ni/Cu de 1,4, enquanto

que o S1 apresenta 0,8. Esses números parecem estar muito bem amarrados com a curva desenhada na Figure 33a (ataque seletivo), porém bastante distantes das amostras evidenciadas pela Figure 33b (rocha total). Este fato só vem reforçar a utilidade e importância da utilização do ataque seletivo no estudo da geoquímica de sulfetos em amostras com sulfetos disseminados.
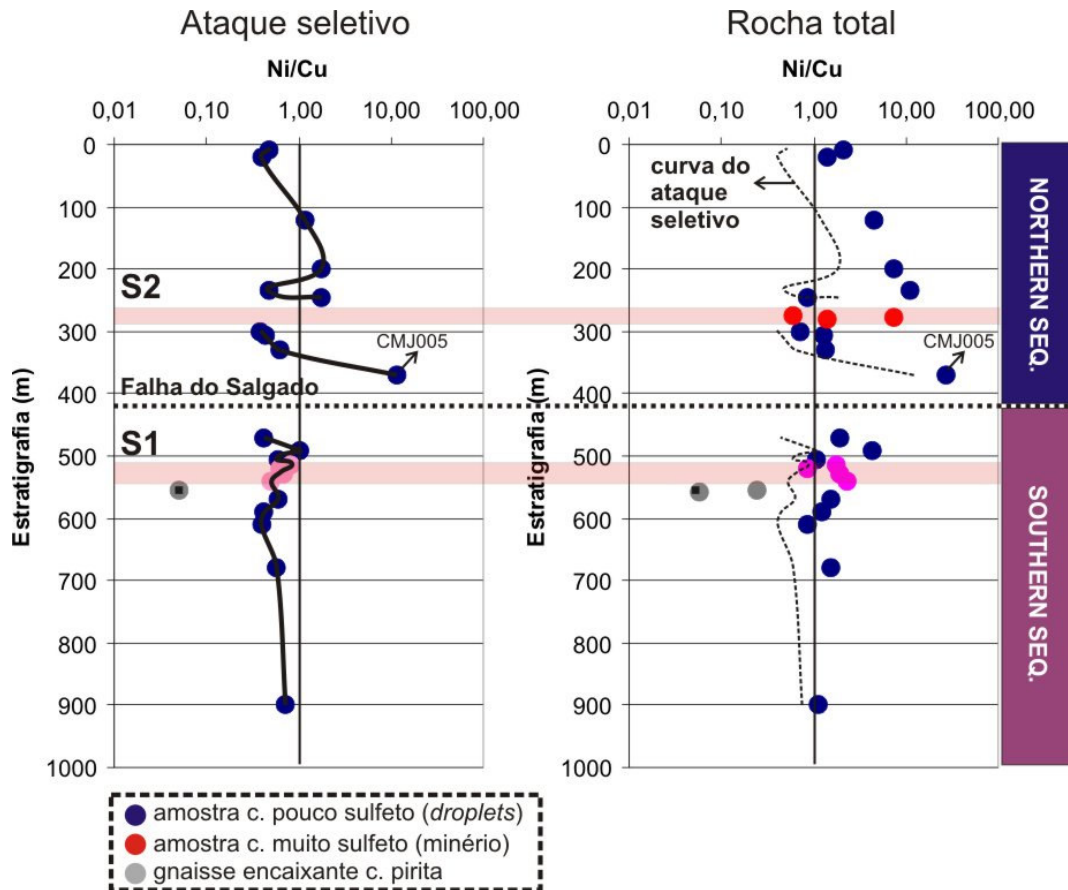

Figura 33 – Razão Ni/Cu contra estratigrafia do complexo AB: (a) amostras que foram analisadas pelo método bromo-metanol seletivo e (b) amostras analisadas como rocha total.

A Figura 34 mostra em diagrama onde se situam os diferentes tipos de depósitos magmáticos em relação a seus conteúdos de Ni e Cu. Vale reforçar que se fizéssemos uso das razões Ni/Cu obtidas por análise de rocha total, muitas amostras da Sequencia Norte e algumas da Sequencia Sul estariam desenhadas no campo dos komatiítos, o que obviamente, não tem nenhum senso científico.
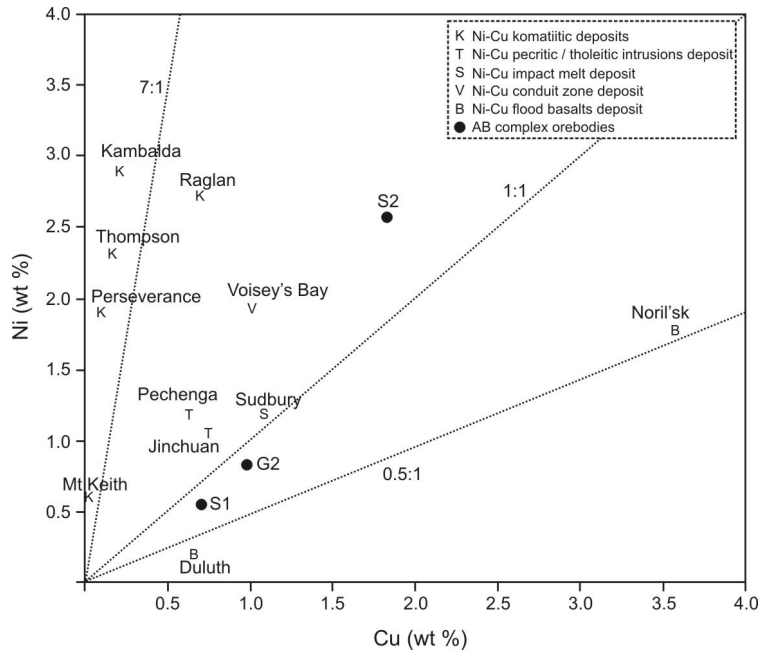
Figura 34 – Diagrama evidenciando conteúdos de Ni e Cu nos corpos de minério do complexo AB.

Deste modo, o ataque seletivo com abertura branda de bromo-metanol é uma eficiênte ferramenta para estudo da geoquímica de *droplets* e, portanto, da evolução do magma silicático durante o fracionamento magmático em complexos máficos acamadados. Este método é hoje ainda de uso muito restrito, porém é amplamente utilizado pela empresa Outokumpu Oy que trabalha com diversos depósitos magmáticos Ni-Cu ou polimetálicos de baixo teor na Finlândia.

Referências

Naldrett, A.J. (2004). Magmatic Sulfide Deposits – Geology, Geochemistry and Exploration. Springer. Berlin, Germany. 724 pp.

Nilson, A.A. (1981). The nature of Americano do Brasil mafic-ultramafic complex and associated sulfide mineralization, Goiás, Brazil. PhD Thesis, University of Western Ontario, 460 pp.

Pentinnen, U., Palosaari, V., Siura, T. (1977) – Selective dissolution and determination of sulfides in nickel ores by the bromine-methanol method. Bulletin of Geological Society of Finland 49(2), 79 – 84.

Votorantim Metais (2007). Geological model of Americano do Brasil ore deposits. Unpublished internal report.

Anexo 2 - Isótopos de enxofre em LA-MC-ICPMS

Isótopos de S, assim como outros isótopos estáveis, são amplamente utilizados para identificação de um dado processo e/ou condições físico-químicas de fluidos mineralizantes. É bastante disseminado na literatura científica sobre depósitos magmáticos, a importância da assimilação de fontes externas de enxofre pelo magma básico na formação de grande depósitos Ni-Cu-PGE (Naldrett, 1966, Keays, 1995 e Li *et al*, 2001). Um exemplo disso é o depósito gigante de Noril'sk-Talnakh, que tem assinaturas de contaminação por enxofre de evaporitos e provavelmente também por sulfetos de folhelhos piritosos (Godlevsky e Grienko (1963), Grinenko (1985) e Li *et al.* (2003)). Outros depósitos grandes como Stillwater (Zientek e Ripley (1990)), Bushveld (Buchanan *et al.* (1981)) e sua intrusão satélite Uitikomst (Li *et al.* (2002)), também possuem assinaturas de assimilação de fonte externa de enxofre. Este trabalho demonstrou uma possível assimilação restrita por gnaisse piritoso, o mesmo tipo de rocha que Ryan *et al.* (1995) sugeriu contaminar o magma básico que formou o depósito de Voisey's Bay no Canadá.

Durante esta pesquisa, foi implantado no Laboratório de Geocronologia do IG/UnB, o método de análise de isótopos de enxofre com LA-MC-ICPMS (Laser Ablation - Multi Collector - Induced Coupled Plasma Mass Spectometer) no equipamento Finnigan-Neptune acoplado ao laser New Wave UP 213. Este método permite análises pontuais de sulfetos e sulfatos, envolvendo pouca preparação de amostras, em granulação de até 100 μm e podendo-se evitar imperfeições no cristal. O processo de implantação do método foi desenvolvido junto com Karin M. Bender, doutoranda no IG/UnB. Uma publicação sobre o método desenvolvido e suas aplicações foi recentemente apresentada por Bender, K.M., Buhn, B.M., Mota-e-Silva, J., Chaves, J.G.S (2008) no VI *South American Symposium on Isotope Geology* em San Carlos de Bariloche, Argentina. Uma síntese da metodologia segue nos parágrafos seguintes.

Dentre os quatro isótopos de enxofre existentes na natureza, conforme evidenciado na Tabela 16, os trabalhos acadêmicos têm tratado mais intensamente dos S32, S33 e S34, entre os quais o S32 e o S34 são mais abundantes e amplamente utilizados no meio científico, e foram objetos de estudo desta pesquisa.

Tabela 16 – Isótopos de enxofre e suas abundâncias relativas (Rosman e Taylor, 1998)

Massa atômica	Abundância natural (%)
32	94.93
33	0.76
34	4.29
36	0.02

A maior dificuldade em análises de isótopos de enxofre é resolver o problema das interferências poliatômicas (Tabela 17) no espectrômetro. As interferências mais importantes estão relacionadas aos átomos de oxigênio. Para evita-las o espectrômetro deve ser ajustado para "*medium resolution*" de tal modo que no "*mass scan*" consiga-se um patamar antes da curva de influência do oxigênio (Figura 35). O isótopo S33 deve ficar no "*center cup*" que é o *Faraday cup* central, enquanto que S32 e S34 ficarão nos *Faraday cups* vizinhos.

Tabela 17 – Isótopos de enxofre e suas interferências poliatômicas típicas (Bendall *et al.*, 2006)

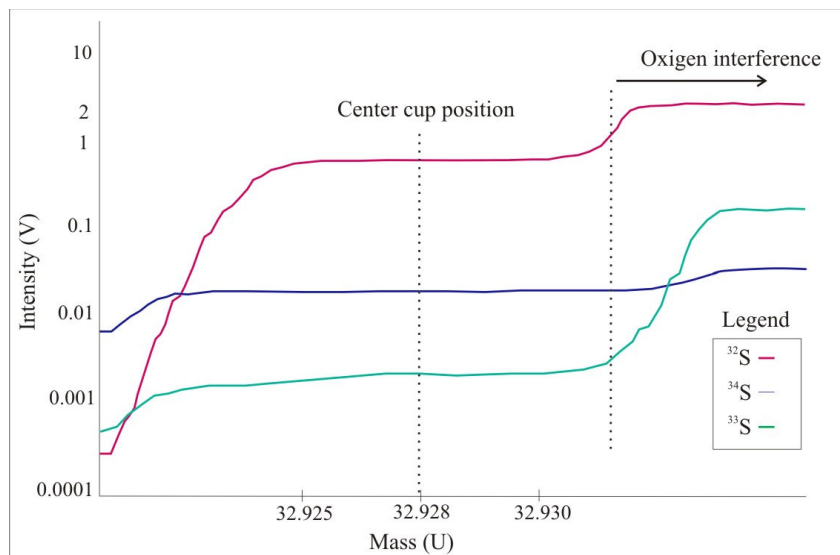| Isótopo	Massa	Resolução (m/Δm)
S32	31.97207	
O16–O16	31.98983	1800
S33	32.97146	
S32–H1	32.9799	3907
S34	33.96787	
S33–H1	33.97928	2977
O16–O18	33.99407	1296
S36	35.96708	
Ar36	35.96755	76526

Figura 35 – Curvas de intensidade no "*mass scan*" do programa de operação do MC-ICPMS com *laser ablation*. Reparar nos patamares bem definidos dos isótopos de S de massas 32 e 34, enquanto que o de massa 33 mostra-se imperfeito (Bender *et al*, 2008).

Para calibração da posição dos *Faraday cups*, foram feitas amostras em solução, a fim de evitar heterogeneidades. Foram preparadas seis soluções, sendo duas delas com amostras padrão adquiridas no *National Institute of Standards & Technology* e quatro que se consituíram em padrões internos, com utilização de grãos minerais bem formados e homogêneos. Uma delas foi pirita secundária remobilizada em plano de falha e outra primária do depósito S1, ambos do complexo Americano do Brasil. As outras foram calcopirita e pirrotita do depósito de Ni de Boa Vista do Greenstone Belt de Crixás-GO. Os grãos foram separados utlizando-se de cominuição, peneiramento, separação isodinâmica magnética no Frantz e catação com lupa binocular. As amostras padrão (NBS123-esfalerita e NBS127-barita, National Institute of Standards & Technology, 1992) ja se encontravam prontos para serem dissolvidas, em grãos limpos e homogêneos.

Os grãos foram dissolvidos em HNO_3 concentrado em bombas fechadas submetidas a três minutos de aquecimento em aparelho microondas regulado em potência máxima. As amostras foram evaporadas em chapa quente (*clean box*) dentro da capela e posteriormente re-dissolvidas em HNO_3 de modo a gerar uma solução com 5 ppm de concentração de enxofre.

As amostras para o laser foram simplesmente moídas, sendo que os fragmentos de rocha contendo sulfetos foram separados manualmente e *mounts* foram montados utilizando-se lamina de vidro, durex dupla-face, invólucro de plástico e resina

de endurecimento rápido (Epofix). Depois de endurecido, os *mounts* foram lixados e polidos com pasta de diamante. Um rápido ataque com HNO$_3$ 2% e vibração ultrasônica em água nanopura, garantiu que a superfície ficasse isenta de impurezas ou crostas de oxidação.

As duas soluções com os padrões internacionais foram lidas repetidas vezes juntamente com as quatro soluções com as amostras de Crixás e Americano do Brasil. Utilizando-se de ciclos de leitura (PAAB / PAAB / etc) de amostra padrão (P), branco (B) e amostra (A) e correção *standard-sample breacketing* em curva linear conseguiu-se bons patamares de detecção dos isótopos e valores S34/S32 para os padrões internos. Esta correção visou eliminar os efeitos de *drift* do instrumento e o próprio fracionamento de isótopos, porém este efeito decai em curva logarítmica, ou seja, tem efeito muito mais forte nas primeiras horas de trabalho.

Após essa etapa passou-se para as análises com *laser ablation*, propriamente ditas. Seguindo a mesma metodologia de seqüência de análises e correções matemáticas da fase de análises em solução, a série foi repetida por 16 vezes para as quatro amostras. Nesta etapa identificou-se duas amostras com boa homogeneidade dos grãos e boa reprodutibilidade das análises. Essas amostras foram a pirita do corpo S1 (Figura 36) do complexo de Americano do Brasil e calcopirita do depósito de Boa Vista no Greenstone Belt de Crixás-GO (Tabela 18).
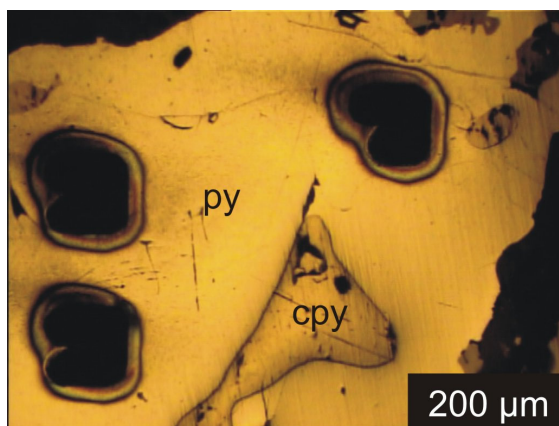

Figura 36 – Pirita do corpo S1 do complexo Americano do Brasil com três "tiros" de laser em geometria raster. Esta amostra tornou-se um dos padrões internos do laboratório.

Tabela 18 – Dois padrões internos, suas razões isotópicas e seus erros.

Padrões	32S/34S	2σ (0/00)	32S/34S	1σ (0/00)
cpy	22.2601	0.9107	22.2580	0.2305
py	22.1925	0.7626	22.1913	0.2592

As configurações dos equipamentos estão explicitados na Tabela 19.

Tabela 19 – Melhor configuração alcançada para os equipamentos durante os trabalhos com isótopos de enxofre.

Laser		ICPMS	
Freqüência (Hz)	9	Fluxo de gás Ar (l/min)	0.857
Geometria	Raster	RF Power (W)	928
Energia (mJ)	0.023 (38%)	Resolução	média
Diâmetro (μm)	65	Ciclos	40 (1s cada)
Fluxo de gás He (l/min)	0.35		

A análise de isótopos de S, apesar de ser uma ferramenta eficiênte, tem uma implantação do método relativamente simples. Equipamentos LA-MC-ICPMS, ou até espectômetros mais simples, podem ser configurados e ajustados para realizar leituras de isótopos S32 e S34. Os problemas com interferências poliatômicas devem ser resolvidos com uma resolução mais fina no aparelho, o que por sua vez, causa uma diminuição no sinal captado. Todavia, isso não é um problema uma vez que a quantidade de S liberado na abertura de sulfetos e sulfatos é muito grande. Um desafio certamente mais árduo é calibrar o equipamento para leituras de isótopos S33. Este isótopo de abundância muito baixa na natureza (0,76% de acordo com Rosman e Taylor, 1998), vem gradativamente se tornando parte das pesquisas com isótpos estáveis, e assim, ganhando importância nos estudos científicos. No entanto, o S33 não foi o foco da atual pesquisa.

Referências

Bendall, C., Lahaye, Y., Fiebig, J., Weyer, S. and Brey, G.P. (2006). *In situ* sulfur isotope analysis by laser ablation MC-ICPMS. Applied Geochemistry, 21: 782-787.

Bender, K.M., Buhn, B.M., Mota-e-Silva, J., Chaves, J.G.S. (2008). 32S/34S Isotope analyses by laser ablation MC-ICPMS: Method and application. VI South American Symposium on Isotope Geology. San Carlos de Bariloche, Argentina.

Buchanan, D.L., Nolan, J., Suddaby, P., Rouse, J.E., Viljoen, M.J., Davenport, J.W.L., (1981). The genesis of sulfide mineralization in a portion of the Potgietersrus Limb of the Bushveld intrusion. Economic Geology, 76: 568–579.

Godlevsky M N e Grienko L N. (1963). Some data on the isotopic composition of sulfur in the sulfides of the Noril'sk deposit. Geochemistry, 1: 335–341.

Grinenko L N. (1985). Sources of sulfur of the nickeliferous and barren gabbro-dolerite intrusions of the northwest Siberian platform. International Geology Review, 28: 695–708.

Keays, R.R., (1995). The role of komatiitic and picritic magmatism and S-saturation in the formation of ore deposits. Lithos 34: 1–18.

Li C, Naldrett A J, Ripely E M. (2001). Critical factors for the formation of a nickel-copper deposit in an evolved magma system: lessons from a comparison of the Pants Lake and Voisey's Bay sulfide occurrences in Labrador, Canada. Mineralium Deposita, 36: 85–92.

Li C., Ripley, E.M., Maier, W.D., Gomwe, T.E.S. (2002). Olivine and sulfur isotopic compositions of the Uitkomst Ni–Cu sulfide ore-bearing complex, South Africa: evidence for sulfur contamination and multiple magma emplacements. Chemical Geology, 188: 149– 159.

Li C., Ripley E.M., Naldrett A.J. (2003). Compositional variations of olivine and sulfur isotopes in the Noril'sk and Talnakh Intrusions, Siberia: implications for ore-forming processes in dynamic magma conduits. Economic Geology, 98: 69–86.

Naldrett, A.J. (1966). The role of sulphurization in the gneiss of iron-nickel sulphide deposito of the porcupine district, Ontario. Transactions LXIX, 147-155.

National Institute of Standards & Technology (1992). Report of Investigation, reference materials 8553-8557.

Rosman, K.J.R. e Taylor, P.D.P. (1998). Isotopic Compositions of the Elements 1997. Pure and Applieed Chemistry, 70: 217-236.

Ryan, B., Wardle, R., Gower, C., Nunn, G., (1995). Nickel–copper sulfide mineralization in Labrador: the Voisey Bay discovery and its exploration implications. Current Research Newfoundland Department of Natural Resources, Geological Survey Report 95-1, 177–204.

Zientek, M.L., Ripley, E.M., (1990). Sulfur isotope studies of the Stillwater intrusion and associated rocks, Montana. Economic Geology, 85: 376–391.